A STUDY OF LINE INTENSITIES IN THE SPECTRUM OF θ URSAE MAJORIS

By

HUGH OSCAR PEEBLES

Bachelor of Science
University of Texas
Austin, Texas
1955

Master of Science
Oklahoma State University
Stillwater, Oklahoma
1960

Submitted to the Faculty of the Graduate School of
the Oklahoma State University
in partial fulfillment of the requirements
for the degree of
DOCTOR OF PHILOSOPHY
May, 1964

OKLAHOMA
STATE UNIVERSITY
LIBRARY
JAN 8 1965

A STUDY OF LINE INTENSITIES
IN THE SPECTRUM OF
θ URSAE MAJORIS

Thesis Approved:

Leon W. Schroeder
Thesis Adviser

W E Harrington

Francis C. Todd

E E Kohnke

H H Mendenhall

Dean of the Graduate School

570290

ACKNOWLEDGMENTS

The author wishes to express his appreciation to Dr. Leon W. Schroeder for his constant guidance and encouragement during this investigation. The study was initiated at Dr. Schroeder's suggestion and carried out with the θ Ursae Majoris tracings which he supplied.

Indebtedness is acknowledged to Dr. K. O. Wright of the Dominion Astrophysical Observatory who provided the θ Ursae Majoris spectrograms, both for the tracings and for reproduction in the text.

The work was supported in part by a grant from the Office of Naval Research, Geography Branch, under Contract No. Nonr(G)-00017-61, administered through the Research Foundation of the Oklahoma State University.

The author also wishes to acknowledge the support he received from a National Defense Education Act fellowship during the three years this research was in progress.

TABLE OF CONTENTS

LIST OF TABLES

LIST OF FIGURES

LIST OF PLATES

CHAPTER I

INTRODUCTION

Much useful information concerning the properties of a stellar atmosphere can be obtained from a study of the intensities of the absorption lines appearing in the stellar spectrum. A commonly employed method of analyzing absorption line intensities involves the application of idealized curves of growth. The purpose of this paper is to describe the use of this approach, called "grobanalyse" by German workers, in a study of the spectrum of the star θ Ursae Majoris*.

The advantage of the curve of growth lies in the fact that it may be used to handle many observational data, namely, the equivalent widths of the lines. The equivalent width of a line is a readily obtainable quantity, whereas the actual shape or profile of a line, which is required for the use of the more refined model atmosphere techniques, is difficult to determine, especially for weak lines. The disadvantage of the curve of growth arises from its being a statistical procedure which ignores information that might be obtainable from the shapes of certain lines.

The curve of growth was introduced by Minnaert and Slob (1931) and developed and applied by many other workers. Menzel (1936) first

---

*θ Ursae Majoris is listed by Johnson and Morgan (1953) as a subgiant (spectral type F6, luminosity class IV). Its visual magnitude is 3.3 and its coordinates are $\alpha(1900) = 9^h26^m$, $\delta(1900) = +52^o8'$ (Keenan and Morgan, 1951).

developed the theory as it applies to the Schuster-Schwarzschild (S-S) model atmosphere--wherein the entire continuous spectrum is produced by a sharply defined radiating surface or photosphere, overlaid by a reversing layer which produces all the line absorption but no continuous absorption. Such an approximation can be considered quite representative for the lines of neutral metals (e.g., Ca I and Na I in the sun) where the number of absorbers diminishes with optical depth because of increased ionization with increased temperature. The other extreme approximation, where the lines originate in the same layers as does the continuous spectrum, is embodied in the Milne-Eddington (M-E) approximation of a ratio of line to continuous absorption coefficient which is constant with depth. Strömgren (1937) has found, at least in some cases, that the variation of this ratio with optical depth is sufficiently small to permit a mean value to be employed over the layers important in line formation, in which case the M-E model can be used. The true situation for any line lies between the two extremes represented by the S-S and M-E models.

Wrubel (1949, 1950, 1956) has computed theoretical curves of growth based upon the M-E model for pure scattering and for pure absorption. The processes of pure scattering and pure absorption are the two extreme mechanisms by which a line may be formed. Also, Wrubel (1954a) has published curves for the S-S model with pure scattering. All of Wrubel's curves of growth are based upon Chandrasekhar's exact solutions of the equation of transfer and therefore are regarded as the most accurate available for the above mentioned models. Theoretical curves of growth for the S-S and M-E models with pure absorption have been calculated by Hunger (1956).

Although these idealized curves can be brought into approximate coincidence (Wrubel, 1954b, and Hunger, 1956), significant differences exist. However, the scatter in the observations is usually large enough that it is difficult to determine with any degree of certainty which of the idealized curves is best fit by the observations; hence, it was deemed advisable to apply all four sets of curves to the study of the spectrum of θ Ursae Majoris. The four sets of curves applied in this study are those for pure scattering by Wrubel for the M-E and S-S models and Hunger's M-E and S-S pure absorption curves. For reasons to be discussed in Chapter II, Hunger's M-E pure absorption curves were used rather than those by Wrubel for this same model.

This investigation was restricted to those lines for which laboratory absolute f-values are reasonably well known. Recently, Corliss and Bozman (1962) published a list of experimentally determined absolute f-values for 25,000 spectral lines of seventy elements. Due to the availability of this extensive tabulation, there appeared to be no necessity for using theoretically calculated f-values; such quantities determined by laboratory measures are considered to be more reliable that those calculated from theory. Other experimentally determined f-values employed in this investigation are those of King and King (1938) for Fe I and Ti I, Hill and King (1951) for Cr I, and Carter (1949) for Fe I. Also, the solar log X_f's of Wright (1948) were used to augment the Ti II data.

Only lines with wavelengths in excess of 4000 angstroms were used, since the spectrum is quite complex to the violet of λ4000. Also, many lines in this region are on the broad wings of the H and K lines of ionized calcium.

Equivalent widths have been measured for 359 lines of Ca I, Ti I, Ti II, Cr I, Mn I, Fe I, Co I, and Ni I. The spectral region covered is λλ4000-6500, and only those lines which were sufficiently well resolved and unblended were used. Kinetic velocities, damping constants, excitation temperatures, and abundances were determined using the theoretical curves of growth based upon both the M-E and S-S models. Results were obtained for the extreme cases of pure scattering and pure absorption for the two models.

CHAPTER II

THE CURVE OF GROWTH

Definition

The curve of growth is the relation between the intensity of an absorption line and the number of absorbing atoms active in producing the line.

The Intensity of an Absorption Line

The term "intensity" here means the total amount of energy subtracted from the continuous spectrum by the absorption line and is best specified by a quantity called the "equivalent width," W, of the line. The profile of a line is the plot of the flux at each point in the line versus the wavelength. Hence, the area enclosed by the profile and the continuum is the total amount of energy absorbed in the line. The equivalent width is the width of the rectangle having this same area and with a height equal to that of the adjacent continuum. These relations are shown in Figure 1.

The advantages of expressing the intensity of a line in terms of the equivalent width are that W is much less affected by the finite resolution of the spectrograph than is the line profile, and W is independent of the Doppler effects of stellar rotation and large scale turbulence in the stellar atmosphere.

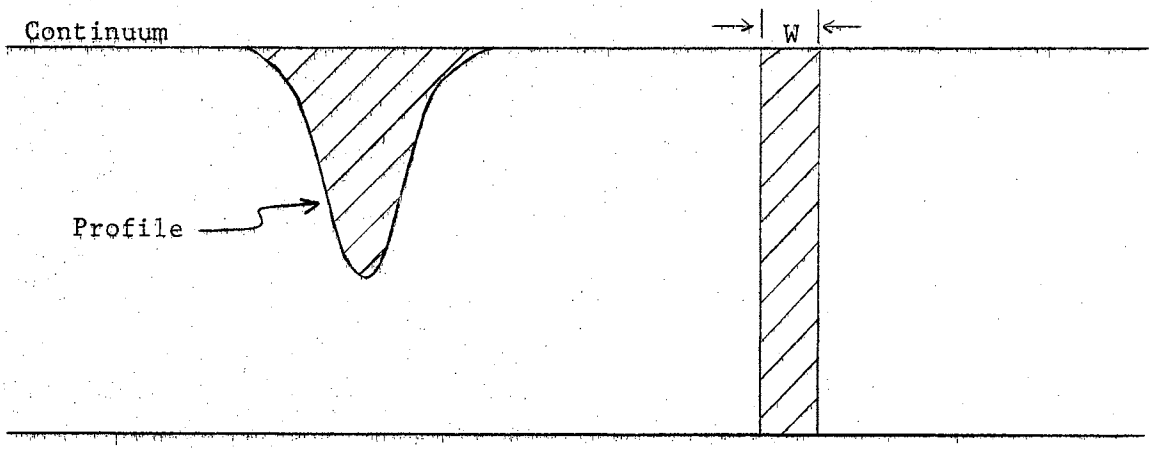

Figure 1. The Equivalent Width, W, of a Spectral Line.

The Number of Absorbing Atoms

The number of absorbing atoms for a line originating from a level n and terminating on level j is given by $N_n f_{nj}$, where N_n is the number of atoms in level n, and f_{nj} is the f-value or oscillator strength of the transition from level n to level j. When an atom in level n is exposed to radiation of all frequencies it may absorb any one of several different quanta. In specifying the number of absorbing atoms for a particular line it is necessary to include the f-value to take into account the probability of the atom absorbing the particular quantum corresponding to the transition in question. The f-values depend only upon the structure of the atom, and may be computed from theory or measured in the laboratory.

Observed Curves of Growth

Lines Produced in an Absorption Tube

Let us consider the growth of a particular line as the number of absorbers is increased. This "growth" of a line may be observed in the

laboratory by varying the concentration of the element under investigation in an absorption tube. Lines with strengths depending upon the concentration are formed when light from an incandescent source shines through the tube. When the number of absorbers is small the principal contributor to the equivalent width is thermal Doppler broadening, with the result that W is proportional to Nf. Hence, plotting log W ("log" represents the logarithm to the base ten) versus log Nf for small values of Nf gives a portion of the curve of growth which is linear and has slope equal to unity. Increasing the number of absorbers causes the center of the line to become saturated, and a linear relation between W and Nf no longer exists. The point of departure from linearity is called the "knee" of the curve of growth. Beyond the knee W increases slowly, being proportional to the square root of the natural logarithm of Nf. As the number of absorbers is increased still more, the damping portion of the absorption coefficient is reached. Here the number of atoms is large enough to sufficiently perturb the energy levels so that an appreciable amount of absorption occurs away from the saturated center of the line. Thus the line begins to grow more rapidly. In this portion of the curve of growth W is proportional to the square root of Nf.

This discussion assumes that the temperature of the absorbing atoms is a particular constant value. The position of the knee of the curve of growth varies with the temperature. As the temperature increases, the Maxwellian velocity distribution becomes more extended, and saturation occurs at a greater line width, giving a higher knee on the curve of growth. Also, the point at which the damping portion of the curve begins moves closer to the knee as the value of the damping parameter

increases. The damping parameter, a, is the ratio of the effective natural line width to the Doppler width. Figure 2 illustrates these relations.

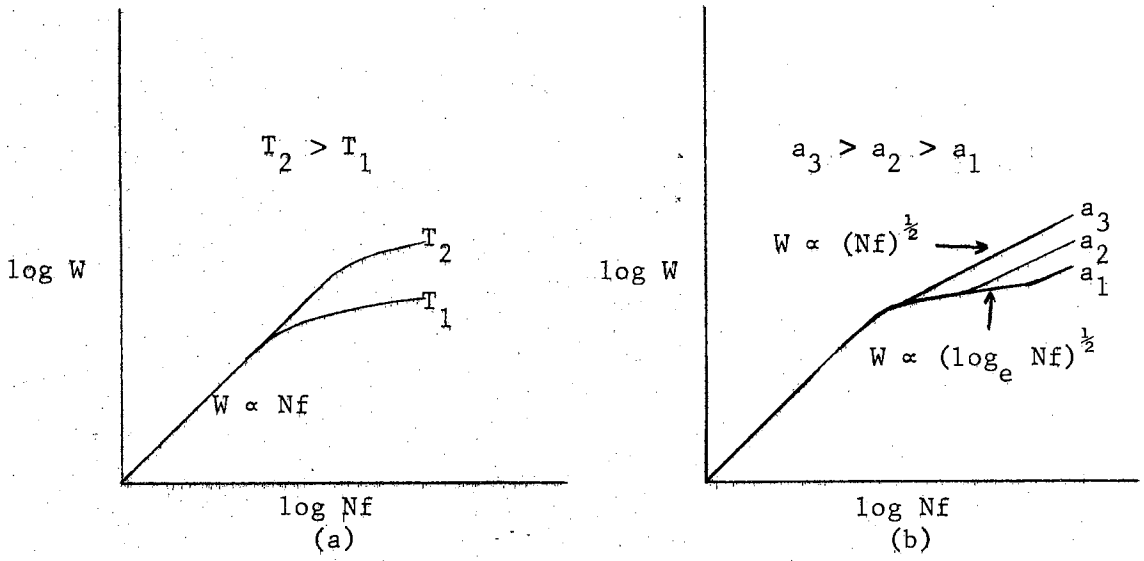

Figure 2. Effects of Temperature (a) and Damping (b) on the Curve of Growth.

Lines Produced in a Stellar Atmosphere

The discussion thus far has dealt with the growth of a single line as the number of absorbing atoms is increased. A single line cannot be observed to grow in a stellar spectrum because $N_n f_{nj}$ does not change. However, in going from one line to another of the same element, $N_n f_{nj}$ does change, since f_{nj} varies from line to line, and N_n also varies if the lines arise from different levels. Again a curve of growth results from the relation between the equivalent widths of the various lines and the corresponding values of $N_n f_{nj}$.

In beginning a study of a stellar spectrum, the values of N_n are not known, and one of the objectives of a curve of growth study is to

determine these quantities. The procedures employed for this purpose are described later in this chapter.

In applying the curve of growth technique to many different lines of an element it is necessary to assume that all the lines are formed at the same temperature. The temperature in a stellar atmosphere increases roughly as $\tau^{\frac{1}{4}}$, where τ is the optical depth. Thus the assumption is made that all the lines are formed at a particular depth in the atmosphere. This may be a poor assumption for weak lines and the wings of strong lines where the absorption coefficient is small. In this case the line is formed in a thick layer through which the temperature may change appreciably. In the center of a strong line the absorption coefficient is large, and the line is effectively formed in a thin layer in which the temperature may be practically constant. Considering non-resonant lines of a neutral atom, the temperature in the outer layers of the atmosphere may be too low to appreciably excite the atoms to levels capable of absorbing these lines. In very deep layers of the atmosphere ionization will reduce the number of absorbers to a negligible number. The lines are consequently formed in intermediate layers, and the temperature in this case is characteristic of these layers.

It is also necessary to assume that a particular value of the damping parameter can be taken as representative for all the strong lines. This assumption is somewhat questionable, since the damping parameter is known to differ from line to line. However, this effect does not come into play for weak lines, and it is usually possible to determine a value for the damping parameter that fits the observations reasonably well.

As mentioned earlier, the position of the knee of the curve of growth depends upon the temperature. Another factor which may influence the position of the knee is microturbulence, i.e., turbulent motions of the gases of the atmosphere where these motions or eddies are confined within the layer in which the lines are produced. The presence of microturbulence increases the widths of the lines thus increasing the number of absorbers required for saturation of the line center. Hence, the position of the knee is elevated. Effects of microturbulence are especially evident in curves of growth for giant and supergiant stars. Struve and Elvey (1934) first called attention to this phenomenon.

Theoretical Curves of Growth

Calculations of theoretical curves of growth are based upon various assumptions as to the structure of stellar atmospheres and the mechanism of line formation.

The Schuster-Schwarzschild Model

The Schuster-Schwarzschild (S-S) model depicts the atmosphere as consisting of a "reversing layer" of depth H overlying a sharply defined radiating surface or photosphere. The continuous spectrum is produced below the photosphere, and the reversing layer is the region of line formation. The optical depth of the reversing layer is a function of the absorption coefficient of the line, and there is no continuous absorption in the reversing layer. A portion of the radiation incident upon the photosphere from below is transmitted while the remainder is diffusely reflected. The transmitted energy is subject to selective absorption and scattering. Radiation returned to the photosphere is

absorbed there by continuous absorption. For a point in the wing of a line the optical thickness of the reversing layer is small, while it is much greater in the line core. This model is a good approximation for neutral metals where the number of absorbers diminishes rapidly with depth because of increased ionization with increased temperature.

The Milne-Eddington Model

In the Milne-Eddington (M-E) model the lines and the continuum are formed in the same region. For each frequency the ratio of the line absorption coefficient to the continuous absorption coefficient ($\ell_\upsilon / \varkappa_\upsilon = \eta_\upsilon$) is assumed to be constant with depth, although ℓ_υ and $\varkappa_\upsilon$ may individually change with depth. In the line wings there are few absorptions and reemissions, and consequently the emergent radiation follows a short path through the atmosphere. In the line center the quanta follow longer paths (many absorptions and reemissions) and the probability of continuous absorption is greater (say due to H^- in stars like the sun) and the energy may be lost.

Thus, in both models a selective process followed by continuous absorption forms the line. Figure 3 illustrates these two idealized models.

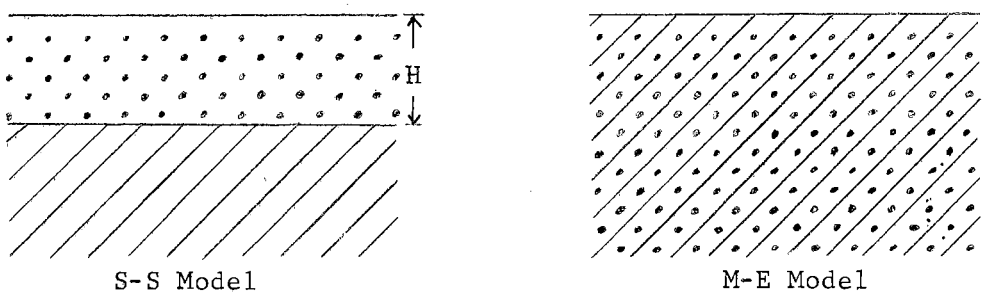

Figure 3. The S-S and M-E Models. Dots represent selective absorption and emission; hatches represent continuous absorption.

The Formation of a Line

The mechanism of spectral line formation is determined by conditions existing in the atmosphere. If the atmosphere is in a state of radiative equilibrium, then for each quantum absorbed a like quantum is emitted. This process is called "scattering." Scattering is coherent if the frequency of the emitted quantum is exactly the same as the frequency of the absorbed quantum. If the frequency of the emitted quantum is slightly different from that of the absorbed quantum, the scattering is non-coherent. If the atmosphere is in "local thermodynamic equilibrium," i.e., Kirchhoff's law holds at each point of the atmosphere for the local temperature, then the lines are formed by the process of "absorption." Here there is no one-to-one correspondence between the absorbed frequency and the emitted frequency, and the absorbed quantum is "lost."

Hence, a spectral line may be formed by scattering or absorption or by some combination of the two.

The Theoretical Curves Used in This Study

The four sets of theoretical curves used in this investigation are as follows: 1) M-E pure scattering by Wrubel, 2) S-S pure scattering by Wrubel, 3) M-E pure absorption by Hunger, and 4) S-S pure absorption by Hunger.

Curves for M-E pure absorption have also been calculated by Wrubel and published in an article by Aller (1960). The calculations were based upon Chandrasekhar's exact solution of the equation of transfer and, therefore, should be the most accurate available for the M-E pure absorption case. However, these curves include only two values (-1 and

-3) of log a, where a is the damping parameter. Because of this limitation they have not been employed in this study.

The integral equation for the equivalent width, W, is

$$\frac{W}{b} = \int_{-\infty}^{+\infty}(1 - R)d\upsilon, \tag{1}$$

where b is the Doppler width of the line, R, the "residual intensity," is the ratio of the flux of the radiation at a point in the line to the flux in the adjacent continuum, and υ is the distance from the center of the line in units of the Doppler width. Here $\upsilon = (\lambda - \lambda_o)/b$, where λ is the wavelength at a point in the line, and λ_o is the wavelength at the center of the line. Also, $b = \lambda_o v/c$, where v is the most probable velocity of the atoms and c is the velocity of light.

It should be noted that the velocity v includes both the effects of thermal and microturbulent motions. That is,

$$v = \sqrt{v_{th}^2 + v_{turb}^2}, \tag{2}$$

where v_{th} is the most probable thermal velocity, and v_{turb} is the most probable velocity of the microturbulence. It is assumed that the turbulent elements have a random distribution of velocities. The thermal velocity is given by

$$v_{th} = \sqrt{\frac{2kT}{M}}, \tag{3}$$

where k is Boltzmann's constant, T is the kinetic temperature, and M is the mass of the atom producing the lines.

The residual intensity, R, is found from the solution of the equation describing the transfer of radiation through a stellar atmosphere. R depends upon assumptions as to the atmospheric model and the mechanism of line formation. In his calculations of theoretical curves of growth,

Wrubel employed the expressions for R resulting from Chandrasekhar's exact solutions of the equation of transfer. Expressions for R which follow from the work of Unsöld (1955) were used by Hunger in his calculations of theoretical curves of growth.

Both Wrubel's and Hunger's curves employ the assumption that the Planck function varies linearly with optical depth in the continuum; i.e., $B_\nu(T) = B^o + B^1\tau_\nu$. This leads to a limb darkening law in the continuum that is linear in cos θ, where θ is the angle between the line of sight and the normal to the stellar surface. In the S-S model this is expressed as $I = I^o + I^1 \cos\theta$, and in the M-E model as $I = B^o + B^1\cos\theta$. The effect of the addition of an exponential term to the linear expression for the Planck function has been investigated by Hunger (1956). He concluded that the addition of such a term has negligible effect and is therefore unnecessary.

The expression for the residual intensity, as given by Chandrasekhar and used in Wrubel's calculations, involves the ratio of the limb darkening coefficients, I^o/I^1 or B^o/B^1. Pure scattering curves are available for the S-S model with I^o/I^1 equal to ¼, ½, 1, and 2, and for the M-E model with B^o/B^1 equal to 1/3, 2/3, 4/3, and 10/3.

Equation (1), with the appropriate expressions for R, was employed by Wrubel in his calculations. Consequently, the ordinate of his curves is log W/b. Hunger divided Equation (1) by R_c, the "limiting depth" of the line, to obtain

$$\frac{W}{2R_c b} = \int_o^\infty \frac{1 - R}{R_c}\, d\sigma , \qquad (4)$$

where

$$R_c = \frac{1}{1 + \frac{3}{2}\frac{B^o}{B^1}} , \qquad (5)$$

and the symmetry of the integral about ν equal to zero has been taken into account. The ordinate of Hunger's curves is log $W/2R_c b$. For the cases of M-E and S-S pure absorption, the ratio $(1-R)/R_c$ is independent of the limb darkening coefficients. This results from the particular expressions for R used by Hunger. Therefore, Hunger's formulation of the curve of growth for M-E and S-S pure absorption avoids the necessity of having to calculate separate curves for each value of B^o/B^1. It is to be noted, however, that the limb darkening is still taken into account by Hunger since B^o/B^1 is involved in the ordinate of his curves.

In the calculations of theoretical curves of growth the damping constant, a, is considered to be a free parameter. Wrubel's pure scattering curves were calculated for values of log a running from -3.0 to -1.0 in steps of 0.4. The pure absorption curves published by Hunger were computed for values of log a running from -4.3 to +0.7 in steps of 0.5. He also included a curve for log a = $-\infty$.

For the M-E model (both scattering and absorption) R is a function of η_o, where

$$\eta_o = \frac{\ell_o}{\overline{\kappa}} . \qquad (6)$$

ℓ_o is the fictitious absorption coefficient at the center of the line, and $\overline{\kappa}$ is the mean continuous absorption coefficient. The abscissa for both the M-E scattering and M-E absorption curves is log η_o. In Hunger's notation the abscissa is log C, but, as he points out, $C = \eta_o$ for M-E pure absorption.

For the transition from level n to level j, η_o is given by

$$\eta_o = \frac{\ell_o}{\overline{\kappa}} = \frac{\pi^{\frac{1}{2}} e^2 \lambda^2 N_n f_{nj}}{mc^2 b \rho \overline{\kappa}} , \tag{7}$$

where

e = charge of the electron,

m = mass of the electron,

λ = wavelength of the line in question,

N_n = number of atoms in level n per unit volume,

f_{nj} = oscillator strength of the transition from level n to level j,

c = speed of light,

b = Doppler width of the line, and

ρ = density of the stellar material.

Here $\overline{\kappa}$ is the mean absorption coefficient per gram of stellar material.

Using the relation $b = \lambda v/c$, it follows that

$$\log \eta_o = \log N_n/\rho\overline{\kappa} + \log C + \log f_{nj}\lambda + \log c/v, \tag{8}$$

where

$$C = \frac{\pi^{\frac{1}{2}} e^2}{mc^2} . \tag{9}$$

The residual intensity, R, in the S-S model is a function of τ_o, the fictitious optical depth at the center of the line. For S-S pure scattering Wrubel uses $\log \tau_o$ as abscissa while Hunger, for S-S pure absorption, uses $\log C$, where $C = \frac{3}{2}\tau_o$ in this case. Hence, Hunger's abscissa differs from that of Wrubel by the additive constant log 3/2.

$$\tau_o = \ell_o \rho H = \frac{\pi^{\frac{1}{2}} e^2 \lambda^2 N_n f_{nj} H}{mc^2 b} , \tag{10}$$

where H is the depth of the reversing layer. Then

$$\log \tau_o = \log N_n H + \log C + \log f_{nj}\lambda + \log c/v . \tag{11}$$

The Idealized Situation

If 1) the atmosphere were built on either the M-E or the S-S model,
2) the temperature and density were constant throughout the atmosphere,
3) turbulence were negligible,
4) the effects of broadening were constant with depth,
5) measurements for many lines from a single level were available,
6) the lines were formed either by pure scattering or pure absorption, and
7) absolute f-values were known,

then 1) the damping constant could be found,
2) the temperature could be determined, and
3) the abundance of the element could be determined,

all from the curve of growth.

For such an idealized situation the procedure, for the S-S pure scattering model for example, would be as follows: plot log W/λ against log $f\lambda$ and superpose this observed curve of growth upon the theoretical curves drawn to the same scale; shift vertically and horizontally with no rotation until the curves are brought into coincidence; obtain log a by noting which theoretical curve best fits the damping portion of the observed curve; from the vertical shift determine log c/v and thus v; from this value of v calculate the kinetic temperature using Equation (3), since $v = v_{th}$ in the absence of turbulence; from the horizontal shift, which gives log $N_n H$ + log C + log c/v, find log $N_n H$.

Departures from the idealized conditions may place severe limitations on the curve of growth technique.

Reduction of Curve of Growth Data

The Boltzmann Equation

In practice, a large number of lines all arising from the same level of excitation usually are not available. Hence, lines arising from different levels are plotted on the same curve of growth. For this purpose the assumption is made that an excitation temperature can be specified so that the distribution of atoms in the various energy levels is given by the Boltzmann equation, i.e.,

$$N_n = \frac{Ng_n}{u} \exp(-\chi_e/kT), \tag{12}$$

where

N = total number of atoms per unit volume of the element in question,

$g_n = 2J + 1$ = statistical weight of level n,

χ_e = excitation potential of level n,

k = Boltzmann's constant,

T = excitation temperature, and

u = the partition function $= \sum g_i w \exp(-\chi_{e,i}/kT)$ summed over all levels in the atom. w is a correction for pressure effects.

By replacing N_n in Equations (8) and (11) by the expression in Equation (12), it follows that

$$\log \eta_o = \log N/\rho\overline{\mu} + \log C + \log g_n f_{nj} \lambda - \log u + \log c/v - \theta\chi_e, \tag{13}$$

and

$$\log \tau_o = \log NH + \log C + \log g_n f_{nj} \lambda - \log u + \log c/v - \theta\chi_e, \tag{14}$$

where $\theta = 5040/T$, if χ_e is expressed in electron volts.

The Method of Analysis

For purposes of the following discussion, let us confine our attention to the application of the S-S pure scattering model to the analysis of the lines belonging to a single element in a particular stage of ionization.

Notice that all the terms on the right-hand side of Equation (14), except log gfλ* and $\theta\chi_e$, are constant for all the lines. For a group of lines that all arise from the same atomic term, χ_e is practically constant; therefore, log gfλ is the only variable quantity involved in the abscissa of a curve of growth limited to such a group. The ordinate of the theoretical curves can be written as

$$\log W/b = \log W/\lambda + \log c/v, \qquad (15)$$

where log c/v is assumed to be constant for all the lines. Hence, plots that can be compared to the theoretical curves can be obtained as follows: all lines arising from the same atomic term are plotted together on transparent paper with log gfλ as abscissa and log W/λ as ordinate.

Each plot obtained in this manner, i.e., by taking the lines in groups corresponding to particular atomic terms, defines a portion of the observed curve of growth. These plots are then superposed upon plots of the theoretical curves, drawn to the same scale, and shifted vertically and horizontally (with no axial rotation) until the best fit is obtained. If enough strong lines are available, a value of log a can be determined by choosing, from among the theoretical curves for various values of log a, the curve that best fits the plots containing the strong lines.

---

*To simplify the notation, the subscripts on g and f will be omitted henceforth.

If plots are available which fit around the knee of the curve of growth, it is possible to obtain log c/v from the vertical shift--since

$$\text{vertical shift} = \log W/b - \log W/\lambda = \log c/v. \qquad (16)$$

It should be noted that the same vertical shift must be used for all plots, since log c/v is assumed to be the same for all the lines.

The horizontal shift yields $\Delta \log X$, where

$$\Delta \log X = \log \tau_o - \log gf\lambda. \qquad (17)$$

Also,

$$\Delta \log X = [\log NH + \log C - \log u + \log c/v] - \theta\chi_e, \qquad (18)$$

which can be seen by referring to Equation (14). In Equation (18), the quantity in brackets is constant for all the lines. Hence, plotting $\Delta \log X$ versus χ_e for each of the different terms should give a straight line with slope equal to $-\theta$. The excitation temperature can be found since $T = 5040/\theta$.

From Equation (18) it is apparent that $\Delta \log X + \theta\chi_e$ is equal to a constant, henceforth called the "shift." Then

$$\text{shift} = \log NH + \log C - \log u + \log c/v. \qquad (19)$$

Consequently, the abundance is given by

$$\log NH = \text{shift} - \log C + \log u - \log c/v. \qquad (20)$$

From the values of the shift and log c/v determined as described above, log NH can be calculated from Equation (20) with the aid of log C, which is a known constant (-12.30), and log u, which has been tabulated by Aller (1960). Since N is the number of atoms per cubic centimeter and H is the depth of the reversing layer, NH is the number of atoms in a one square centimeter column of the reversing layer.

The above discussion describing the application of the S-S pure scattering model can be made valid for the other three models by a few

simple alterations. These changes are outlined in the paragraphs to follow.

The discussion relating to the application of the S-S pure scattering model can be made valid for M-E pure scattering by replacing log gfλ by log gfλ + Δlog η_o, τ_o by η_o, and NH by $N/\rho\overline{\kappa}$. The addition of Δlog η_o to log gfλ takes into account limb darkening effects. As mentioned earlier, Wrubel's curves have been calculated for several values of B^o/B^1, or I^o/I^1, with a separate curve resulting for each value. Since these quantities depend upon the wavelength, and therefore vary from line to line, each line should fit on a different curve of growth. This effect is negligibly small for the S-S pure scattering model and need not be considered. For M-E pure scattering, however, in order to plot all lines on the same curve of growth, say for B^o/B^1 = 2/3, it is necessary to add a quantity, Δlog η_o, to the value of log gfλ for each line. This shifts the abscissa of the line by the proper amount to take into account the limb darkening effect. These limb darkening corrections can be determined by interpolating in the tables published by Wrubel for the case of M-E pure scattering.

Hunger's curves for M-E and S-S pure absorption do not depend upon the limb darkening coefficients. Limb darkening effects are taken into account by the inclusion of R_c in the ordinates. R_c can be calculated for each line from Equation (5), using appropriate values of B^o/B^1. To convert the discussion relating to S-S pure scattering to one applying to M-E and S-S pure absorption proceed as follows: M-E model--replace W by $W/2R_c$, τ_o by η_o, and NH by $N/\rho\overline{\kappa}$; S-S model--replace W by $W/2R_c$, τ_o by $3\tau_o/2$, and "shift" by "shift" + log 3/2. The log 3/2 comes about because the abscissa here is log $3\tau_o/2$, not simply log τ_o.

In the M-E model the abundance of the element is expressed as $N/\rho\overline{\kappa}$. N/ρ is the number of atoms of the element in question per gram of stellar material, and $1/\overline{\kappa}$ is a measure of the number of grams of stellar material in a one square centimeter column of the atmosphere. Hence, $N/\rho\overline{\kappa}$ is a measure of the number of atoms in a one square centimeter column of the atmosphere.

If the element being studied exists in several stages of ionization, then the total abundance is given by the Saha equation. In logarithmic form,

$$\log N_1/N_o = - \log P_e - \theta\chi_i + 2.5 \log T - 0.48 + \log 2u_1/u_o, \quad (21)$$

where χ_i is the ionization potential in electron volts, P_e is the electron pressure in dynes per cm^2, N_1 is the number of singly ionized atoms per cm^3, N_o is the number of neutral atoms per cm^3, u_1 is the partition function of the singly ionized atoms, and u_o is the partition function of the neutral atoms. The equation may be successively applied to include all significant stages of ionization.

Summary of Steps Involved in a Curve of Growth Analysis

1) Obtain spectrograms of the star to be investigated.--It is necessary to use spectra of the highest dispersion possible so that effects of blending will be minimized.

2) From these plates obtain microphotometer tracings.--Microphotometer tracings are plots of the density of the spectral image versus the wavelength.

3) Obtain intensitometer tracings.--The intensitometer converts the density of the image into intensity. Calibration involves the use of sources of known intensity. The central portion of the density-intensity

curve for the plate is used.

At the Dominion Astrophysical Observatory steps two and three were performed separately. At other observatories, Mt. Wilson for example, the two may be combined into a single operation. Line profiles may also be obtained by photoelectric spectrophotometry. The instruments and procedures used in these various techniques have been described by Wright (1962).

4) Draw in the continuum.--The location of the continuum is a great source of error. The continuum can be drawn directly on the intensitometer tracing or first drawn on the microphotometer tracing and then transferred. The procedure employed depends upon which seems to be the most reliable for the wavelength region concerned.

5) Identify the lines and approximate the profiles.--If the apparent line profile is irregular or asymmetric, several tracings may be compared to determine if the variations are real. A possible cause for irregularities and asymmetry is blending. In drawing the profiles these possible effects of blending should be taken into account. Concerning the approximation of the profiles a question arises: should the profiles be drawn so that the wings are inversely proportional to ν^2, as theory indicates, or should the profiles be assumed to be triangular in shape as some workers do? The procedure indicated by theory was followed in this investigation.

6) Determine equivalent widths.--The following steps are needed: a) planimeter the lines to determine the area enclosed by the profile and the continuum, b) measure the height of the continuum, c) measure the dispersion, and d) calculate the equivalent width. Deutsch (1954) has discussed the effect of the finite width of the microphotometer

analyzing slit on the equivalent width. He found that as the slit opening increased so did the measured equivalent width.

7) Bring together lines arising from the same term and plot log W/λ (or log $W/2R_c\lambda$) versus log $gf\lambda$ on transparent paper.--Appropriate limb darkening corrections should be included.

8) Fit these plots to the theoretical curves of growth.--Then, a) the theoretical curve which is best fit by the strong lines gives log a, b) log c/v is obtained from the vertical shift, c) the excitation temperature is found from the slope, determined by the least squares method, of the straight line that best fits the plot of Δlog X versus χ_e, and d) the abundance is determined from the horizontal shift.

Steps 7 and 8 must be repeated for each element and each degree of ionization.

9) Apply the Saha equation to get the total abundance of all observed elements.

CHAPTER III

OBSERVATIONAL MATERIAL

Spectrograms and Tracings

The θ Ursae Majoris spectrograms used in this study were taken at the Cassegrain focus of the 72-inch telescope of the Dominion Astrophysical Observatory by Dr. K. O. Wright. Some representative spectrograms are shown in Plate I.

The dispersion varied, depending upon the spectrograph used. For the Littrow spectrograph with the Wood grating (15,000 lines/inch) the dispersion was approximately 7.5 A/mm for the second order spectra in the range λλ4800-6750; for third order spectra in the range λλ3750-4500, the dispersion was about 4.5 A/mm. When the Bausch and Lomb grating No. 496 (30,000 lines/inch) was used in the second order, the dispersion was about 3.2 A/mm. For the three-prism spectrograph the dispersion varied from about 5 A/mm to 15 A/mm over the wavelength range studied.

The microphotometer and intensitometer tracings were made at Victoria by Dr. Leon W. Schroeder. The magnification of the tracings is 200. Details of the spectrograms and tracings are given in Table I.

Figure 4 is a reproduction of a portion of one of the microphotometer tracings showing the estimated position of the continuum and the profiles of some representative lines.

Plate I

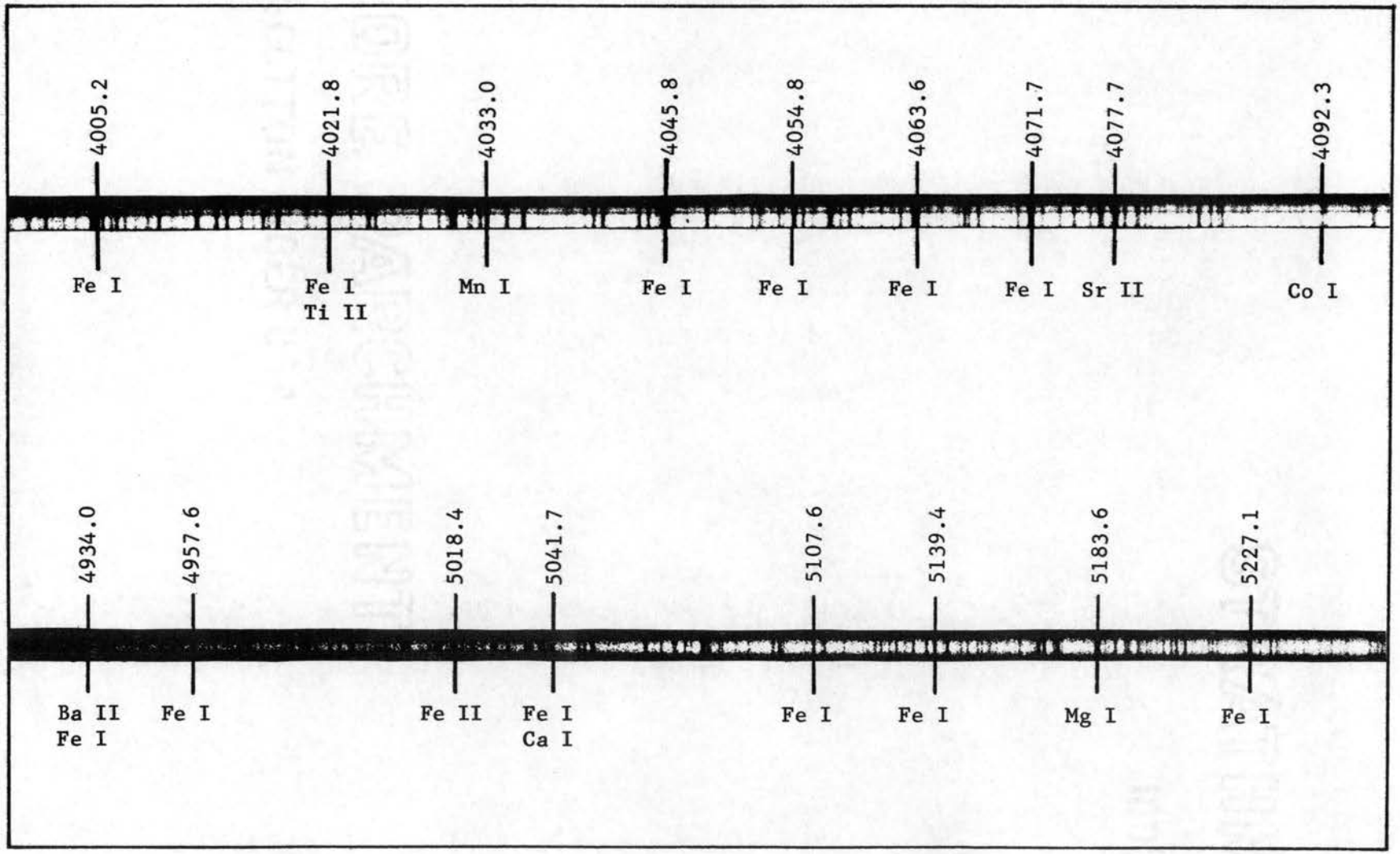

Spectrum of θ Ursae Majoris in the Regions λλ4000-4100 and 4915-5260. Wavelengths and identifications have been marked for representative lines. The spectrogram at the top was made with a grating, while that at the bottom was made with a three prism spectrograph.

TABLE I

VICTORIA PLATE, MICROPHOTOMETER, AND INTENSITOMETER DATA FOR θ URSAE MAJORIS

Victoria Plate Number	Microphotometer & Intensitometer Tracing Number	Spectrograph	Wavelength Range (Angstroms)
55224	1808	Grating*-2nd Order	3900-4080
55053	1828	Grating*-2nd Order	3990-4085
38157	1827	Grating -3rd Order	4000-4210
50092	1797	Prism	4120-4250
55225	1793	Grating*-2nd Order	4180-4315
55054	1811	Grating*-2nd Order	4210-4340
50092	1796	Prism	4250-4580
34599	1807	Grating -3rd Order	4275-4455
55225	1792	Grating*-2nd Order	4300-4480
37112	1914	Grating*-2nd Order	4310-4900
37075	1915	Grating*-2nd Order	4310-4900
55054	1810	Grating*-2nd Order	4335-4495
31421	1799	Prism	4600-5020
38133	1816	Grating -2nd Order	4700-4830
38133	1815	Grating -2nd Order	4825-5180
31421	1798	Prism	5015-5710
37111	1812	Grating -3rd Order	5130-5450
37074	1800	Grating -2nd Order	5160-5450
34800	1814	Grating -2nd Order	5165-5510
36796	1818	Grating -2nd Order	5600-6010
34799	1817	Grating -2nd Order	6000-6325
36795	1819	Grating -2nd Order	6200-6700

*The asterisk refers to grating spectra made with the Bausch and Lomb grating No. 496, or 169 in the cases of plates 37112 and 37075. All other grating spectra were made with the Wood grating. Prism spectrograms were made with the three prism spectrograph.

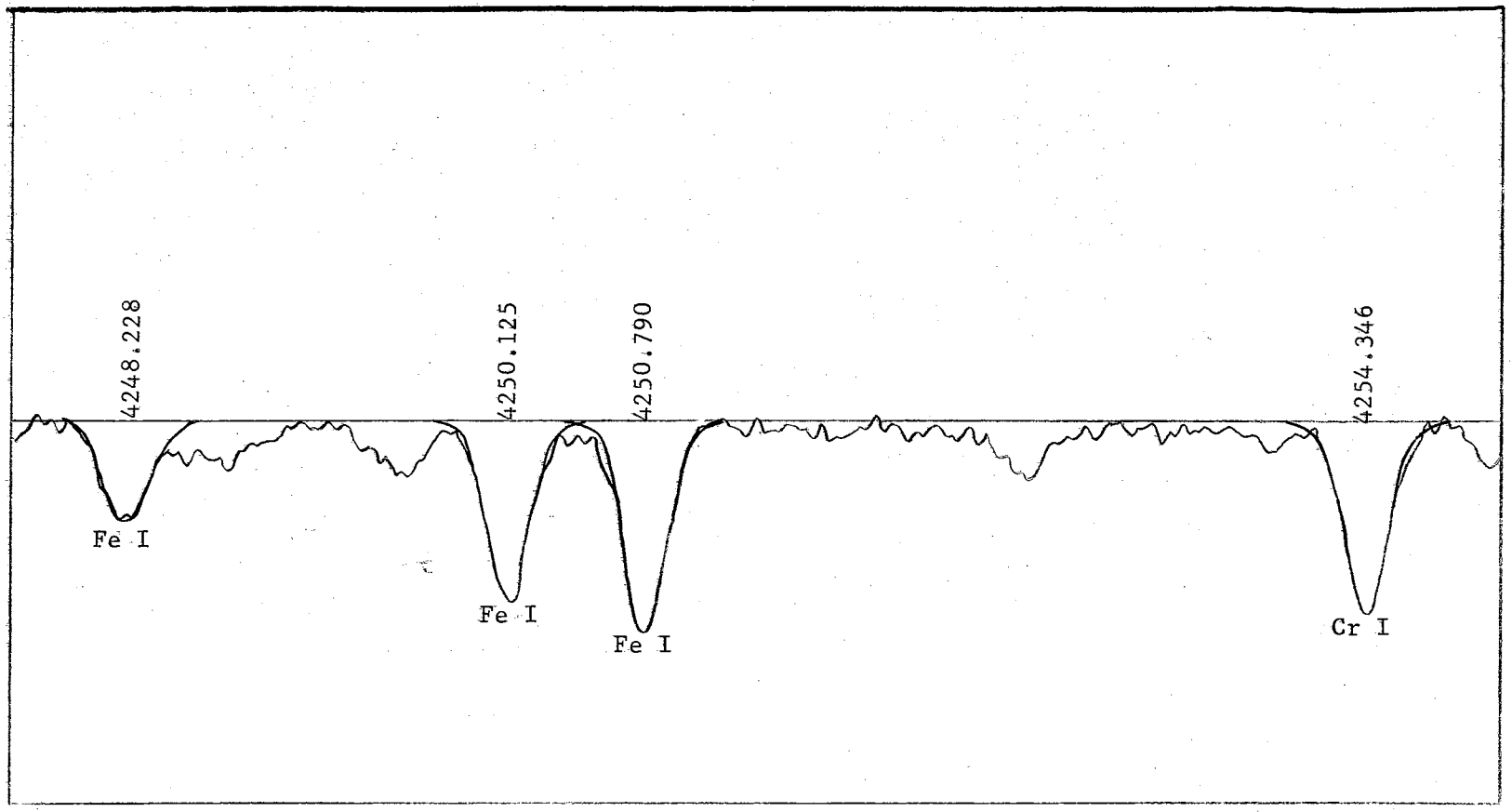

Figure 4. Microphotometer Tracing of the Spectrum of θ Ursae Majoris in the Region λλ4248-4255. A line has been drawn indicating the estimated position of the continuum and four representative profiles are drawn for lines whose equivalent widths were measured. Wavelengths and identifications have been marked.

Location of the Continuum

For the most part, the continuum was drawn directly on the intensitometer tracings as the average of the galvanometer deflections due to plate grain in the regions between the lines. In a few cases, however, the position of the continuum was more apparent on the microphotometer tracing and hence was first drawn there and then transferred to the intensitometer tracing.

Approximation of the Profiles

Theory indicates that the shape of the wings exhibited by the stronger lines should be inversely proportional to the square of ν, the distance from the line center in units of the Doppler width. An attempt was made to take this into account when drawing the profiles of the stronger lines. The shapes of the wings were readily apparent for very strong lines, expecially when there were no nearby lines to produce blending effects in the wings. When blending was serious the wings were roughly approximated.

Identification of the Lines

The lines were identified by referring to the tables published by Swensson (1946) in his paper "The Spectrum of Procyon." Identifications could be made in this way because the spectrum of Procyon (spectral type F5, luminosity class IV) is quite similar to that of θ Ursae Majoris. Also, the θ Ursae Majoris tracings were compared with similar ones for Procyon which were used by Schroeder (1958) in his study of that star. The work by Charlotte E. Moore (1945), A Multiplet Table

of Astrophysical Interest, Revised Edition, was also consulted for purposes of line identification.

Selection of Lines

The selection of lines to be used in this study was based upon the following considerations; effects of blending, the availability of f-values, and the number of lines available for a particular element. These are discussed in detail in the paragraphs to follow.

Effects of Blending

Equivalent widths were measured only for lines which were believed to be substantially free of blending effects in the central portions of the profiles. These effects were tolerated when present in the wings of the strong lines, since this was almost always the case. Decisions as to whether or not blending was serious enough to preclude the use of a line were based upon Swensson's line identifications for Procyon. Any line listed by Swensson as having more than one contributor was discarded. Also, the selected lines were restricted to those with wavelengths greater than 4000 angstroms. To the violet of λ4000 the spectrum is very complex, and many lines in this region are on the broad wings of the H and K lines of ionized calcium.

Availability of f-Values

An extensive bibliography on transition probabilities has been published by Glennon and Wiese (1962). This paper proved to be of valuable assistance in gathering information concerning f-values.

Wright (1948) has pointed out that oscillator strengths measured in the laboratory are more accurate than those calculated theoretically. Corliss and Bozman (1962) have published laboratory absolute f-values for 25,000 lines between 2000 and 9000 angstroms for 112 spectra of 70 elements. Their work was done at the National Bureau of Standards, and henceforth these f-values will be referred to as "NBS f-values." The existence of this extensive work should greatly reduce the use of theoretically calculated f-values in studies of the type presented in this paper. However, some limitations are present in these listings. Due to the relatively low temperature (about 5100^{o}K) of the copper arc used to excite the lines, the weaker lines of several of the spectra, Ti II for example, were not excited sufficiently for measurement. Hence, no f-values are given for these lines. The accuracy of the NBS f-values is admittedly not as great as for f-values measured by more refined and laborious techniques, but the NBS measurements are almost certainly more reliable than theoretical f-values. The principal usefulness of the NBS tables lies in the large number of values made available, the wide range of wavelength covered, and the fact that the scale is absolute.

Tables of laboratory oscillator strengths for Fe I and Ti I have been published by the Kings (1938), for another group of Fe I lines by Carter (1949), and for Cr I by Hill and King (1951). All of these measurements are considered to be quite accurate. These f-values are on relative scales.

All of the above mentioned works were used as sources of f-values, although the NBS tables were the major source. Most of the lines for which f-values are given by the Kings, Carter, and Hill are also included

in the NBS tabulations; but due to the more accurate nature of the measures of the Kings, Carter, and Hill, it was considered advisable to make independent analyses of the curves of growth for Fe I, Ti I, and Cr I using these oscillator strengths. The results obtained for the different sets of f-values could then be compared. Also, the Kings' and Carter's f-values for Fe I were not combined, but were used to derive independent results.

As mentioned above, there was found to be a shortage in the NBS tables of f-values for the weaker lines of Ti II. This was the only ionized element considered suitable for investigation here, and thus offered the only opportunity to compare abundances of the neutral and ionized atoms. To improve the accuracy of the results obtained for Ti II, it was decided to supplement the available data by including a number of weaker lines for which Wright (1948) has tabulated solar log X_f-values. These can be converted to f-values in the manner described in Wright's paper, i.e., by means of the relation

$$\log gf\lambda = \log X_f + 5040\ \chi_e/T, \qquad (22)$$

where χ_e is the excitation potential in electron volts of the lower level of the transition in question, and $T = 4700^{\circ}K$ is a mean value, suggested by Wright, of the excitation temperature for the sun. The application of this equation puts the derived f-values on a relative scale. Values were calculated for ten lines of Ti II which are common to Wright's and the NBS tabulations, and the average value of the differences between these and the corresponding NBS quantities was used to convert to an absolute scale, that of the NBS. Figure 5 compares the derived oscillator strengths (on the absolute scale) with the NBS values for these common lines.

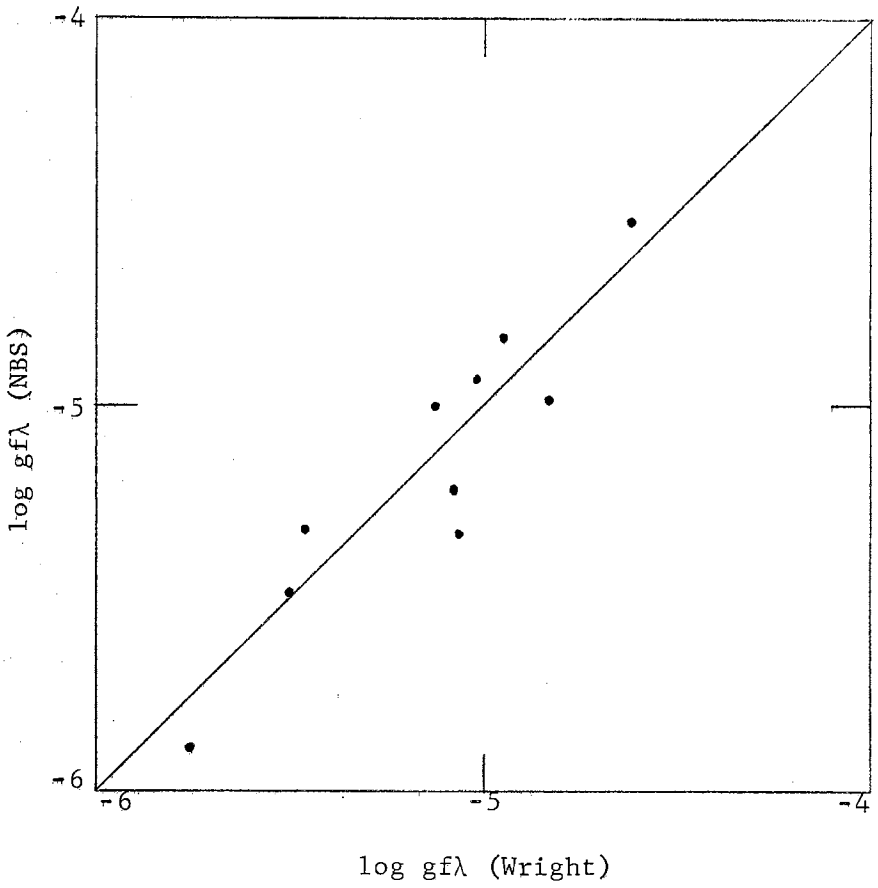

Figure 5. Comparison of Ti II f-Values Derived From Wright's log X_f's With NBS f-Values for Ten Common Lines.

Number of Lines Available for a Particular Element

The reliability of the results obtained by the method of curve of growth analysis employed in this study depends strongly upon the number of lines available for the element being investigated. Hence, it was felt that results derived from only a few lines would be of doubtful value. Of the elements studied, Co I was represented by twelve lines. Elements with fewer lines available were not considered for analysis.

Table II lists the eight atoms and ions studied, the sources providing the f-values, and the number of lines available for each set of f-values.

TABLE II

LIST OF ATOMS AND IONS STUDIED IN THIS INVESTIGATION

Atom or Ion	Source of f-values	No. of Lines	Atom or Ion	Source of f-values	No. of Lines
Ca I	NBS	21	Mn I	NBS	22
Ti I	NBS	55	Fe I	NBS	115
Ti I	King	17	Fe I	King	30
Ti II	NBS & Wright	27	Fe I	Carter	29
Cr I	NBS	65	Co I	NBS	12
Cr I	Hill & King	36	Ni I	NBS	32

Determination of Equivalent Widths

The determination of equivalent widths first involves measurement of the area enclosed by the line profile and the continuum. These areas were obtained using an Ott rolling disc planimeter. Each line was measured twice, each measurement consisting of two circuits of the profile with the planimeter. The continuum height was taken as the average of the values adjacent to the line. For each tracing the dispersion was taken at various points along the spectrum and a straight line fitted to a plot of dispersion against wavelength. For the calculation of equivalent widths the dispersion was then read from these plots. W was calculated in milliangstroms. Due to overlapping and duplication of the spectrograms, some lines were represented by as many as seven profiles, a few by only one. The equivalent width, in all cases, was taken as the average with all measures assigned equal weight. For a representative group of lines, Figure 6 compares the equivalent widths measured on different tracings with the corresponding average values. Every tracing used in this study is represented in this plot by at least one measurement of W.

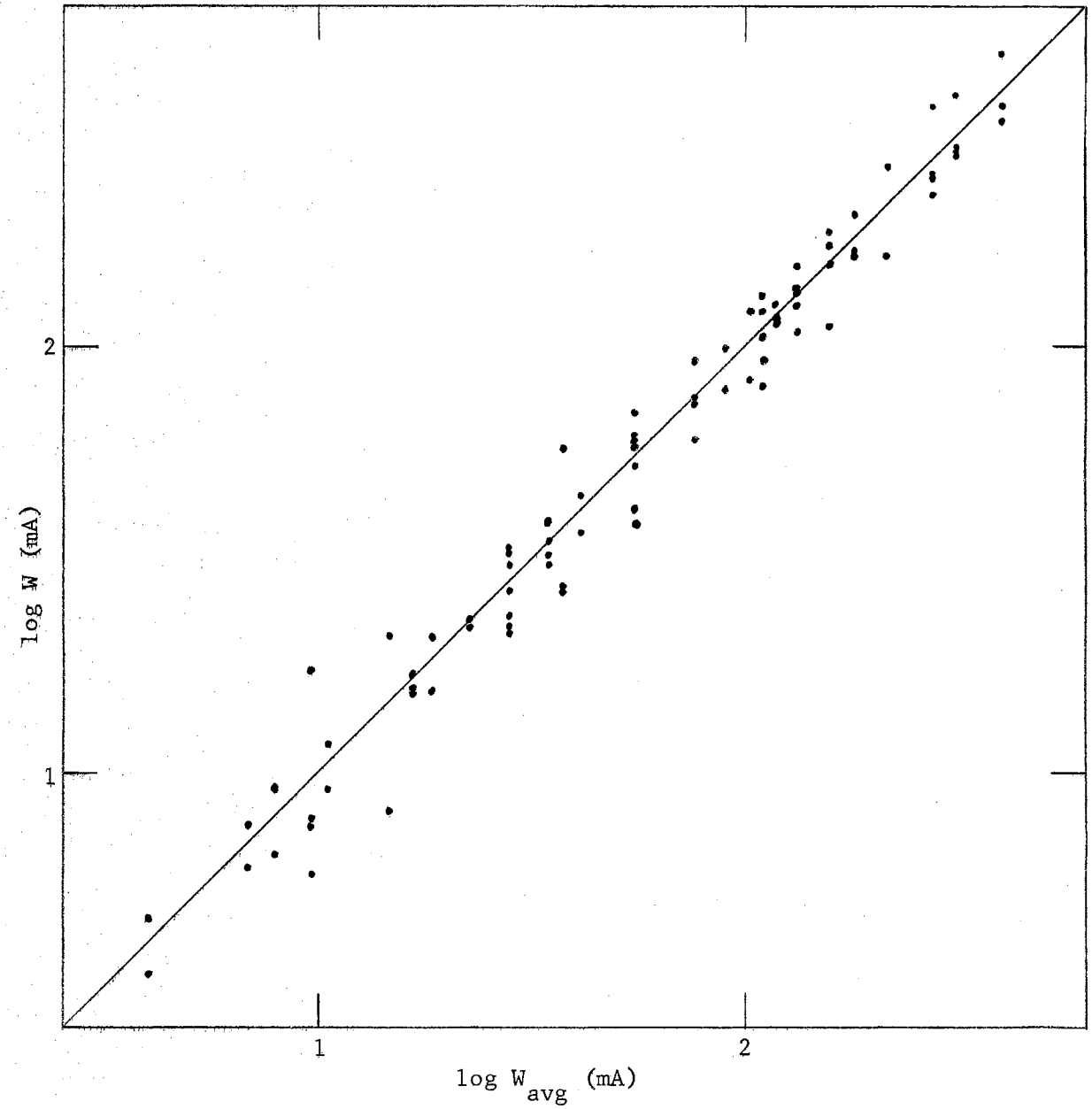

Figure 6. Comparison of Equivalent Widths Measured on Different Tracings With the Average Values for a Representative Group of Lines. The scale is logarithmic with the average values as abscissae and the values obtained from different tracings as ordinates. A set of points forming a vertical array represents the values of W measured for a particular line. The 45-degree line gives the position of the average.

Thackeray's (1936) relation was applied to increase the measured equivalent widths of the lines located in the wings of the Balmer lines. This relation is

$$W = \frac{W_b}{r_w} , \qquad (23)$$

where W_b is the measured equivalent width referred to the wing as the continuum, r_w is the ratio of the intensity of the wing to the intensity of the true continuum at the center of the line being studied, and W is the equivalent width the line would have if no blending occurred. This relation is not exact but should be sufficiently accurate to permit the use of such lines.

Table of Equivalent Width Measures

Equivalent widths obtained in this study are listed in Table III along with other quantities used in the analysis. A section is included for each element studied, and these are arranged according to increasing atomic weight. Within each section the lines are tabulated in the order of increasing wavelength.

Column 1 lists the wavelength in angstroms as given by Miss Moore (1945) in the Revised Multiplet Table (RMT).

Column 2 gives the RMT multiplet number.

Column 3 lists the excitation potential of the lower level of the transition, in electron volts.

Column 4 gives log gfλ, where the wavelength is in centimeters. This column is divided into two sub-columns. The sub-column on the left, headed by "NBS," contains values of log gfλ taken from the NBS tables. The sub-column on the right, headed by "Other," contains

TABLE III

LINE INTENSITIES IN THE SPECTRUM OF θ URSAE MAJORIS

λ RMT	Multiplet RMT	χ_e	log gfλ NBS	log gfλ Other	Number of Measures	W	log $\frac{W}{\lambda}$	Δlog η_o
	Ca I							
4226.728	2	0.00	-4.92		3	400	-4.02	+0.15
4283.010	5	1.88	-4.74		3	119	-4.56	+0.18
4289.364	5	1.87	-4.79		3	114	-4.58	+0.18
4298.986	5	1.88	-4.83		3	137	-4.50	+0.17
4425.441	4	1.87	-4.68		5	132	-4.53	+0.17
4434.960	4	1.88	-4.34		4	167	-4.42	+0.16
4434.688	4	1.88	-4.90		4	134	-4.52	+0.17
4526.935	36	2.70	-5.15		2	69	-4.82	+0.14
4578.558	23	2.51	-5.16		2	80	-4.76	+0.14
5262.244	22	2.51	-4.55		3	119	-4.64	+0.06
5512.979	48	2.92	-4.89		1	106	-4.71	+0.04
5581.971	21	2.51	-4.61		1	79	-4.85	+0.04
5588.757	21	2.51	-3.84		1	177	-4.50	+0.04
5590.120	21	2.51	-4.69		1	66	-4.93	+0.03
5601.285	21	2.51	-4.61		2	123	-4.66	+0.04
6102.722	3	1.87	-4.83		1	121	-4.70	-0.01
6122.219	3	1.88	-4.38		1	173	-4.55	-0.01
6162.172	3	1.89	-4.20		1	183	-4.53	-0.01
6166.443	20	2.51	-4.95		1	36	-5.23	-0.01
6439.073	18	2.51	-3.89		1	181	-4.55	-0.03
6493.780	18	2.51	-4.24		1	121	-4.73	-0.03
	Ti I							
4008.046	187	2.11	-4.23		3	38	-5.03	+0.15
4008.926	12	0.02	-5.18	-2.22	3	108	-4.57	+0.19
4016.264	186	2.13	-4.52		2	7	-5.77	+0.12

TABLE III (Continued)

λ RMT	Multiplet RMT	χ_e	log gfλ NBS	log gfλ Other	Number of Measures	W	log $\frac{W}{\lambda}$	Δlog η_o
	Ti I (Continued)							
4060.263	80	1.05	-4.54		2	15	-5.44	+0.12
4166.311	163	1.87	-4.74		1	8	-5.70	+0.12
4169.330	163	1.88	-4.44		2	6	-5.82	+0.11
4186.119	129	1.50	-4.19		1	21	-5.30	+0.12
4265.723	162	1.87	-4.84		2	4	-6.03	+0.11
4281.371	44	0.81	-5.42		1	7	-5.79	+0.11
4286.006	44	0.82	-4.49	-1.48	4	79	-4.73	+0.17
4287.405	44	0.83	-4.51	-1.48	5	37	-5.06	+0.14
4305.910	44	0.84	-3.65	-0.70	5	200	-4.33	+0.15
4321.655	235	2.23	-3.80		7	28	-5.19	+0.13
4326.359	43	0.82	-5.25		4	15	-5.45	+0.11
4417.274	161	1.88	-4.09		6	14	-5.51	+0.11
4427.098	128	1.50	-3.85		1	14	-5.49	+0.11
4453.708	160	1.87	-3.99		4	19	-5.38	+0.11
4465.807	146	1.73	-4.12		4	18	-5.41	+0.11
4518.022	42	0.82	-4.49	-1.47	4	59	-4.88	+0.14
4533.238	42	0.84	-3.70	-0.64	4	151	-4.48	+0.15
4534.782	42	0.83	-3.93	-0.80	4	108	-4.62	+0.15
4548.764	42	0.82	-4.52		2	42	-5.03	+0.12
4555.486	42	0.84	-4.62	-1.60	4	66	-4.84	+0.14
4617.269	145	1.74	-3.63	-0.80	3	44	-5.02	+0.11
4623.098	145	1.73	-3.94		2	22	-5.33	+0.09
4639.369	145	1.73	-4.24		2	19	-5.39	+0.09
4639.669	145	1.74	-4.27		2	11	-5.65	+0.09
4645.193	145	1.73	-4.46		2	15	-5.51	+0.09
4656.468	6	0.00	-5.48	-2.49	4	38	-5.08	+0.11
4681.908	6	0.05	-5.32	-2.21	4	92	-4.71	+0.13
4758.120	233	2.24	-3.61		3	22	-5.33	+0.08

TABLE III (Continued)

λ RMT	Multiplet RMT	χ_e	log gfλ NBS	log gfλ Other	Number of Measures	W	log $\frac{W}{\lambda}$	Δlog η_o
	Ti I (Continued)							
4759.272	233	2.25	-3.60		3	25	-5.27	+0.09
4799.797	242	2.26	-4.05		3	30	-5.21	+0.08
4805.416	260	2.33	-3.97		3	12	-5.62	+0.08
4820.410	126	1.50	-4.55		2	19	-5.42	+0.07
4840.874	53	0.90	-4.79		3	23	-5.33	+0.07
4913.616	157	1.87	-3.98		1	18	-5.45	+0.07
4919.867	200	2.15	-4.10		1	11	-5.64	+0.07
4981.732	38	0.84	-3.73	-0.59	2	123	-4.61	+0.09
5016.162	38	0.84	-4.74	-1.64	2	54	-4.97	+0.07
5024.842	38	0.81	-4.77	-1.69	2	74	-4.83	+0.08
5025.570	173	2.03	-3.86		2	41	-5.09	+0.07
5039.959	5	0.02	-5.26	-2.17	2	66	-4.88	+0.07
5043.578	38	0.83	-5.60		2	14	-5.55	+0.06
5152.185	4	0.02	-6.02		1	11	-5.67	+0.05
5173.742	4	0.00	-5.35	-2.16	5	74	-4.84	+0.06
5194.043	183	2.09	-4.36		2	8	-5.86	+0.05
5201.096	183	2.08	-4.50		1	8	-5.83	+0.05
5210.386	4	0.05	-5.18	-1.90	4	62	-4.93	+0.06
5224.301	183	2.13	-3.86		2	18	-5.46	+0.05
5689.465	249	2.29	-4.16		1	12	-5.68	+0.02
5713.895	249	2.28	-4.53		1	13	-5.65	+0.02
5766.330	309	3.28	-3.44		1	14	-5.60	+0.01
5866.453	72	1.06	-4.77		1	14	-5.62	+0.01
5918.548	71	1.06	-5.31		1	14	-5.61	+0.01
	Ti II							
4300.052	41	1.18	-4.92		4	218	-4.30	+0.15
4301.928	41	1.16	-5.32		4	152	-4.45	+0.16

TABLE III (Continued)

λ RMT	Multiplet RMT	χ_e	log gfλ NBS	log gfλ Other	Number of Measures	W	log $\frac{W}{\lambda}$	Δlog η_o
	Ti II (Continued)							
4312.861	41	1.18	-5.31		7	176	-4.39	+0.16
4316.807	94	2.04		-5.94	7	55	-4.90	+0.15
4337.916	20	1.08	-5.14		6	159*	-4.44	+0.16
4344.291	20	1.08	-5.95		4	104*	-4.62	+0.18
4394.057	51	1.22		-5.90	6	110	-4.60	+0.18
4395.031	19	1.08	-4.82		6	223	-4.29	+0.15
4395.848	61	1.24		-6.37	6	87	-4.71	+0.17
4409.519	61	1.23		-6.96	2	37	-5.08	+0.13
4417.718	40	1.16	-5.48		6	129	-4.53	+0.17
4421.949	93	2.05		-5.92	6	63	-4.85	+0.16
4443.802	19	1.08	-5.00		5	173	-4.41	+0.16
4450.487	19	1.08	-5.88		5	137	-4.51	+0.17
4468.493	31	1.13	-4.93		5	189	-4.37	+0.15
4533.966	50	1.23	-4.84		3	253	-4.25	+0.13
4563.761	50	1.22	-5.21		3	194	-4.37	+0.14
4568.312	60	1.22		-7.20	2	46	-5.00	+0.12
4571.971	82	1.56	-4.52		3	245	-4.27	+0.13
4708.663	49	1.23		-6.80	2	68	-4.84	+0.12
4779.986	92	2.04		-5.94	3	84	-4.76	+0.11
4805.105	92	2.05	-4.98		2	155	-4.49	+0.11
5129.143	86	1.88	-5.12		2	137	-4.57	+0.07
5185.90	86	1.88		-5.88	4	76	-4.83	+0.06
5336.809	69	1.57	-5.52		4	85	-4.80	+0.06
5381.020	69	1.56		-6.57	3	72	-4.88	+0.05
5418.802	69	1.57		-6.61	3	59	-4.96	+0.04

TABLE III (Continued)

λ RMT	Multiplet RMT	χ_e	log gfλ NBS	log gfλ Other	Number of Measures	W	log $\frac{W}{\lambda}$	Δlog η_o
	Cr I							
4001.444	268	3.87	-3.35		2	36	-5.04	+0.15
4022.263	268	3.87	-3.61		3	15	-5.42	+0.12
4039.100	251	3.83	-3.26		2	29	-5.15	+0.13
4065.716	279	4.09	-4.75		1	6	-5.85	+0.12
4120.613	65	2.70	-4.60	-0.57	1	16	-5.40	+0.12
4126.521	35	2.53	-4.24	-0.51	2	15	-5.43	+0.12
4197.234	249	3.83	-3.90		3	11	-5.58	+0.12
4208.357	249	3.83	-3.96		1	4	-6.03	+0.11
4209.368	248	3.83	-3.49		1	15	-5.45	+0.12
4211.349	133	3.00	-4.36		2	11	-5.60	+0.12
4254.346	1	0.00	-4.64	-1.37	3	180	-4.37	+0.16
4272.910	96	2.89	-4.46	-0.61	3	16	-5.42	+0.11
4274.803	1	0.00	-4.76	-1.47	3	172	-4.40	+0.16
4289.721	1	0.00	-4.95	-1.61	4	219	-4.29	+0.15
4337.566	22	0.96	-5.12	-1.80	6	93*	-4.67	+0.17
4339.450	22	0.98	-4.94		4	54*	-4.90	+0.15
4339.718	22	0.96	-5.43		4	25*	-5.23	+0.13
4344.507	22	1.00	-4.69	-1.43	2	97*	-4.65	+0.18
4346.833	104	2.97	-4.16	-0.27	5	29*	-5.18	+0.13
4351.051	22	0.96	-5.43		2	48	-4.96	+0.14
4373.254	22	0.98	-6.15		4	10	-5.66	+0.11
4381.112	64	2.70	-4.62	-0.68	1	5	-5.93	+0.10
4384.977	22	1.03	-5.24		3	46	-4.98	+0.14
4387.496	103	2.99	-4.25	-0.41	4	37	-5.08	+0.13
4410.304	129	3.00	-4.63		2	7	-5.79	+0.11
4412.250	22	1.03	-6.42		4	12	-5.57	+0.11
4458.538	127	3.00	-3.98	-0.21	3	35	-5.10	+0.12

TABLE III (Continued)

λ RMT	Multiplet RMT	χ_e	log gfλ NBS	log gfλ Other	Number of Measures	W	log $\frac{W}{\lambda}$	$\Delta \log \eta_o$
	Cr I (Continued)							
4511.903	150	3.07	-3.98	+0.01	4	37	-5.09	+0.12
4535.146	33	2.53	-4.82		2	15	-5.50	+0.10
4545.956	10	0.94	-5.31	-1.99	4	84	-4.73	+0.14
4591.394	21	0.96	-5.52	-2.27	5	58	-4.90	+0.12
4600.752	21	1.00	-5.36	-1.85	5	86	-4.73	+0.13
4616.137	21	0.98	-5.29	-1.90	4	70	-4.82	+0.13
4626.188	21	0.96	-5.33	-1.89	4	65	-4.85	+0.13
4639.538	186	3.10	-4.27		1	35	-5.12	+0.10
4646.174	21	1.03	-4.82	-1.45	4	132	-4.55	+0.14
4649.461	32	2.53	-4.97		2	15	-5.49	+0.09
4651.285	21	0.98	-5.30	-2.00	4	61	-4.88	+0.12
4652.158	21	1.00	-5.12	-1.54	4	76	-4.79	+0.13
4708.040	186	3.15	-3.63	+0.35	5	40	-5.08	+0.10
4718.429	186	3.18	-3.51	+0.36	5	56	-4.93	+0.11
4724.416	145	3.07	-4.31		2	12	-5.58	+0.08
4730.711	145	3.07	-3.94		2	29	-5.21	+0.09
4745.308	61	2.70	-5.09		2	11	-5.66	+0.08
4756.113	145	3.09	-3.45	+0.41	5	55	-4.94	+0.10
4764.294	231	3.54	-3.94		2	24	-5.30	+0.09
4836.857	144	3.09	-4.85		3	13	-5.56	+0.07
4922.267	143	3.09	-3.60	+0.18	2	156	-4.50	+0.10
4936.334	166	3.10	-3.98	-0.20	2	41	-5.08	+0.07
4954.811	166	3.11	-3.97	-0.20	2	60	-4.92	+0.08
4964.928	9	0.94	-6.60		1	30	-5.22	+0.07
5110.751	60	2.70	-4.96		2	11	-5.66	+0.05
5206.039	7	0.94	-4.27	-0.83	4	164	-4.50	+0.07
5238.971	59	2.70	-4.17		1	20	-5.43	+0.05
5243.395	201	3.38	-4.29		4	27	-5.28	+0.05
5247.564	18	0.96	-5.72	-2.29	4	55	-4.98	+0.06
5296.686	18	0.98	-5.64	-2.06	4	76	-4.84	+0.06
5297.360	94	2.89	-4.42	+0.03	4	82	-4.81	+0.06

TABLE III (Continued)

λ RMT	Multiplet RMT	χ_e	log gfλ NBS	log gfλ Other	Number of Measures	W	log $\frac{W}{\lambda}$	Δlog η_o
	Cr I (Continued)							
5298.269	18	0.98	-5.35	-1.85	4	146	-4.56	+0.06
5329.12	94	2.90	-4.40	-0.12	4	57	-4.97	+0.05
5345.807	18	1.00	-5.25	-1.66	4	84	-4.80	+0.06
5348.319	18	1.00	-5.56	-1.84	4	55	-4.99	+0.05
5390.394	191	3.35	-4.83		3	26	-5.31	+0.03
5409.791	18	1.03	-4.97	-1.38	3	119	-4.66	+0.05
5712.778	119	3.00	-4.81		1	9	-5.79	+0.02
	Mn I							
4018.102	5	2.11	-4.05		4	143	-4.45	+0.18
4030.755	2	0.00	-4.87		4	286	-4.15	+0.15
4033.073	2	0.00	-5.03		4	225	-4.25	+0.15
4034.490	2	0.00	-5.27		4	181	-4.35	+0.16
4055.543	5	2.13	-3.92		3	113	-4.56	+0.19
4059.392	29	3.06	-4.17		2	31	-5.12	+0.14
4070.279	5	2.18	-4.69		4	33	-5.09	+0.14
4079.422	5	2.18	-4.29		2	87	-4.67	+0.18
4082.944	5	2.17	-4.14		3	55	-4.87	+0.16
4257.659	23	2.94	-3.98		3	15	-5.46	+0.12
4265.924	23	2.93	-4.00		2	23	-5.27	+0.12
4453.005	22	2.93	-4.29		2	18	-5.39	+0.11
4457.045	28	3.06	-4.65		2	11	-5.59	+0.11
4470.138	22	2.93	-4.20		4	23	-5.29	+0.11
4502.220	22	2.91	-4.17		3	28	-5.21	+0.11
4709.715	21	2.88	-4.38		4	30	-5.19	+0.10
4739.108	21	2.93	-4.44		4	25	-5.28	+0.09
4754.042	16	2.27	-4.19		4	129	-4.57	+0.12
4765.859	21	2.93	-4.07		3	67	-4.07	+0.11

TABLE III (Continued)

λ RMT	Multiplet RMT	χ_e	log gfλ NBS	log gfλ Other	Number of Measures	W	log $\frac{W}{\lambda}$	Δlog η_o
	Mn I (Continued)							
4766.430	21	2.91	-3.87		4	85	-4.75	+0.11
4783.420	16	2.29	-4.21		4	158	-4.48	+0.11
4823.516	16	2.31	-4.17		4	180	-4.43	+0.11
	Fe I							
4005.246	43	1.55	-4.46	-1.32	3	284	-4.15	+0.15
4009.714	72	2.21	-4.86		3	103	-4.59	+0.19
4045.815	43	1.48	-3.67	-0.62	4	558	-3.86	+0.15
4062.446	359	2.83	-4.33		3	98	-4.62	+0.19
4063.597	43	1.55	-4.00	-0.76	4	372	-4.04	+0.15
4071.740	43	1.60	-4.03	-0.81	4	329	-4.09	+0.15
4107.492	354	2.82	-4.23		2	85*	-4.68	+0.18
4134.681	357	2.82	-4.23		1	123	-4.53	+0.18
4143.871	43	1.55	-4.50	-1.24	2	265	-4.19	+0.15
4147.673	42	1.48	-5.87		1	103	-4.60	+0.19
4154.502	355	2.82	-4.24		1	123	-4.53	+0.18
4175.640	354	2.83	-4.29		3	102	-4.61	+0.18
4181.758	354	2.82	-3.95		3	154	-4.43	+0.17
4187.044	152	2.44	-4.12		3	129	-4.51	+0.18
4187.802	152	2.41	-4.15		2	180	-4.37	+0.16
4191.436	152	2.46	-4.32		2	150	-4.45	+0.17
4199.098	522	3.03	-3.56		3	133	-4.50	+0.18
4202.031	42	1.48	-4.67	-1.43	3	228	-4.27	+0.15
4206.702	3	0.05		-4.60	3	116	-4.56	+0.17
4216.186	3	0.00	-7.47	-4.05	3	137	-4.49	+0.18
4219.364	800	3.56	-3.51	-3.70C	3	141	-4.48	+0.17
4222.219	152	2.44	-4.64	-4.99C	3	120	-4.55	+0.18
4227.434	693	3.32	-3.37	-3.76C	3	231	-4.26	+0.15

TABLE III (Continued)

λ RMT	Multiplet RMT	χ_e	log gfλ NBS	log gfλ Other	Number of Measures	W	log $\frac{W}{\lambda}$	Δlog η_o
	Fe I (Continued)							
4233.608	152	2.47	-4.17	-4.66C	3	140	-4.48	+0.17
4235.942	152	2.41	-4.04	-4.44C	3	207	-4.31	+0.16
4238.816	693	3.38	-3.97	-4.06C	3	139	-4.48	+0.17
4247.432	693	3.35	-3.98	-4.11C	3	154	-4.44	+0.17
4248.228	482	3.06		-4.44C	3	93	-4.66	+0.18
4250.125	152	2.46	-4.15	-4.60C	3	156	-4.43	+0.17
4250.790	42	1.55	-4.75	-1.43	3	177	-4.38	+0.16
4260.479	152	2.39	-3.75	-4.19C	2	223	-4.28	+0.15
4271.159	152	2.44	-4.18	-4.48C	3	184	-4.37	+0.16
4271.764	42	1.48	-4.21	-0.98	3	276	-4.19	+0.15
4282.406	71	2.17	-4.63	-4.74C	4	144	-4.47	+0.17
4291.466	3	0.05		-4.71	4	89	-4.68	+0.17
4325.765	42	1.60	-4.12	-0.78	4	372	-4.07	+0.14
4337.049	41	1.55	-5.55	-2.25	4	158*	-4.44	+0.17
4352.737	71	2.21	-4.90		6	159	-4.44	+0.16
4369.774	518	3.03	-4.55		5	131	-4.52	+0.17
4375.932	2	0.00	-6.93	-3.72	4	139	-4.50	+0.17
4383.547	41	1.48	-4.01	-0.60	4	397	-4.04	+0.14
4389.244	2	0.05		-4.98	4	44	-5.00	+0.14
4404.752	41	1.55	-4.25	-0.88	4	313	-4.15	+0.14
4415.125	41	1.60	-4.45	-1.36	4	276	-4.20	+0.14
4427.312	2	0.05	-6.89	-3.72	4	156	-4.45	+0.16
4430.618	68	2.21		-6.74C	4	118	-4.57	+0.17
4442.343	68	2.19	-4.85	-5.28C	3	138	-4.51	+0.17
4443.197	350	2.85	-4.59	-3.99C	3	120	-4.57	+0.17
4447.722	68	2.21	-4.83	-5.23C	3	134	-4.52	+0.17
4454.383	350	2.82		-4.69C	3	109	-4.61	+0.17
4461.654	2	0.09	-7.16	-3.89	3	197	-4.36	+0.16

TABLE III (Continued)

λ RMT	Multiplet RMT	χ_e	log gfλ NBS	log gfλ Other	Number of Measures	W	log $\frac{W}{\lambda}$	Δlog η_o
	Fe I (Continued)							
4466.554	350	2.82	-4.15		3	152	-4.47	+0.16
4489.741	2	0.12		-4.55	3	113	-4.60	+0.16
4494.568	68	2.19	-4.79	-4.99C	1	161	-4.45	+0.15
4531.152	39	1.48	-5.97	-6.09C	1	265	-4.23	+0.13
4602.944	39	1.48	-5.89	-2.26	2	119	-4.59	+0.14
4736.780	554	3.20	-4.40		3	137	-4.54	+0.12
4859.748	318	2.86	-4.66		4	145*	-4.53	+0.10
4871.323	318	2.85	-4.19		4	195*	-4.40	+0.10
4872.144	318	2.87	-4.41		4	191*	-4.41	+0.10
4890.762	318	2.86	-4.42		4	193	-4.40	+0.10
4891.496	318	2.84	-4.09		4	235	-4.32	+0.09
4918.999	318	2.85	-4.28		2	203	-4.38	+0.09
4920.509	318	2.82	-3.94		2	269	-4.26	+0.08
5001.871	965	3.86	-4.06		2	170	-4.47	+0.08
5005.720	984	3.87	-4.14		1	145	-4.54	+0.09
5006.126	318	2.82	-4.63		1	145	-4.54	+0.09
5049.825	114	2.27	-5.28		2	144	-4.54	+0.08
5051.636	16	0.91	-6.93		2	155	-4.51	+0.08
5068.774	383	2.93	-4.93		2	117	-4.64	+0.08
5083.342	16	0.95	-6.98		2	119	-4.63	+0.08
5110.414	1	0.00	-7.54	-4.41	2	161	-4.50	+0.08
5133.692	1092	4.16	-3.58		3	142	-4.56	+0.07
5191.460	383	3.03	-4.24	-4.63C	4	152	-4.53	+0.07
5192.350	383	2.99	-4.10	-4.46C	4	145	-4.55	+0.07
5194.943	36	1.55	-5.83	-6.30C	4	106	-4.69	+0.07
5216.278	36	1.60	-5.86	-6.28C	4	122	-4.63	+0.07
5225.533	1	0.11		-9.03C	1	59	-4.95	+0.06
5232.946	383	2.93	-3.91	-4.29C	4	194	-4.43	+0.06

TABLE III (Continued)

λ RMT	Multiplet RMT	χ_e	log gfλ NBS	log gfλ Other	Number of Measures	W	$\log \frac{W}{\lambda}$	$\Delta \log \eta_o$
	Fe I (Continued)							
5250.650	66	2.19		-6.23C	4	82	-4.81	+0.06
5266.562	383	2.99	-4.20	-4.61C	4	142	-4.57	+0.06
5269.541	15	0.86	-5.67	-2.05	4	202	-4.42	+0.06
5281.796	383	3.03	-4.56		4	106	-4.70	+0.06
5283.628	553	3.23	-4.06		3	161	-4.52	+0.06
5307.365	36	1.60		-7.10C	4	75	-4.85	+0.06
5324.185	553	3.20	-3.84	-4.15C	4	167	-4.50	+0.06
5328.042	15	0.91	-5.70	-2.19	4	265	-4.30	+0.06
5339.935	553	3.25	-4.49		4	102	-4.72	+0.06
5364.874	1146	4.43	-3.75		3	92	-4.77	+0.06
5367.470	1146	4.40	-3.70		3	95	-4.75	+0.06
5369.965	1146	4.35	-3.56		3	117	-4.66	+0.06
5383.374	1146	4.29	-3.41		3	136	-4.60	+0.06
5393.174	553	3.23	-4.37		3	109	-4.69	+0.05
5397.131	15	0.91	-6.12	-2.66	3	170	-4.50	+0.05
5404.144	1165	4.42	-3.29		3	183	-4.47	+0.05
5405.778	15	0.99	-6.05	-2.50	3	167	-4.51	+0.05
5410.913	1165	4.45	-3.56		3	107	-4.70	+0.05
5424.072	1146	4.30	-3.34		3	156	-4.54	+0.05
5429.699	15	0.95	-6.03	-2.56	3	228	-4.38	+0.05
5434.527	15	1.01	-6.17	-2.73	3	160	-4.53	+0.05
5445.045	1163	4.37	-3.81		3	103	-4.72	+0.05
5446.920	15	0.99	-6.12	-2.63	3	222	-4.39	+0.05
5497.519	15	1.01	-6.68		2	174	-4.50	+0.05
5501.469	15	0.95	-6.93		2	146	-4.58	+0.05
5506.782	15	0.99	-6.60		1	154	-4.55	+0.05
5569.625	686	3.40	-4.21		1	124	-4.65	+0.04
5572.849	686	3.38	-4.05		1	146	-4.58	+0.04

TABLE III (Continued)

λ RMT	Multiplet RMT	χ_e	log gfλ NBS	log gfλ Other	Number of Measures	W	log $\frac{W}{\lambda}$	Δlog η_o
	Fe I (Continued)							
5576.097	686	3.42	-4.65		1	86	-4.81	+0.04
5586.763	686	3.35	-3.96		1	193	-4.46	+0.03
5615.652	686	3.32	-3.90		2	215	-4.42	+0.03
5762.992	1107	4.19	-4.05		1	113	-4.71	+0.03
6024.066	1178	4.53	-3.79		1	76	-4.90	0.00
6065.487	207	2.60	-5.26		1	99	-4.79	0.00
6137.696	207	2.58	-5.06		1	114	-4.73	-0.01
6230.728	207	2.55	-5.10		2	134	-4.67	-0.01
6246.334	816	3.59	-4.52		2	77	-4.91	-0.01
6252.561	169	2.39	-5.47		2	108	-4.76	-0.01
6265.140	62	2.17	-6.07		2	64	-4.99	-0.01
6301.515	816	3.64	-4.54		2	103	-4.79	-0.02
6318.022	168	2.44	-5.81		2	79	-4.90	-0.02
6393.605	168	2.42	-5.52		1	117	-4.74	-0.02
6411.658	816	3.64	-4.32		1	124	-4.71	-0.02
6421.355	111	2.27	-5.77		1	93	-4.84	-0.02
6430.851	62	2.17	-5.78		1	93	-4.84	-0.02
6494.985	168	2.39	-5.08		1	129	-4.70	-0.03
	Co I							
4020.898	16	0.43	-5.98		3	29	-5.14	+0.14
4092.386	29	0.92	-5.13		2	112*	-4.56	+0.19
4110.532	29	1.04	-5.19		2	38*	-5.04	+0.15
4121.318	28	0.92	-4.41		2	90	-4.66	+0.18
4517.094	150	3.11	-4.42		2	23	-5.29	+0.11
4693.190	156	3.22	-4.01		2	18	-5.48	+0.09
4727.936	15	0.43	-7.48		2	14	-5.54	+0.08
5156.366	180	4.04	-3.70		1	50	-5.01	+0.06

TABLE III (Continued)

λ RMT	Multiplet RMT	χ_e	log gfλ NBS	log gfλ Other	Number of Measures	W	log $\frac{W}{\lambda}$	$\Delta \log \eta_o$
	Co I (Continued)							
5212.699	170	3.50	-3.57		1	15	-5.54	+0.05
5342.703	190	4.00	-3.22		2	9	-5.77	+0.04
5343.383	190	4.01	-3.52		3	24	-5.34	+0.04
5369.591	39	1.73	-5.52		1	17	-5.51	+0.04
	Ni I							
4462.460	86	3.45	-4.12		3	57	-4.89	+0.15
4470.483	86	3.38	-3.68		3	67	-4.82	+0.15
4604.994	98	3.47	-3.57		2	72	-4.81	+0.13
4606.231	100	3.58	-4.04		2	23	-5.31	+0.09
4648.659	98	3.40	-3.55		3	75	-4.79	+0.13
4686.218	98	3.58	-3.94		2	35	-5.13	+0.10
4714.421	98	3.37	-3.49		4	136	-4.54	+0.13
4715.778	98	3.53	-4.07		4	53	-4.95	+0.10
4756.519	98	3.47	-3.93		4	67	-4.85	+0.11
4806.996	163	3.66	-3.98		4	35	-5.14	+0.09
4829.028	131	3.53	-4.07		4	99	-4.69	+0.11
4866.267	111	3.52	-3.89		4	66*	-4.87	+0.09
4873.437	111	3.68	-4.06		4	52*	-4.97	+0.09
4904.413	129	3.53	-3.83		3	58	-4.93	+0.08
4918.363	177	3.82	-3.88		2	51	-4.98	+0.08
4935.830	177	3.92	-4.05		2	26	-5.27	+0.07
4980.161	112	3.59	-3.78		2	96	-4.71	+0.09
4984.126	143	3.78	-3.66		1	91	-4.74	+0.09
5000.335	145	3.62	-4.23		1	78	-4.81	+0.08
5012.464	111	3.68	-4.12		2	55	-4.96	+0.07
5017.591	111	3.52	-3.77		2	97	-4.71	+0.08
5035.374	143	3.62	-3.40		2	85	-4.77	+0.08

TABLE III (Continued)

λ RMT	Multiplet RMT	χ_e	log gfλ NBS	log gfλ Other	Number of Measures	W	log $\frac{W}{\lambda}$	Δlog η_o
	Ni I (Continued)							
5080.523	143	3.64	-3.38		2	102	-4.70	+0.08
5081.111	194	3.83	-3.47		2	67	-4.88	+0.07
5084.081	162	3.66	-3.97		2	73	-4.85	+0.07
5099.946	161	3.66	-3.97		2	78	-4.82	+0.07
5115.397	177	3.82	-3.97		2	65	-4.90	+0.07
5146.478	162	3.69	-3.78		3	100	-4.71	+0.07
5155.764	210	3.88	-3.66		3	65	-4.90	+0.06
5176.565	209	3.88	-4.14		5	33	-5.19	+0.05
5578.734	47	1.67	-6.55		1	27	-5.32	+0.02
5592.283	69	1.94	-5.98		1	22	-5.41	+0.02

values of log gfλ from other sources; for Ti I the values in this sub-column are taken from the Kings' tables, for Ti II the values are from Wright, for Cr I the values are from Hill and King, and for Fe I the values are from the Kings' tables and Carter's tables. Carter's values are followed by the letter "C" so that values from the two sources may be distinguished.

Column 5 lists the number of profiles measured for the line.

Column 6 gives the equivalent width in milliangstroms. Equivalent widths of lines found in the wings of the Balmer lines have been corrected according to Thackeray's relation and are indicated by an asterisk. Data pertinent to these lines are listed in Table IV.

Column 7 gives log W/λ, where W and λ have the same units.

Column 8 lists the value of the limb darkening correction, $\Delta\log \eta_o$, for the Milne-Eddington pure scattering model. Such corrections can be obtained by interpolating in the published curve of growth tables. The addition of $\Delta\log \eta_o$ to the abscissa of each line accounts for differences in limb darkening (which depends upon the wavelength) and makes possible the fitting of all lines to a theoretical curve of growth calculated for a single value of B^o/B^1, here taken to be 2/3.

$\Delta\log \eta_o$ is a function of B^o/B^1. Hence, to determine $\Delta\log \eta_o$ for a given line, it is necessary to know the value of B^o/B^1 corresponding to the wavelength of the line. It was assumed that the values of B^o/B^1 for θ Ursae Majoris are approximately the same as for the sun, where the source of continuous opacity is the negative hydrogen ion. This seems to be a valid assumption, inasmuch as the temperature of θ Ursae Majoris is only slightly higher than that of the sun and is certainly much too low for neutral hydrogen and helium to play a

TABLE IV

DATA PERTINENT TO LINES LOCATED ON WINGS OF HYDROGEN LINES

λ(A)	Element	Wing Location	r_w	W(mA) Observed	W(mA) Corrected
4092.386	Co I	Hδ	0.904	102	112
4107.492	Fe I	Hδ	0.832	71	85
4110.532	Co I	Hδ	0.891	34	38
4337.049	Fe I	Hγ	0.808	127	158
4337.566	Cr I	Hγ	0.769	71	93
4337.916	Ti II	Hγ	0.739	117	159
4339.450	Cr I	Hγ	0.561	30	54
4339.718	Cr I	Hγ	0.519	13	25
4344.291	Ti II	Hγ	0.811	84	104
4344.507	Cr I	Hγ	0.832	81	97
4346.833	Cr I	Hγ	0.899	26	29
4859.748	Fe I	Hβ	0.602	87	145
4866.267	Ni I	Hβ	0.821	54	66
4871.323	Fe I	Hβ	0.894	174	195
4872.144	Fe I	Hβ	0.902	172	191
4873.437	Ni I	Hβ	0.913	48	52

prominent role in the continuous absorption. Therefore, the values of B^o/B^1 used in this paper are taken from the solar values observed by Houtgast (1942). The values were read from the plot in Figure 7 which was constructed from Houtgast's data.

$\Delta \log \eta_o$ varies with the intensity of the line, i.e., with log W/b, as well as with B^o/B^1. In order to obtain approximate values of log W/b for each line, log c/v was taken to be approximately equal to 5.00; values in this neighborhood had been obtained from the applications of the other models. Then, using the measured values of log W/λ,

$$\log W/b = \log W/\lambda + 5.00. \qquad (24)$$

The limb darkening corrections are slightly affected by the value of the damping parameter, a. These variations were considered to be negligibly small, however, and the values of $\Delta \log \eta_o$ given in Column 8 are for log a = -1.4.

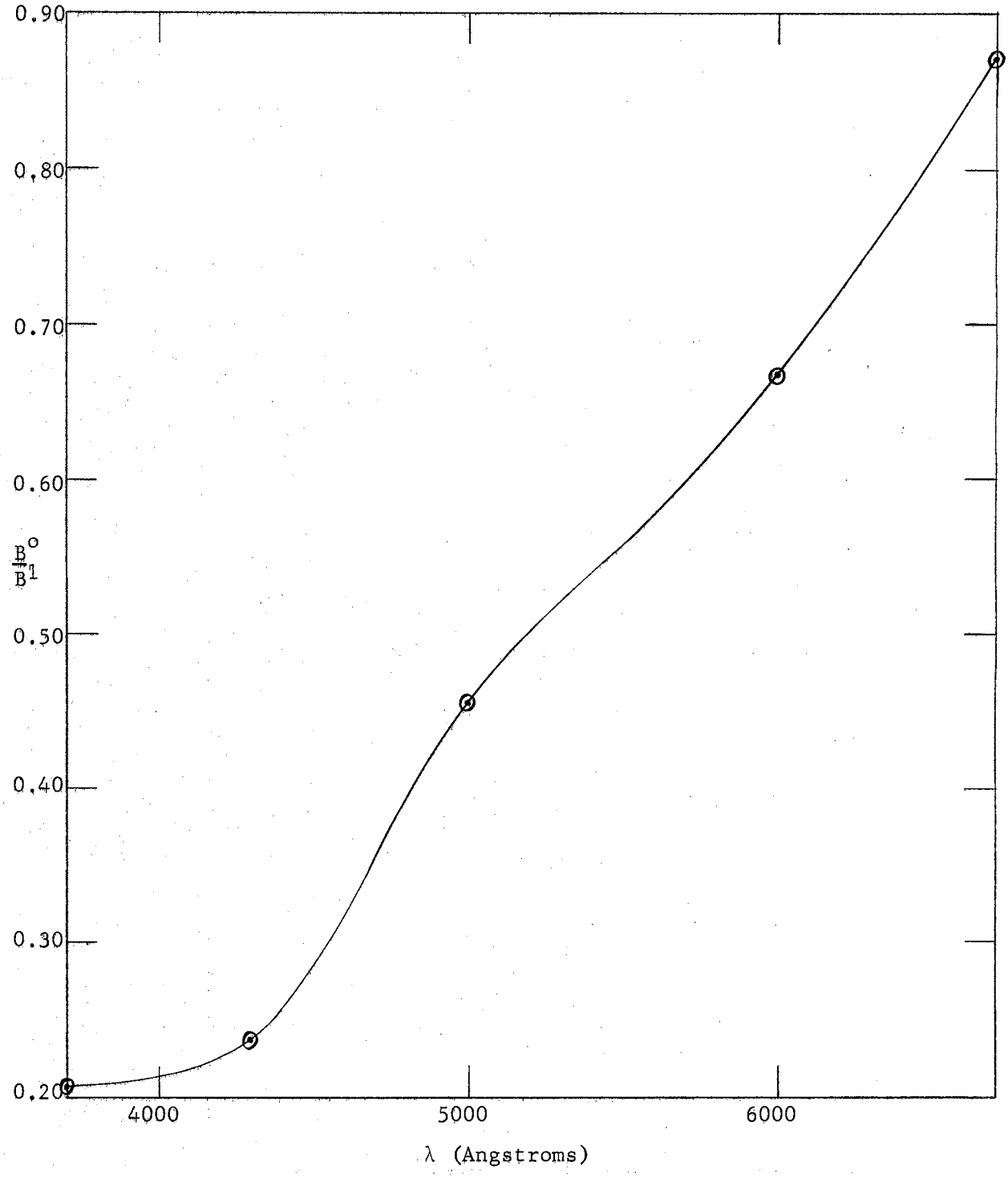

Figure 7, B^o/B^1 Versus Wavelength. The data used to construct the curve are the solar values observed by Houtgast (1942). The circled points are the values given by Houtgast. The points were connected by a smooth curve for purposes of interpolation.

For the S-S pure scattering model, limb darkening corrections are not large enough to be of any consequence and have not been applied in this study.

Limb darkening effects are taken into account in a different way by Hunger in his pure absorption curves. Here, the limiting depth, R_c, which depends upon B^o/B^1, appears in the ordinate of the theoretical curves. The observed curves of growth in the case of pure absorption are plotted with

$$\log W/2R_c\lambda = \log W/\lambda - \log 2R_c \qquad (25)$$

as ordinate. The values of $\log 2R_c$ were read for each line from Table V, which gives $\log 2R_c$ as a function of B^o/B^1. In order to form this table, R_c was calculated from Equation (5) for each value of B^o/B^1 listed.

Comparison of Equivalent Width Measurements With Those of Greenstein

In Figure 8, a comparison is made of the equivalent widths of the θ Ursae Majoris lines measured in this paper and identical lines measured by Greenstein (1948). Inspection of the figure reveals good agreement for values of $\log W/\lambda$ around -4.50. For stronger lines, our values are larger than those of Greenstein, and the reverse is true for the weaker lines. These variances may be due to the different methods used to obtain equivalent widths. In Greenstein's work the profiles were drawn on the microphotometer tracings, line depths measured every millimeter, converted into absorptions, and numerically integrated to obtain the equivalent widths. In this paper the profiles were drawn on the intensitometer tracings rather than the microphotometer tracings. The profiles

were then planimetered to obtain equivalent widths. Consequently, differences might be expected.

TABLE V

LOG $2R_c$ AS A FUNCTION OF B^o/B^1

B^o/B^1	log $2R_c$	B^o/B^1	log $2R_c$	B^o/B^1	log $2R_c$
0.20	+0.19	0.43	+0.08	0.66	0.00
0.21	+0.18	0.44	+0.08	0.67	0.00
0.22	+0.18	0.45	+0.08	0.68	0.00
0.23	+0.17	0.46	+0.07	0.69	-0.01
0.24	+0.17	0.47	+0.07	0.70	-0.01
0.25	+0.16	0.48	+0.07	0.71	-0.01
0.26	+0.16	0.49	+0.06	0.72	-0.02
0.27	+0.15	0.50	+0.06	0.73	-0.02
0.28	+0.15	0.51	+0.05	0.74	-0.02
0.29	+0.14	0.52	+0.05	0.75	-0.03
0.30	+0.14	0.53	+0.05	0.76	-0.03
0.31	+0.14	0.54	+0.04	0.77	-0.03
0.32	+0.13	0.55	+0.04	0.78	-0.04
0.33	+0.13	0.56	+0.04	0.79	-0.04
0.34	+0.12	0.57	+0.03	0.80	-0.04
0.35	+0.12	0.58	+0.03	0.81	-0.04
0.36	+0.11	0.59	+0.03	0.82	-0.05
0.37	+0.11	0.60	+0.02	0.83	-0.05
0.38	+0.10	0.61	+0.02	0.84	-0.05
0.39	+0.10	0.62	+0.02	0.85	-0.06
0.40	+0.10	0.63	+0.01	0.86	-0.06
0.41	+0.09	0.64	+0.01	0.87	-0.06
0.42	+0.09	0.65	+0.01	0.88	-0.06

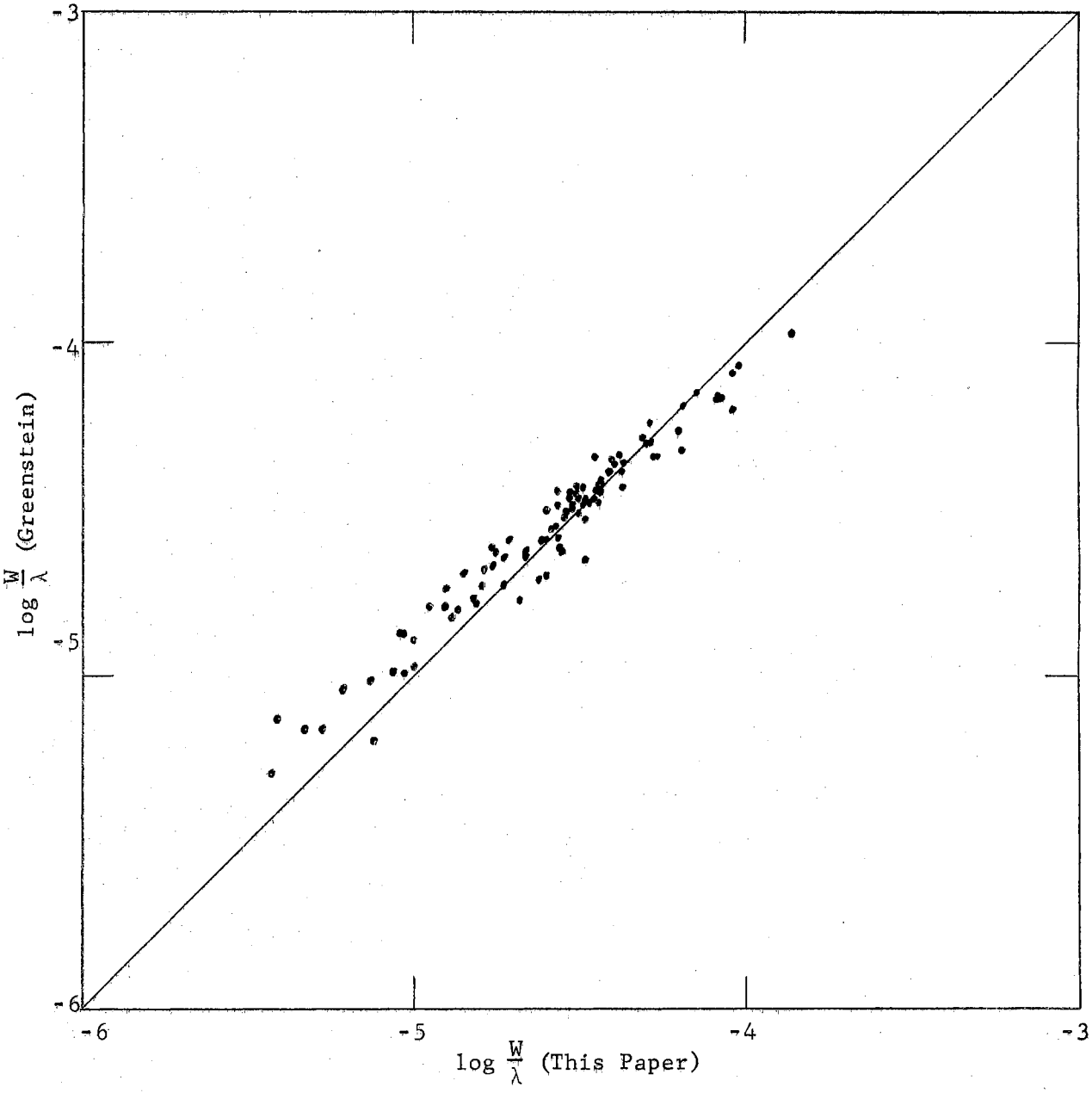

Figure 8. Comparison of Equivalent Widths for Lines Common to This Paper and Greenstein.

CHAPTER IV

RESULTS

Discussion of the Procedures Used in the Reduction of the Data

The general procedures employed in this study to determine log c/v, log a, the excitation temperature, and the abundance from the curve of growth have been discussed in Chapter II. The details involved in the application of these procedures are considered in the following paragraphs. For convenience in the discussion, the designations "Fe I-NBS," "Fe I-King," and "Fe I-Carter" are used to differentiate between the three different sets of data for Fe I corresponding to the three sources of f-values. Similarly, data pertaining to Ti I and Cr I are referred to as "Ti I-NBS," "Ti I-King," "Cr I-NBS," and "Cr I-Hill" data.

Determination of Log c/v

To provide a means for comparing the observed curve of growth for the lines of a given element in a particular stage of ionization with the theoretical curves, the values of log W/λ (or log $W/2R_c\lambda$) for lines which all arise from a given atomic term were plotted against the corresponding values of log $gf\lambda$ (or log $gf\lambda + \Delta\log \eta_o$). Such plots represent portions of the observed curve of growth. Each point on these plots was weighted roughly according to the number of profiles measured in obtaining the equivalent width of the line--the more profiles measured, the more reliable the point. The sizes of the points were made to

indicate the weights, and the larger (more reliable) points were given greater influence in determining the fit of the plot on the theoretical curve of growth.

It is necessary to have a plot which defines the knee of the observed curve of growth in order to determine log c/v. The vertical shift required to fit such a plot on the theoretical curve gives log c/v, as can be seen from Equation (16) of Chapter II. In this manner, values were obtained from the observed curves for Ti I-NBS, Ti I-King, Ti II, Cr I-NBS, Cr I-Hill, Fe I-NBS, and Fe I-King. In each case, four values of log c/v were determined corresponding to the four different atmospheric models. No plots suitable for the determination of log c/v were available for any of the other sets of lines investigated.

Because of the large number of lines available and the relatively small scatter of the points defining the observed curve of growth, the values of log c/v obtained for Fe I-NBS were regarded as more reliable than any of the other determinations. Hence, the Fe I-NBS values of log c/v were adopted for use with the corresponding atmospheric models in the analysis of the lines of Ca I, Mn I, Co I, and Ni I. For Fe I-Carter, the one remaining set of lines, the values of log c/v found for Fe I-King were employed. Since the Kings' f-values were used by Carter to establish a preliminary relative scale for his measurements, these two sets of f-values are closely related. For this reason, the Fe I-King values of log c/v were felt to be the most appropriate choices for use with the Fe I-Carter lines.

Concerning the validity of using the Fe I-NBS values of log c/v in the study of the lines of Ca I, Mn I, Co I, and Ni I, it should be noted that the velocity, v, depends upon the mass of the atom in question.

However, this dependence should be negligibly small, as indicated by the following discussion. Equation (2) of Chapter II can be written as

$$v = \sqrt{\frac{2kT}{M} + v_{turb}^2} \quad , \tag{26}$$

where M is the mass of the atom and T is the kinetic temperature. Before this equation can be used to compare values of v for different atoms, it is necessary to specify a kinetic temperature and a turbulent velocity. It was assumed that the kinetic temperature is approximately equal to the effective temperature, i.e., T = 6210°K as listed by Keenan and Morgan (1951) for stars of class F6 IV. Then, using the mass of the iron atom along with the Fe I-NBS values of log c/v, turbulent velocities were calculated from Equation (26). The four values obtained, corresponding to the four different atmospheric models, were found to range between 2.16×10^5 and 2.67×10^5 cm/sec. Using these estimated values of v_{turb}, Equation (26) was employed to calculate values of v for calcium, which has an atomic mass differing from that of iron by a greater amount than any of the other elements investigated. It was found that the resulting values of log c/v were substantially the same as those for Fe I-NBS. For example, the largest difference between the Fe I-NBS and calcium values for the same atmospheric model amounts to 0.02, which is negligible for the purposes of this investigation. Because of these results, it was felt that the values of log c/v determined for Fe I-NBS were the best approximations available when this quantity could not be determined directly.

Determination of Log a

• If strong lines defining the damping portion of the curve of growth

are available, log a can be determined. For Fe I-NBS, Fe I-King, and Ti II, single plots for a given term were available with enough lines of a sufficient range of intensity to adequately define the transition portion (the section between the knee and the beginning of the damping portion) as well as the damping portion. Since the transition portion of the curve of growth is not perfectly horizontal, the onset of damping occurs at greater intensities as the damping parameter decreases. Hence, fitting the above mentioned plots on the theoretical curves for different values of the damping parameter requires larger vertical shifts for smaller values of log a. However, the vertical shifts were determined by other plots that fit around the knee. In each case, using the appropriate vertical shift, the plot defining the transition and damping* portions was superposed upon theoretical curves of growth for different values of log a. The value belonging to the curve giving the best fit was adopted as characteristic of the element and atmospheric model under investigation.

For Ca I, Cr I-NBS, Cr I-Hill, and Mn I only a few lines were strong enough to fit on the damping portion. Since it was not possible to locate the position of the change from transition to damping with the plots available here, the procedure discussed in the above paragraph could not be used. For each of these cases the value of log a was taken to be that which resulted in the best straight line when $\Delta \log X$ was plotted against $\overline{\chi}_e^*$. This straight line relation is discussed further in the next section which is concerned with the determination of

---

*Since the excitation potentials of the lower levels of the transitions may be slightly different for different lines arising from a particular atomic term, an average value, $\overline{\chi}_e$, was used for each term.

excitation temperatures. A set of values of $\Delta\log X$ was obtained for each value of log a, and $\Delta\log X$ plotted against $\overline{\chi}_e$. The value of log a giving the best straight line was determined by comparing these plots. This rather indirect method for determining log a should not be considered as reliable as the procedure described in the preceding paragraph.

Because of the absence of strong lines, it was not possible to determine values of log a from the lines of Ti I-NBS, Ti I-King, Fe I-Carter, Co I, and Ni I. For a particular atmospheric model, all the theoretical curves of growth for various values of log a are the same below the knee. Hence, the value of log a is of no significance when only weak lines are considered.

Determination of the Excitation Temperature

Equation (18) of Chapter II may be written as

$$\Delta\log X = \text{constant} - \theta\overline{\chi}_e, \qquad (27)$$

where $\overline{\chi}_e$ is the average of the excitation potentials of all the lines arising from a given term. It is apparent from this equation that a straight line relation should exist between $\Delta\log X$ and $\overline{\chi}_e$ with a slope equal to $-\theta$. For each atomic term $\Delta\log X$ was found from the horizontal shift required to fit the corresponding plot on the theoretical curve of growth. The same vertical shift was used for fitting to a particular curve all plots belonging to the same element in a given stage of ionization, although this vertical shift usually changed in going from one atmospheric model to another. The method of least squares was employed to obtain the slope, $-\theta$, of the straight line which best fit the plot of $\Delta\log X$ versus $\overline{\chi}_e$. The excitation temperature was then calculated from $T = 5040/\theta$.

For the purposes of the least squares calculations each value of $\Delta\log X$ was assigned a weight indicative of its apparent reliability. A weight was assigned by considering the number of points on the plot used to determine $\Delta\log X$, the scatter of the points, the extent of the curve of growth defined by the plot, and the fit of the plot on the theoretical curve of growth. Some terms were represented by only one point. In such cases the values of $\Delta\log X$ obtained were given zero weight when there were a sufficient number of other values to adequately determine the straight line relating $\Delta\log X$ and $\overline{\chi}_e$. Also, when a value of $\Delta\log X$ was clearly far off the preliminary straight line, it was given zero weight.

Determination of the Abundance

In Chapter II the equation for the abundance in the case of S-S pure scattering is presented (Equation (20)), and the means of modifying this equation so that it will apply to any of the other models is indicated. Written out in full, the equations giving the abundances for the four models are as follows:

M-E pure scattering and pure absorption--

$$\log N/\rho\overline{\kappa} = \text{shift} - \log C + \log u - \log c/v, \qquad (28)$$

S-S pure scattering--

$$\log NH = \text{shift} - \log C + \log u - \log c/v, \qquad (29)$$

and S-S pure absorption--

$$\log NH = \text{shift} - \log C + \log u - \log c/v + \log 3/2. \qquad (30)$$

When relative f-values were used, as was the case for Ti I-King, Cr I-Hill, Fe I-King, and Fe I-Carter, it was necessary to subtract another quantity, $\Delta\log gf$, from the right-hand sides of Equations (28),

(29), and (30). $\Delta\log gf$ is defined by the following:

$$\Delta\log gf = \log gf_{absolute} - \log gf_{relative} . \qquad (31)$$

The use of relative f-values causes the shifts obtained to be too large by the amount $\Delta\log gf$; hence the subtraction of this quantity. If one or more absolute f-values are known for lines included in the tables of relative f-values, which are on a uniform scale, $\Delta\log gf$ can be calculated from Equation (31). The values used for Ti I-King, Cr I-Hill, Fe I-King, and Fe I-Carter are given later in this chapter when the results obtained from these sets of lines are presented.

As pointed out in Chapter II, shift = $\Delta\log X + \theta\overline{\chi}_e$. From this equation, values of the shift were determined for each atomic term, and weighted average values were calculated using the same weights as employed in the least squares determinations of the excitation temperatures. The weighted average values were used in the abundance computations. The constant C is given by Equation (9) of Chapter II. The values of log u were obtained by interpolating, when necessary, in the tables published by Aller (1960), where log u is given as a function of the excitation temperature.

Values have been determined in this study for the abundances in the atmosphere of θ Ursae Majoris of the neutral atoms of seven elements and the singly ionized atoms of one element, titanium. Titanium was the only element studied where results were obtained for both the neutral and singly ionized atoms. Since second and higher ionizations are negligible, the total abundance of titanium can be obtained by adding the abundances of the neutral and singly ionized atoms. It was found that the contribution of the neutral atoms to the total abundance is

completely negligible as far as the accuracy attained in this study is concerned. Hence, the abundances obtained for singly ionized titanium also represent the total abundances for titanium.

For the other six elements studied, where only the abundances of the neutral atoms were determined, the Saha equation provides a means for estimating the contributions of the ionized atoms to the total abundances. The validity of the results obtained is affected by departures from idealized conditions. Although such departures (e.g., non-uniform distribution of the atoms and ions throughout the stellar atmosphere and deviations from thermodynamic equilibrium) are known to exist, the Saha equation, being the best means available, was applied to estimate the total abundances.

The Saha equation is presented in Chapter II, and for convenience it is restated below:

$$\log \frac{(NH)_1}{(NH)_o} = -\log P_e - \frac{5040}{T} \chi_i + 2.5 \log T - 0.48 + \log \frac{2u_1}{u_o}. \quad (32)$$

As stated here the equation applies to the S-S model. The subscripts 1 and 0 refer respectively to the singly ionized atoms and to the neutral atoms. For application to the M-E model, $(NH)_1$ and $(NH)_o$ are replaced by $(N/\rho\overline{\kappa})_1$ and $(N/\rho\overline{\kappa})_o$.

For purposes of the calculations, the temperature, T, was taken to be equal to the effective temperature, 6210°K, which is characteristic of an optical depth in the atmosphere of 0.6. This is a representative depth for line formation. It should be noted that results obtained from the Saha equation are sensitive to the value used for the temperature, which leads to some uncertainty in the results. The ionization potentials, χ_i, were taken from the Revised Multiplet Table. Values of

the partition functions, u_o and u_1, which depend upon the temperature, were obtained by referring to the tables published by Aller (1960).

The one remaining quantity necessary for the calculations is the electron pressure, P_e. The fact that abundances were determined in this investigation for both neutral and singly ionized atoms of titanium offered the opportunity to calculate values of P_e from the Saha equation. For this purpose, T was taken to be equal to 6210°K as discussed above, and χ_i, u_o, and u_1 were obtained from the above mentioned sources. Since abundances were determined for four different atmospheric models, four values of log P_e, where P_e is in dynes/cm^2, were obtained: 1.36, 1.30, 1.27, and 1.32 which correspond to M-E pure scattering, M-E pure absorption, S-S pure scattering, and S-S pure absorption respectively. The abundances of the neutral atoms determined for Ti I-NBS were used in the calculations. The average of the values obtained for log P_e is 1.31. This average value was used in subsequent calculations.

Since second and higher ionizations are negligible, the total abundance in the S-S model is given by

$$(NH)_{total} = (NH)_o + (NH)_1 = (NH)_o \left[1 + \frac{(NH)_1}{(NH)_o}\right]. \qquad (33)$$

It follows that

$$\log (NH)_{total} = \log (NH)_o + \Delta\log \eta, \qquad (34)$$

where

$$\Delta\log \eta = \log \left[1 + \frac{(NH)_1}{(NH)_o}\right]. \qquad (35)$$

Replacing NH by $N/\rho\bar{\kappa}$ makes the above equations valid for the M-E model. $\Delta\log \eta$ gives the contribution of the ionized atoms to log $(NH)_{total}$ or log $(N/\rho\bar{\kappa})_{total}$. For each of the six elements for which the abundances

of the neutral atoms only were determined, the Saha equation was employed to calculate a value of $(NH)_1/(NH)_o$ from which $\Delta\log\eta$ was obtained. For a given element $(NH)_1/(NH)_o$ and $(N/\rho\overline{\kappa})_1/(N/\rho\overline{\kappa})_o$ have the same value. Hence $\Delta\log\eta$ does not depend upon the atmospheric model.

The results of the determinations of the values of log c/v and log a, the excitation temperatures, and the abundances of the atoms for each set of lines studied are presented in the following paragraphs. The order of presentation is the order in which the sets of lines are listed in Table II of Chapter III.

Results for Ca I

The f-values employed here were those of the NBS. Observational data were available for twenty-one lines belonging to five different lower atomic terms. Table VI lists the terms, the values of $\overline{\chi}_e$ in electron volts, the numbers of lines representing each term, the weights used in the least squares calculations of the excitation temperatures, and the values of $\Delta\log X$ and the shift obtained from the application of each of the four sets of theoretical curves of growth. The values of log c/v listed in the top row of Table VI were adopted from those obtained for Fe I-NBS. This is indicated in the table by enclosing the values in parentheses. The second row gives the values of log a, which were determined by the second method discussed earlier in this chapter for the determination of these quantities, i.e., from the value giving the best straight line relation between $\Delta\log X$ and $\overline{\chi}_e$. The lower portion to the table lists the values of θ, the excitation temperatures with the probable errors derived from the least squares calculations, the values of log u, the weighted shifts, the abundances, and $\Delta\log\eta$.

TABLE VI

CURVE OF GROWTH DATA DERIVED FROM Ca I LINES

				M-E Model				S-S Model			
				Scattering		Absorption		Scattering		Absorption	
log c/v				(5.06)		(5.00)		(5.07)		(5.05)	
log a				-1.8		-1.8		-1.8		-1.8	
Term	$\overline{\chi}_e$	No. of Lines	Weight	Δlog X	Shift	Δlog X	Shift	Δlog X	Shift	Δlog X	Shift
4^1S	0.00	1	1	8.22	8.22	8.16	8.16	8.06	8.06	8.20	8.20
4^3P^o	1.88	9	2	6.27	8.23	6.44	8.13	5.98	8.07	6.45	8.25
3^3D	2.51	9	2	5.60	8.22	5.90	8.16	5.27	8.06	5.80	8.21
3^1D	2.70	1	0	5.87	8.69	5.78	8.21	5.66	8.66	5.69	8.28
4^1P^o	2.92	1	0	6.04	9.09	6.23	8.86	5.66	8.91	6.14	8.94
θ				1.045		0.899		1.112		0.959	
Excitation Temperature (°K)				4825 ± 34		5607 ± 99		4532 ± 23		5256 ± 151	
log u				0.07		0.12		0.05		0.09	
Weighted Shift				8.22		8.15		8.06		8.22	
Abundance	log $N/\rho\overline{\kappa}$			15.53		15.57					
	log NH							15.34		15.38	
Δlog η				3.25							

Figure 9 illustrates the data used in the determination of the excitation temperatures. The straight lines are those which were determined by the method of least squares. In these plots the sizes of the points indicate the weights they were given in the calculations. Circled points indicate zero weights.

The curves of growth obtained for the four models are shown in Figure 10, 11, 12, and 13. The theoretical curves are represented by the solid lines. For M-E and S-S pure scattering the theoretical curves are those calculated for B^o/B^1 and I^o/I^1 equal to 2/3. In each case, the value of log a corresponding to the pictured theoretical curve is indicated on the figure. Also indicated is the value of log c/v used in the analysis. In the figures, different symbols are used to distinguish points representing observed data pertaining to different atomic terms. Following the procedures outlined in this study, each such set of points was fitted individually on the theoretical curve.

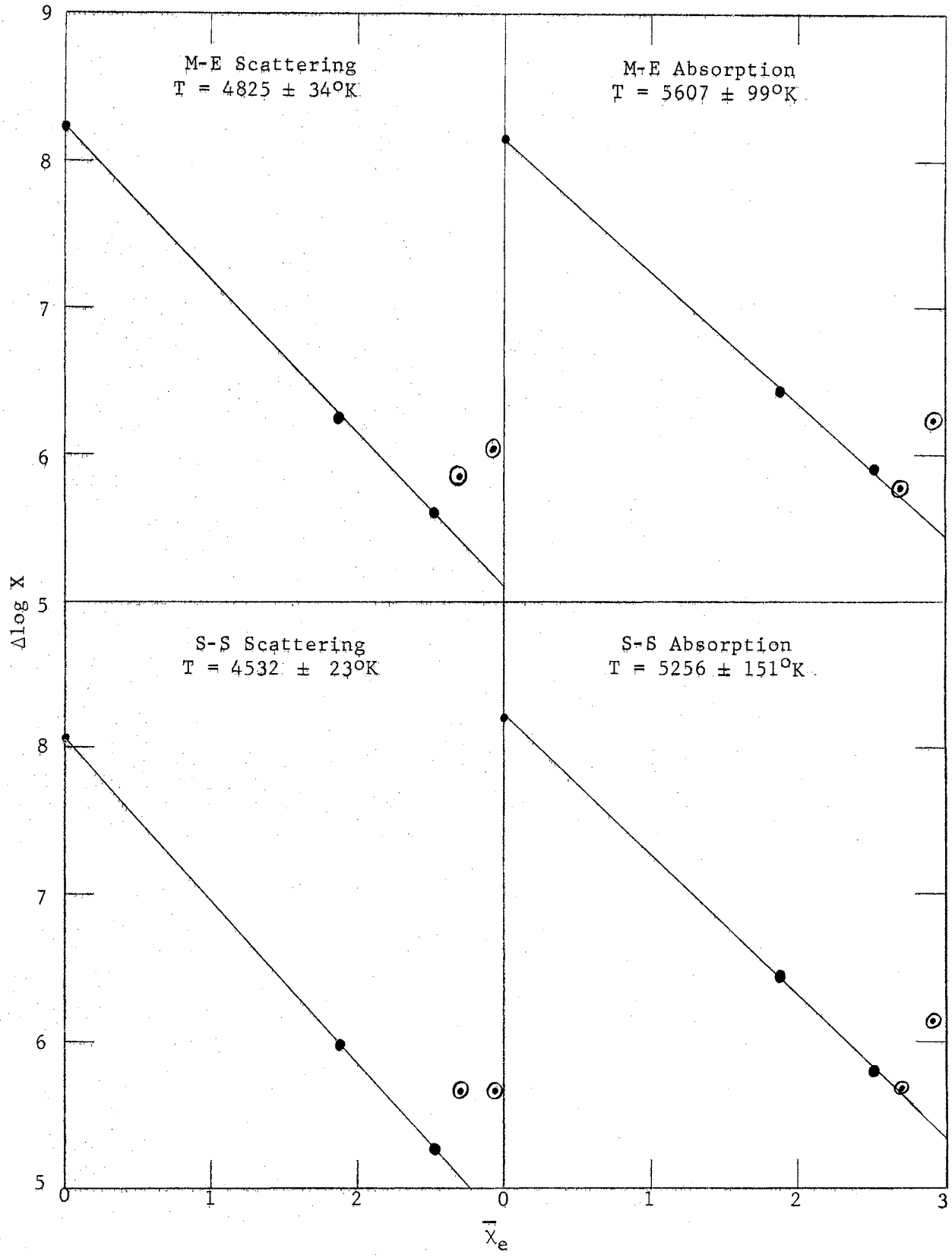

Figure 9. Excitation Temperatures Derived From Ca I Lines.

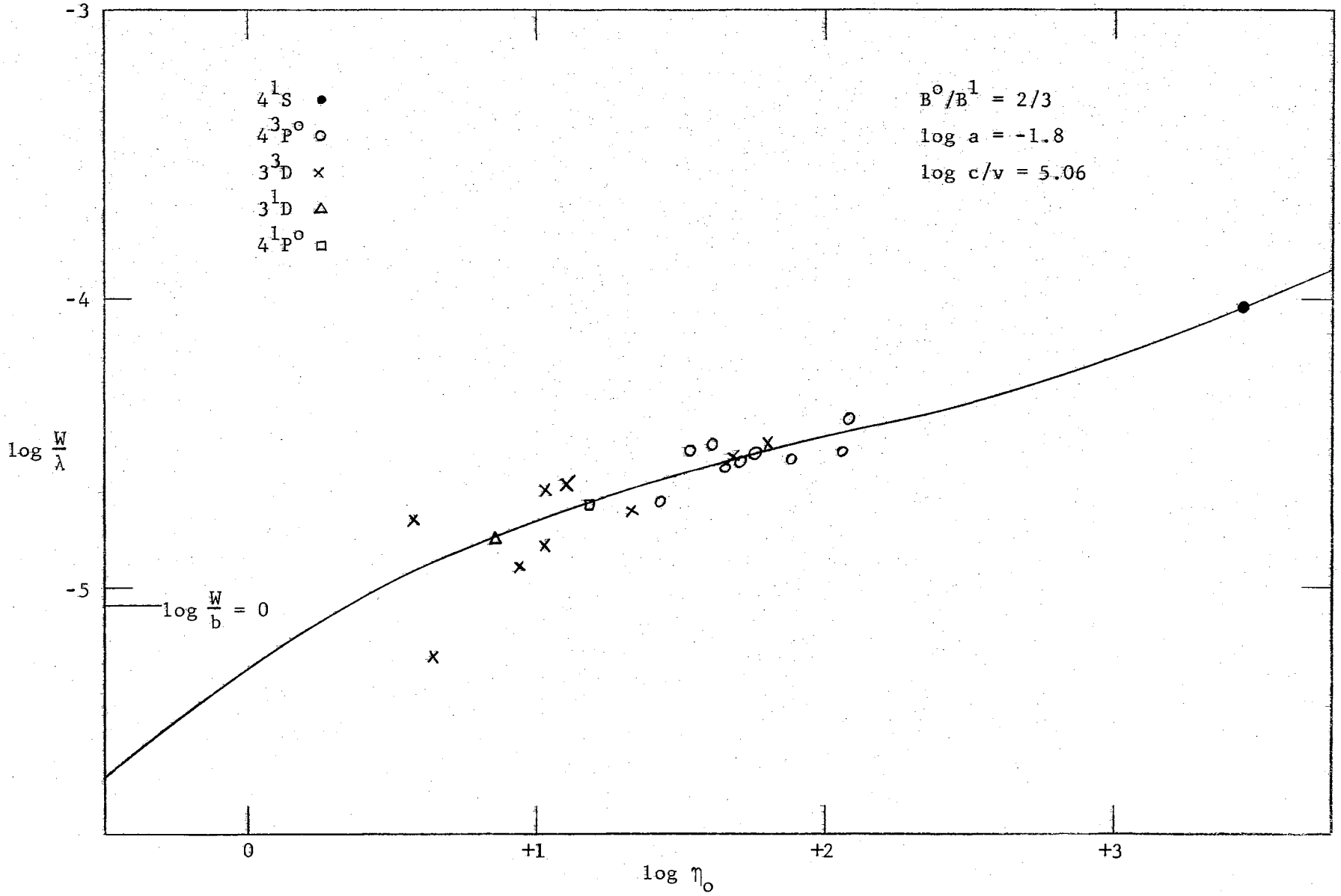

Figure 10. Milne-Eddington Pure Scattering Curve of Growth for Ca I.

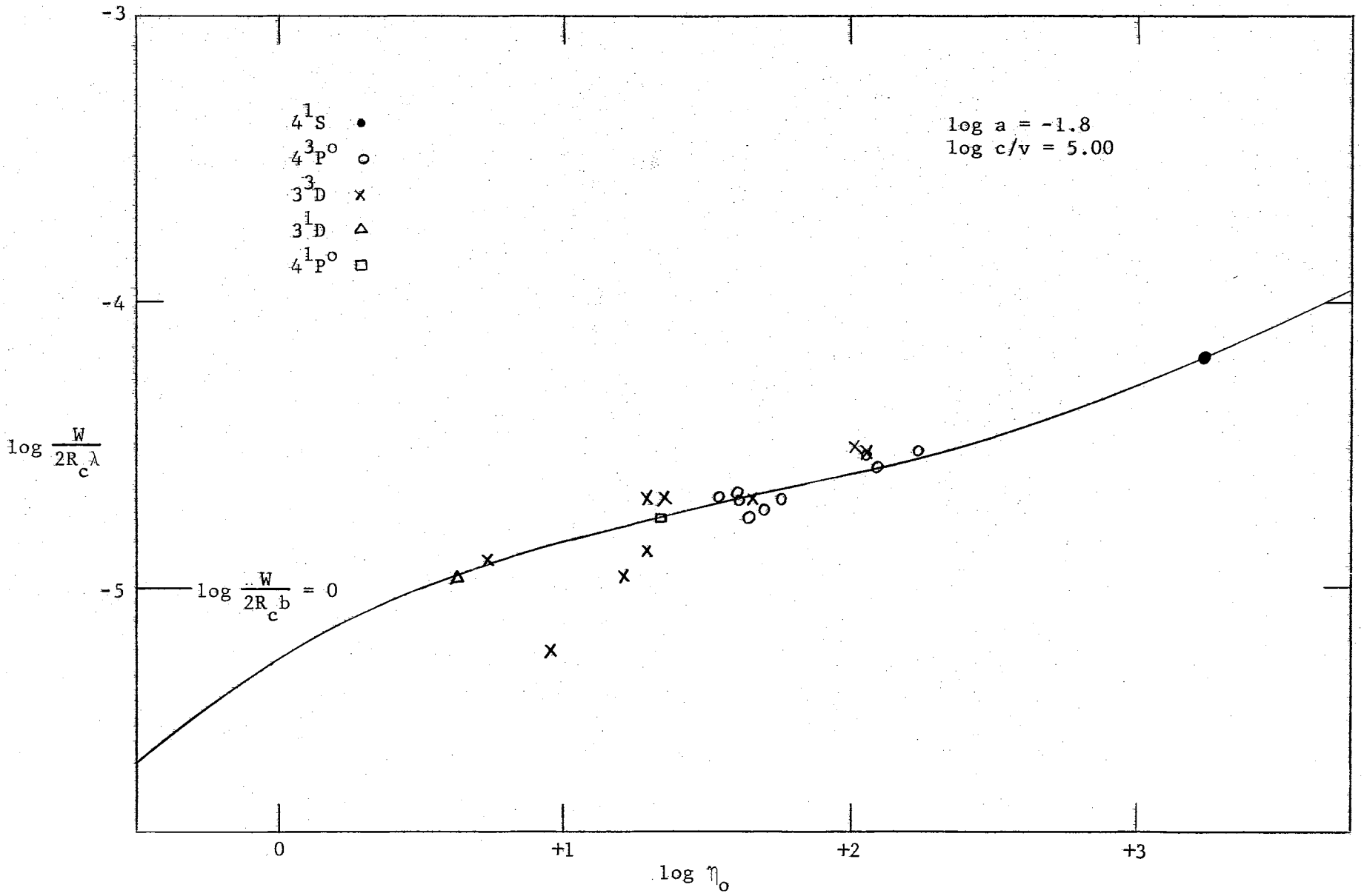

Figure 11. Milne-Eddington Pure Absorption Curve of Growth for Ca I.

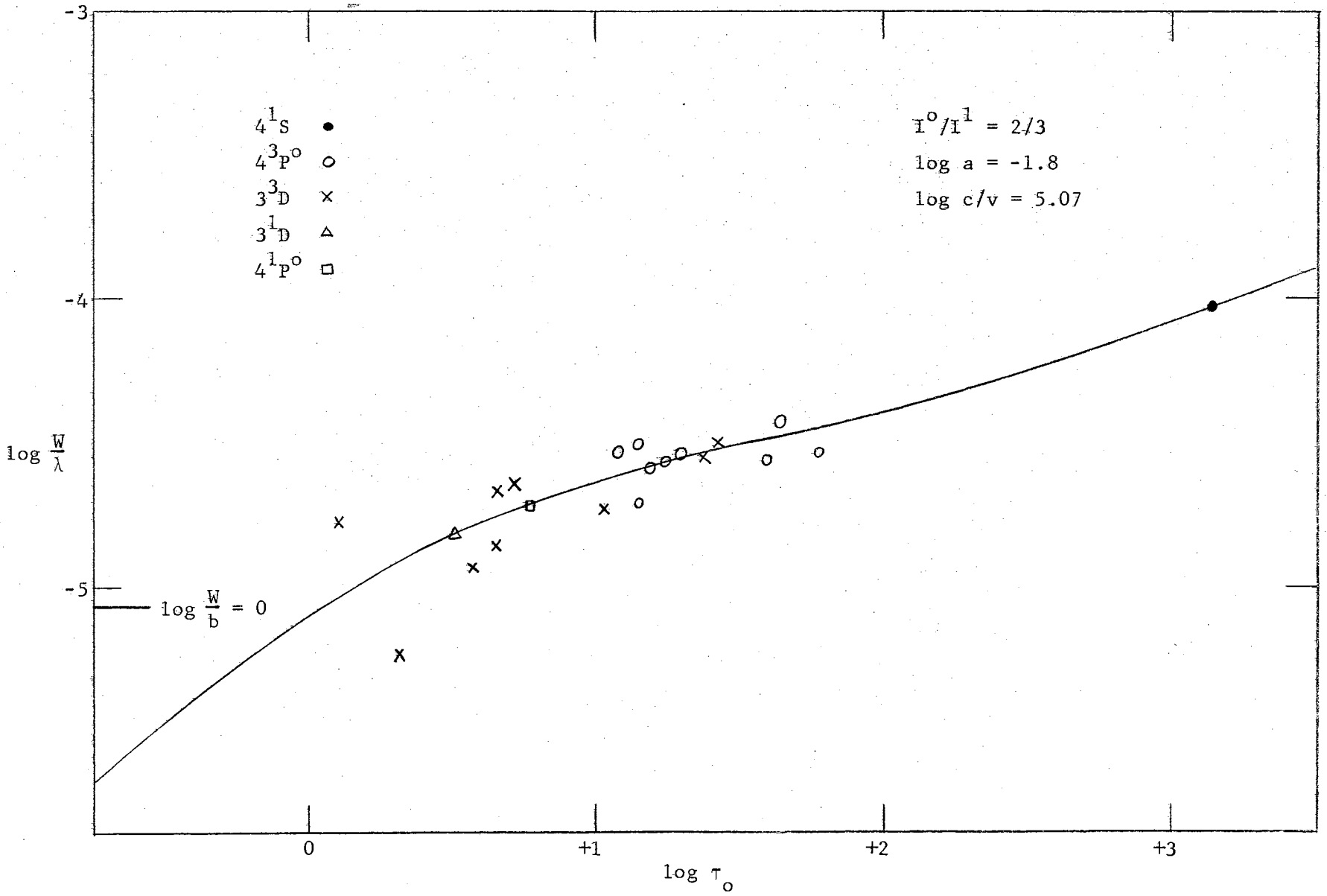

Figure 12. Schuster-Schwarzschild Pure Scattering Curve of Growth for Ca I.

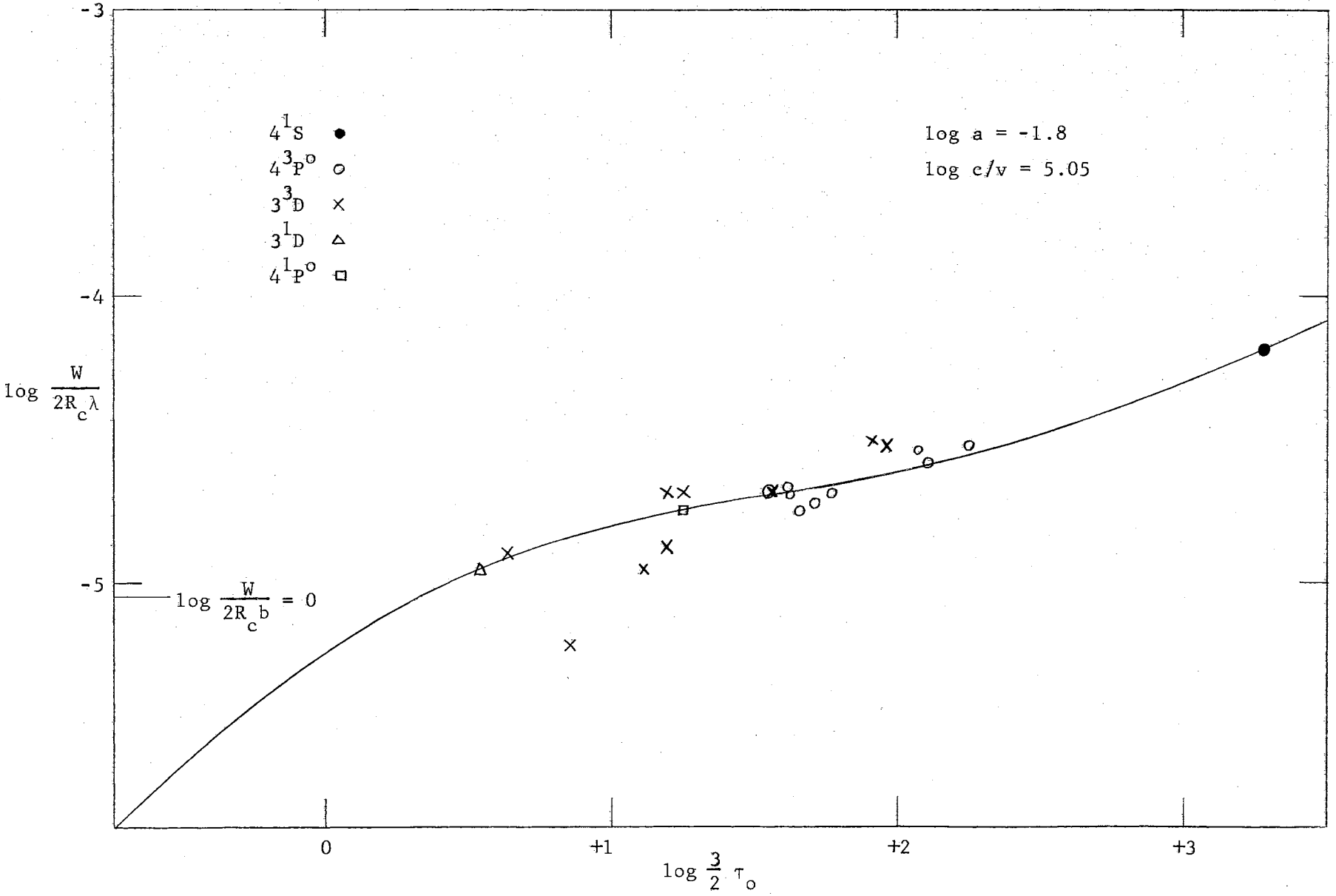

Figure 13. Schuster-Schwarzschild Pure Absorption Curve of Growth for Ca I.

Results for Ti I

Ti I-NBS

The data pertaining to the Ti I-NBS lines are given in Table VII. The values of log c/v were determined from the a^5F plot, which fits around the knee of the curve of growth. No lines strong enough to determine log a were available, and the values listed in the second row of Table VII merely indicate the theoretical curves used for fitting the observed plots. To call attention to this, the values of log a listed in the table are enclosed in parentheses. A value of $\Delta \log \gamma$ for titanium is not given since the abundances obtained for Ti II also represent, as discussed earlier, the total abundances for titanium.

Figure 14 illustrates the excitation temperature data, and Figures 15, 16, 17, and 18 are the curves of growth obtained for Ti I-NBS.

TABLE VII

CURVE OF GROWTH DATA DERIVED FROM Ti I-NBS LINES

				M-E Model				S-S Model			
				Scattering		Absorption		Scattering		Absorption	
log c/v				4.90		4.75		4.95		4.85	
log a				(-1.4)		(-1.8)		(-1.4)		(-1.8)	
Term	$\overline{\chi}_e$	No. of Lines	Weight	Δlog X	Shift	Δlog X	Shift	Δlog X	Shift	Δlog X	Shift
a^3F	0.02	7	2	5.56	5.58	5.36	5.38	5.45	5.47	5.41	5.43
a^5F	0.83	14	4	4.75	5.65	4.52	5.42	4.68	5.56	4.57	5.46
a^1D	0.90	1	0	4.43	5.40	4.23	5.20	4.33	5.29	4.28	5.24
a^3P	1.06	3	1	4.28	5.42	4.07	5.21	4.15	5.28	4.12	5.25
a^1G	1.50	3	1	3.76	5.38	3.55	5.17	3.70	5.30	3.60	5.20
a^5P	1.73	6	2	3.65	5.52	3.43	5.30	3.57	5.41	3.49	5.34
a^3G	1.87	6	2	3.55	5.57	3.34	5.36	3.48	5.47	3.41	5.41
z^5G^o	2.03	1	0	3.83	6.02	3.65	5.84	3.70	5.86	3.69	5.86
z^5F^o	2.11	5	1	3.60	5.88	3.40	5.68	3.55	5.80	3.50	5.76
a^3D	2.15	1	0	3.65	5.97	3.20	5.52	3.29	5.58	3.29	5.59
a^3H	2.24	3	1	3.38	5.80	3.14	5.56	3.30	5.69	3.18	5.57
b^1G	2.26	1	0	3.85	6.29	3.64	6.08	3.73	6.14	3.69	6.11
z^5D^o	2.29	2	0	3.62	6.09	3.50	5.97	3.48	5.92	3.56	6.01

TABLE VII (Continued)

				M-E Model				S-S Model			
				Scattering		Absorption		Scattering		Absorption	
Term	$\overline{\chi}_e$	No. of Lines	Weight	Δlog X	Shift	Δlog X	Shift	Δlog X	Shift	Δlog X	Shift
$c\,^3P$	2.33	1	0	3.26	5.77	3.06	5.58	3.17	5.65	3.16	5.65
$y\,^5G^o$	3.28	1	0	2.82	6.36	2.65	6.19	2.67	6.17	2.73	6.24
θ				1.079		1.080		1.066		1.069	
Excitation Temperature (^oK)				4671 ± 215		4667 ± 206		4728 ± 240		4713 ± 218	
log u				1.45		1.45		1.45		1.45	
Weighted Shift				5.60		5.38		5.50		5.42	
Abundance	log $N/\rho\overline{\kappa}$			14.45		14.38					
	log NH							14.30		14.14	

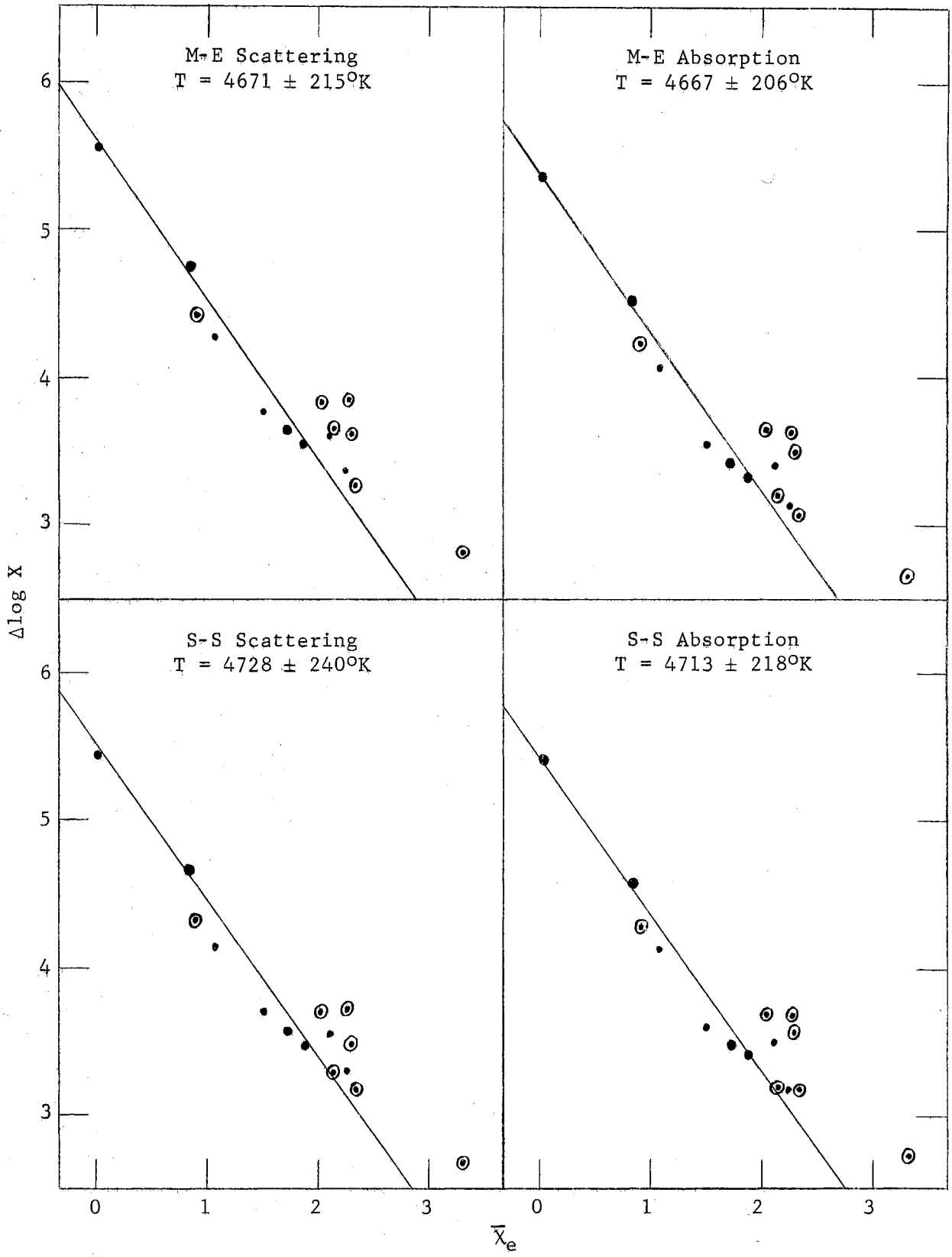

Figure 14. Excitation Temperatures Derived From Ti I-NBS Lines.

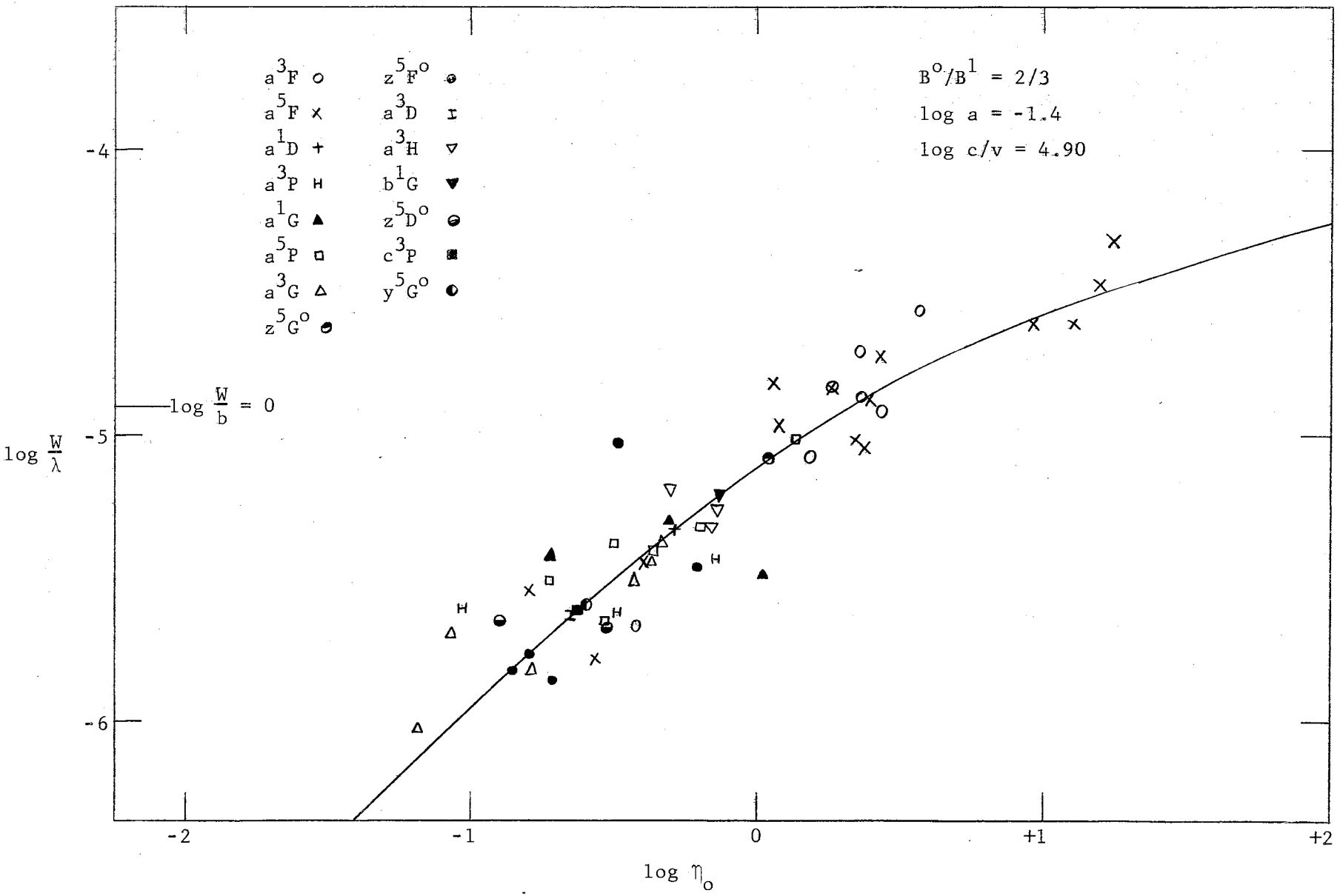

Figure 15. Milne-Eddington Pure Scattering Curve of Growth for Ti I-NBS.

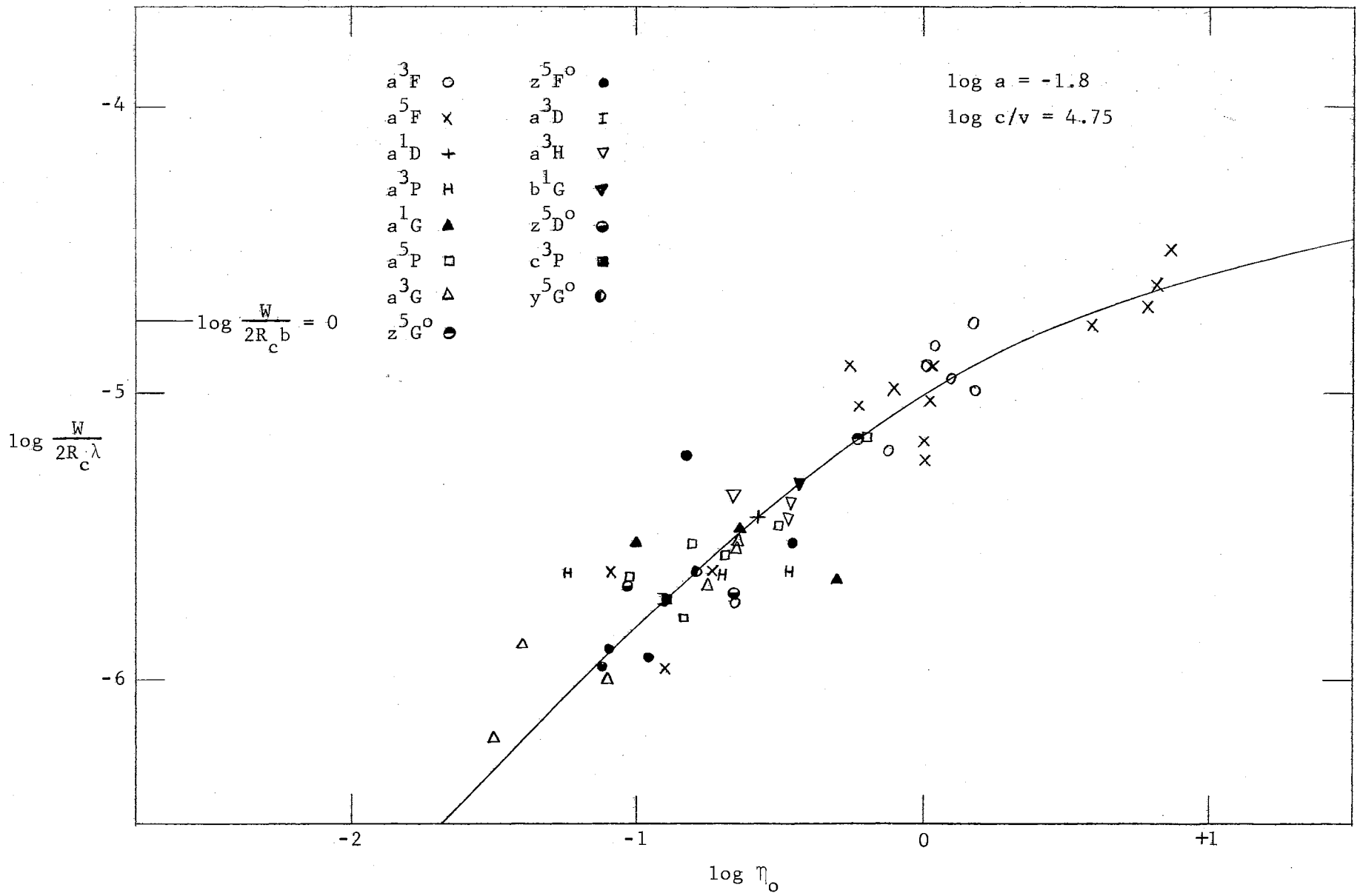

Figure 16. Milne-Eddington Pure Absorption Curve of Growth for Ti I-NBS.

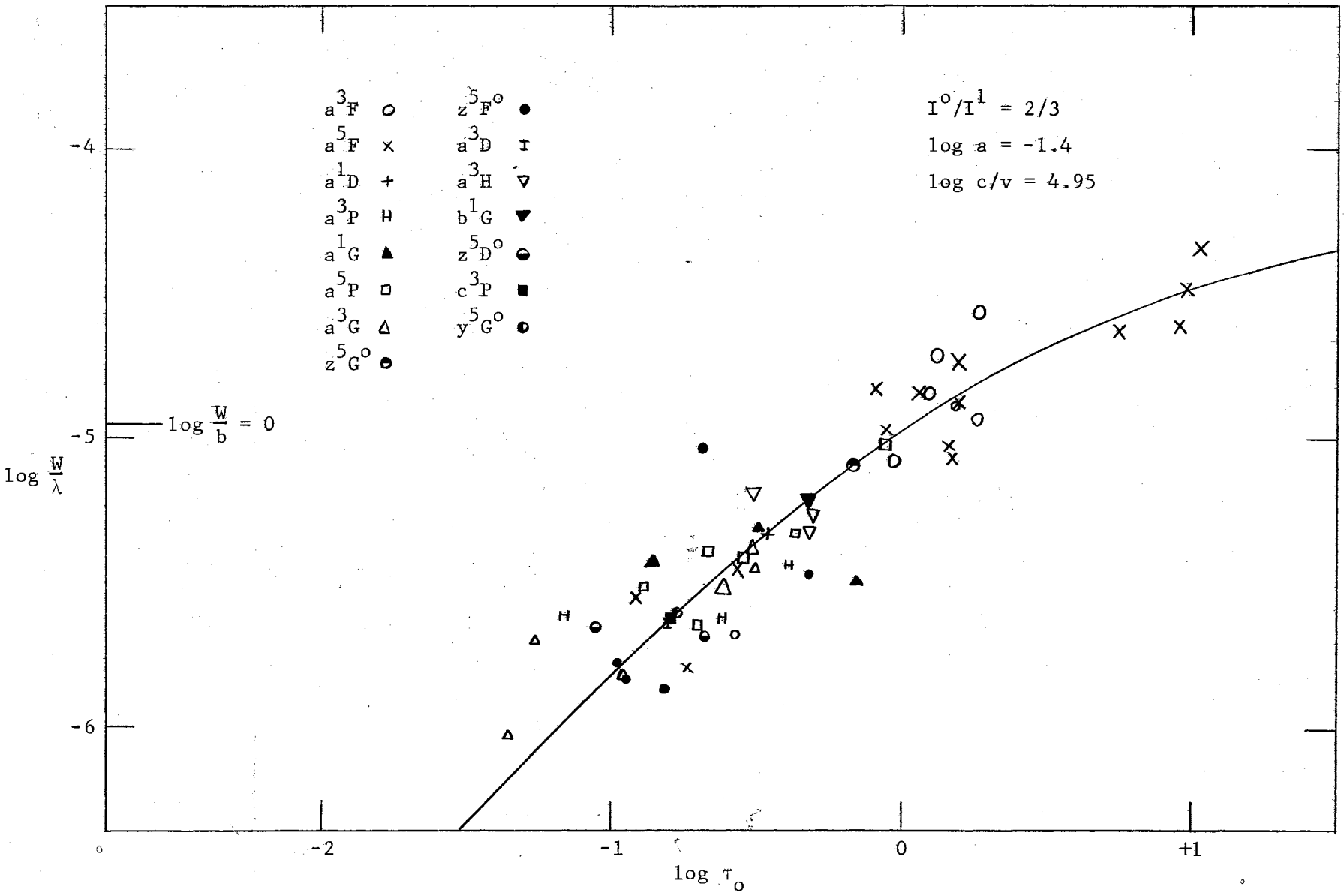

Figure 17. Schuster-Schwarzschild Pure Scattering Curve of Growth for Ti I-NBS.

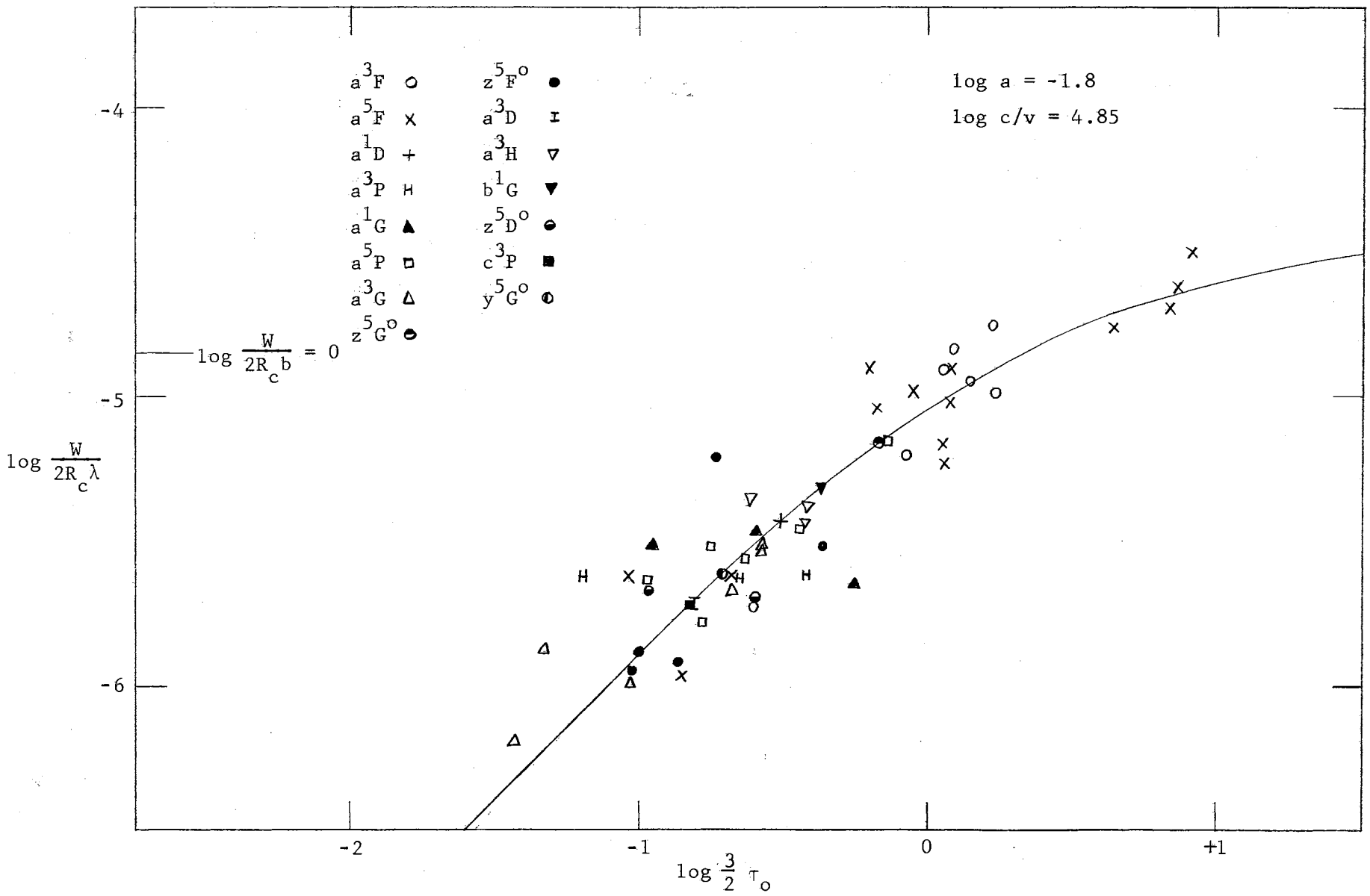

Figure 18. Schuster-Schwarzschild Pure Absorption Curve of Growth for Ti I-NBS.

Ti I-King

The Ti I-King data are presented in Table VIII. The values of log c/v were determined from the a^5F plot. Values of log a could not be determined because of the absence of strong lines, and the values listed indicate the theoretical curves used for fitting the observed plots.

Since the f-values of the Kings are on a relative scale it was necessary to determine a value of Δlog gf for use in the abundance calculations. The absolute f-values of the NBS were not used to obtain a value of Δlog gf since the accuracy of the NBS values is open to some question, and it was desired to keep the determinations for Ti I-NBS and Ti I-King as independent as possible. Allen's (1955) absolute f-values were used for this purpose, giving a value of Δlog gf equal to -3.30. The absolute f-values listed by Allen were determined from the Kings' relative values using f-sum rules and, due to the scarcity of accurate measurements of absolute f-values for Ti I, were regarded as the best available.

The plots of the data used to determine the excitation temperatures are presented in Figure 19, and the curves of growth are illustrated in Figures 20, 21, 22, and 23.

TABLE VIII

CURVE OF GROWTH DATA DERIVED FROM Ti I-KING LINES

				M-E Model				S-S Model			
				Scattering		Absorption		Scattering		Absorption	
log c/v				5.00		4.85		5.04		4.90	
log a				(-1.4)		(-1.8)		(-1.4)		(-1.8)	
Term	$\overline{\chi}_e$	No. of Lines	Weight	Δlog X	Shift	Δlog X	Shift	Δlog X	Shift	Δlog X	Shift
a^3F	0.02	6	2	2.73	2.75	2.50	2.52	2.54	2.56	2.45	2.47
a^5F	0.83	10	4	2.00	2.80	1.78	2.58	1.83	2.60	1.72	2.52
a^5P	1.74	1	1	0.99	2.66	0.75	2.42	0.86	2.48	0.72	2.39
θ				0.962		0.960		0.932		0.959	
Excitation Temperature (^oK)				5239 ± 320		5252 ± 375		5410 ± 310		5257 ± 305	
log u				1.49		1.50		1.51		1.50	
Weighted Shift				2.77		2.54		2.57		2.49	
Abundance	log $N/\rho\overline{\kappa}$			14.86		14.79					
	log NH							14.64		14.51	

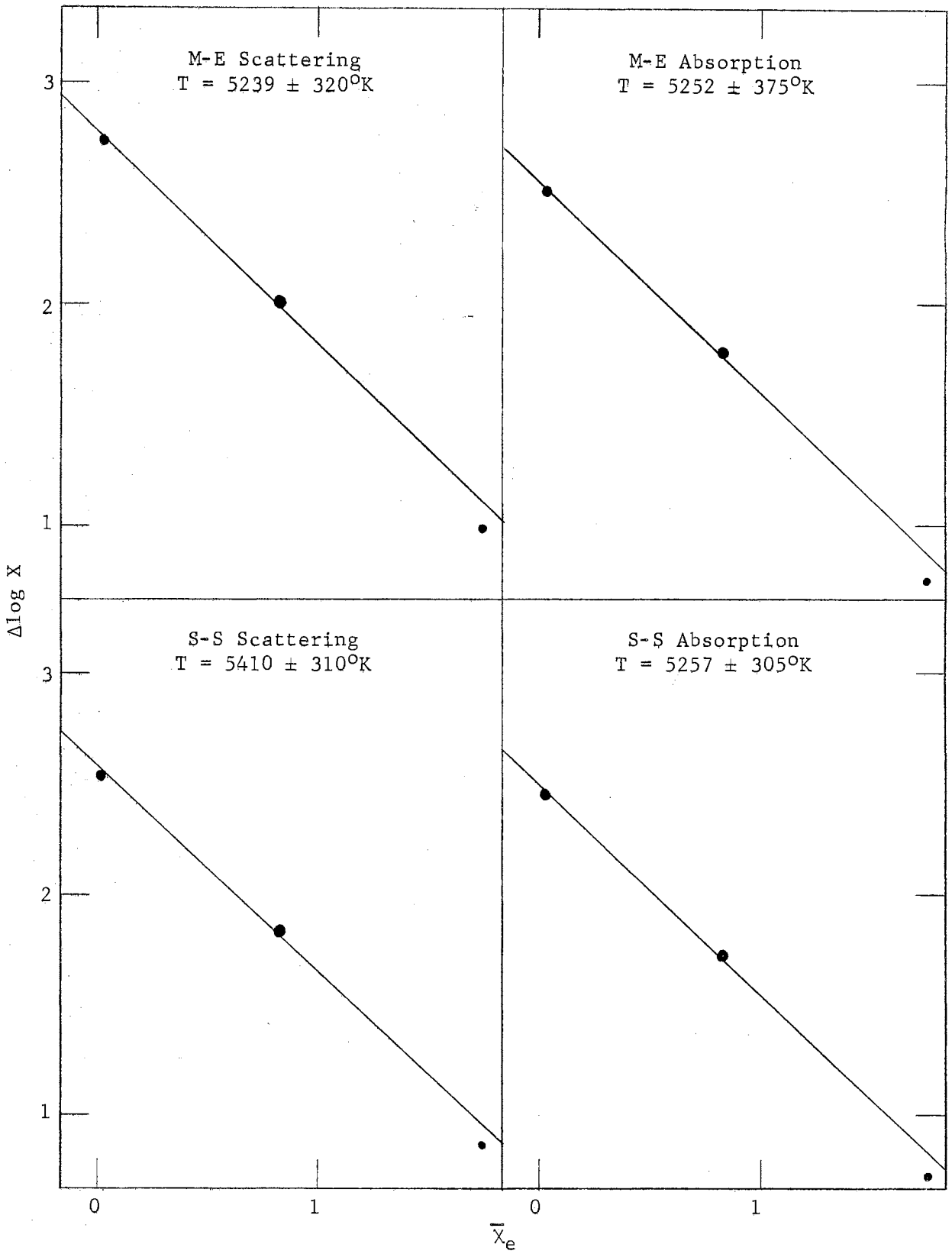

Figure 19. Excitation Temperatures Derived From Ti I-King Lines.

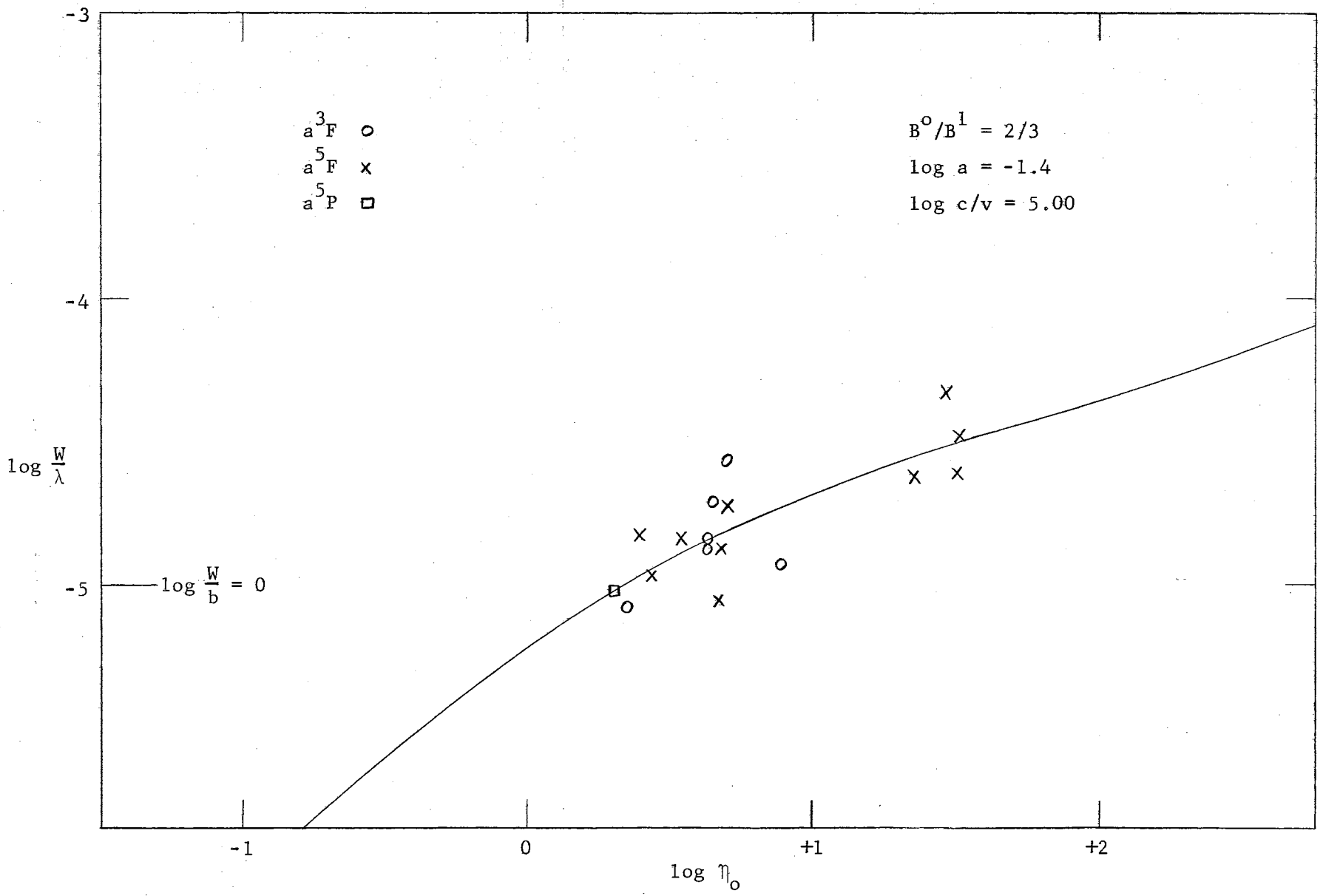

Figure 20. Milne-Eddington Pure Scattering Curve of Growth for Ti I-King.

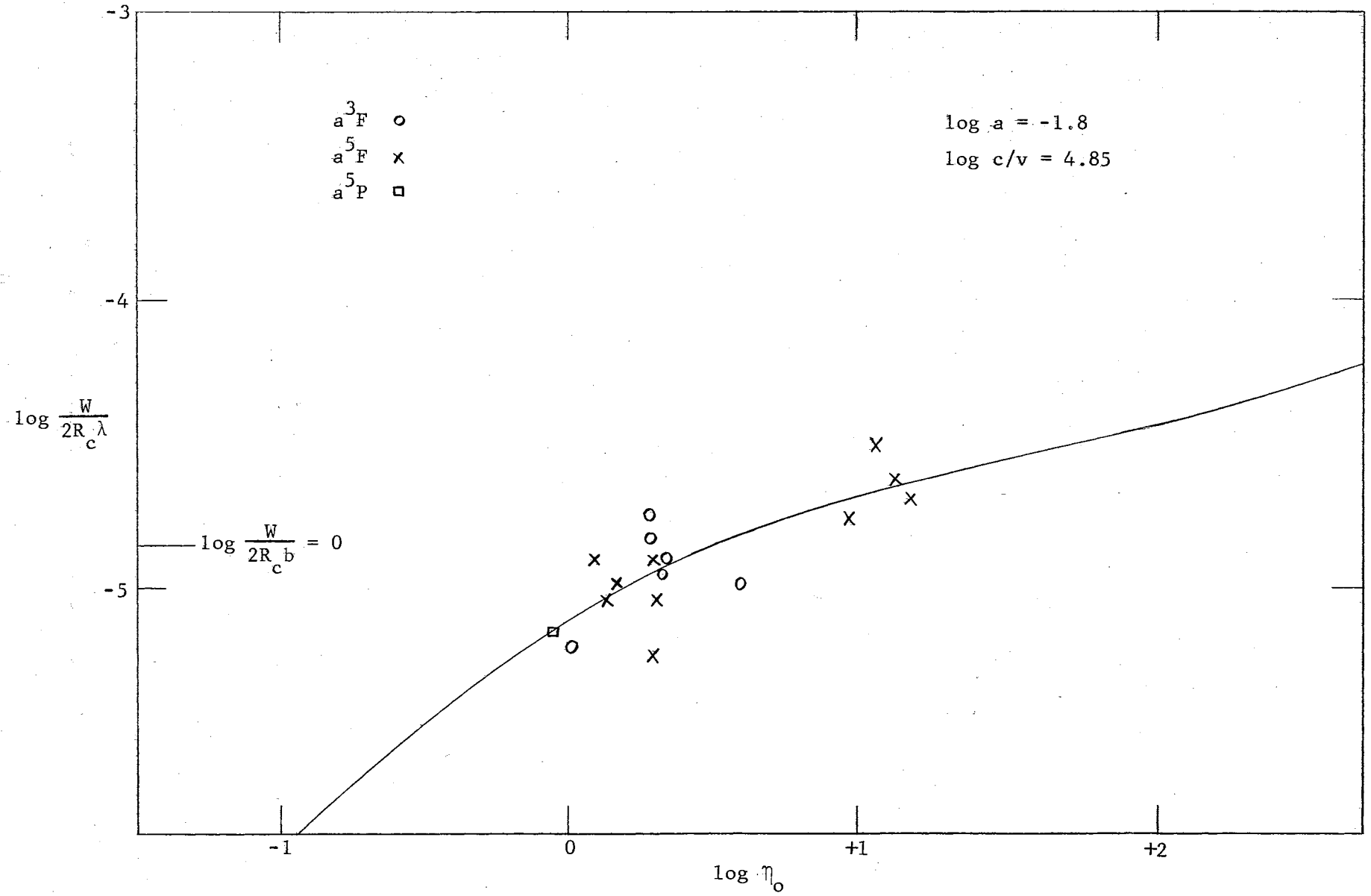

Figure 21. Milne-Eddington Pure Absorption Curve of Growth for Ti I-King.

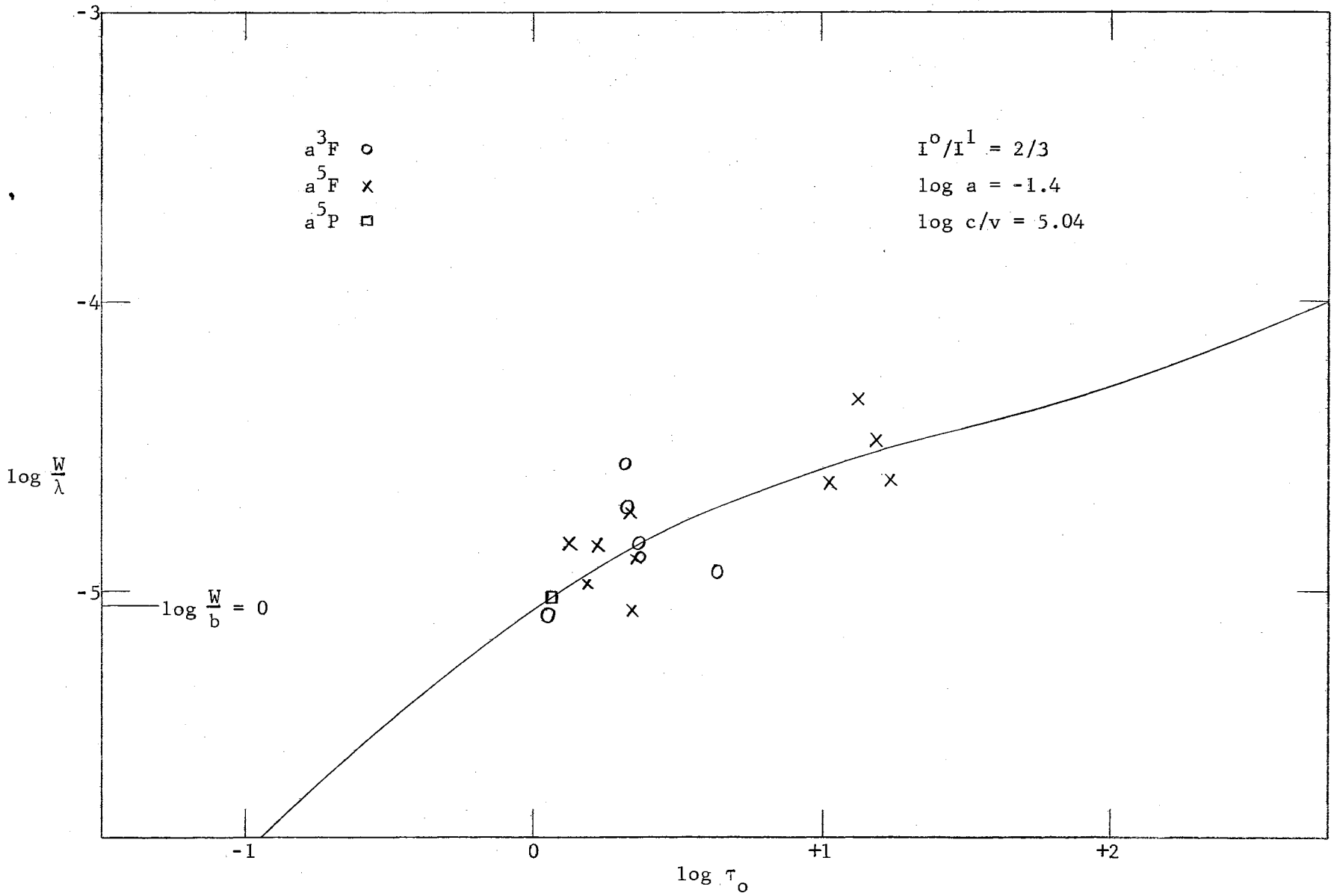

Figure 22. Schuster-Schwarzschild Pure Scattering Curve of Growth for Ti I-King.

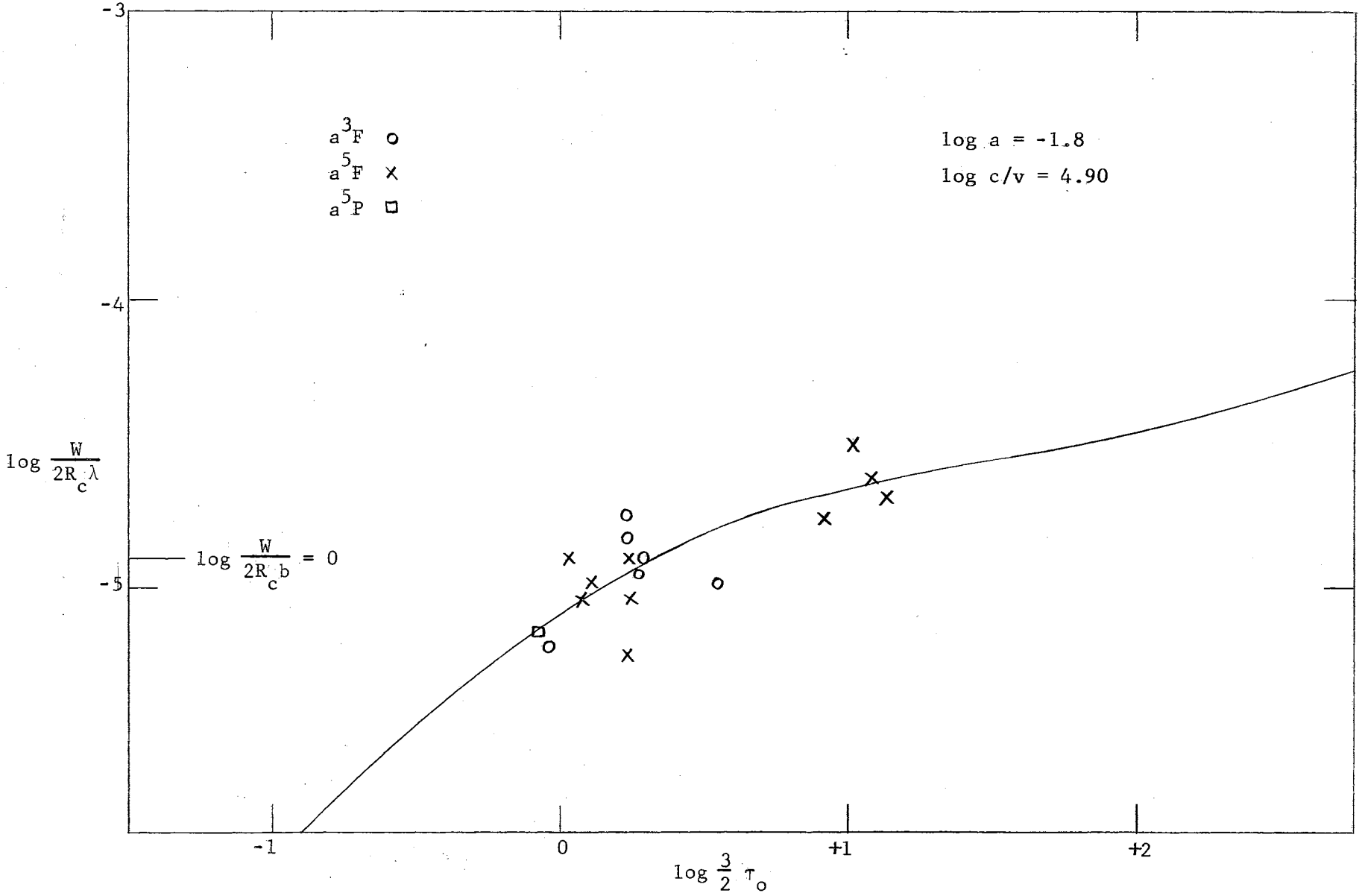

Figure 23. Schuster-Schwarzschild Pure Absorption Curve of Growth for Ti I-King.

Results for Ti II

NBS f-values and values derived from Wright's solar log X_f's were combined for use in the study of the Ti II lines. Table IX gives the results obtained. Since the values of $\overline{\chi}_e$ were the same for the a^2P and b^4P terms, these were combined to form a single plot defining a large portion of the curve of growth. This plot was used to determine both the values of log c/v and log a. The b^2D and a^2H terms were also combined since the respective values of $\overline{\chi}_e$ were practically the same.

The excitation temperatures found from this set of lines are very uncertain. This is made apparent by the four very different values obtained from the application of the four idealized models. The range of χ_e represented by the Ti II lines is quite small. In such a situation, small changes in the values of Δlog X can result in a relatively large change in the slope of the best straight line relating Δlog X and $\overline{\chi}_e$, thus producing a large variation in the excitation temperature.

Figure 24 gives the plots of the data pertaining to the excitation temperature determinations. Figures 25, 26, 27, and 28 are the curves of growth obtained for Ti II.

TABLE IX

CURVE OF GROWTH DATA DERIVED FROM Ti II LINES

				M-E Model				S-S Model			
				Scattering		Absorption		Scattering		Absorption	
log c/v				4.95		5.05		5.00		5.07	
log a				-1.8		-1.3		-1.8		-1.3	
Term	$\bar{\chi}_e$	No. of Lines	Weight	Δlog X	Shift	Δlog X	Shift	Δlog X	Shift	Δlog X	Shift
a^2D	1.08	5	1	6.89	7.72	7.08	7.75	6.82	7.75	6.98	7.66
a^2G	1.13	1	0	6.78	7.64	7.00	7.70	6.72	7.69	6.93	7.64
a^4P	1.17	4	1	6.92	7.81	7.12	7.84	6.84	7.85	7.06	7.80
a^2P	1.23	4	2	7.11	8.05	7.29	8.05	7.00	8.06	7.22	8.00
b^4P	1.23	3									
b^2D	1.57	3	1	6.92	8.12	7.12	8.09	6.75	8.10	7.02	8.01
a^2H	1.56	1									
b^2G	1.88	2	1	6.38	7.82	6.78	7.94	6.18	7.80	6.68	7.87
b^2P	2.05	4	1	6.38	7.95	6.62	7.89	6.24	8.00	6.55	7.84
θ				0.764		0.619		0.860		0.631	
Excitation Temperature (^oK)				6600 ± 478		8141 ± 614		5861 ± 357		7985 ± 608	
log u				1.78		1.86		1.75		1.86	

TABLE IX (Continued)

		M-E Model		S-S Model	
		Scattering	Absorption	Scattering	Absorption
Weighted Shift		7.93	7.94	7.95	7.88
Abundance	log $N/\rho\bar{\pi}$	17.06	17.05		
	log NH			17.00	16.79

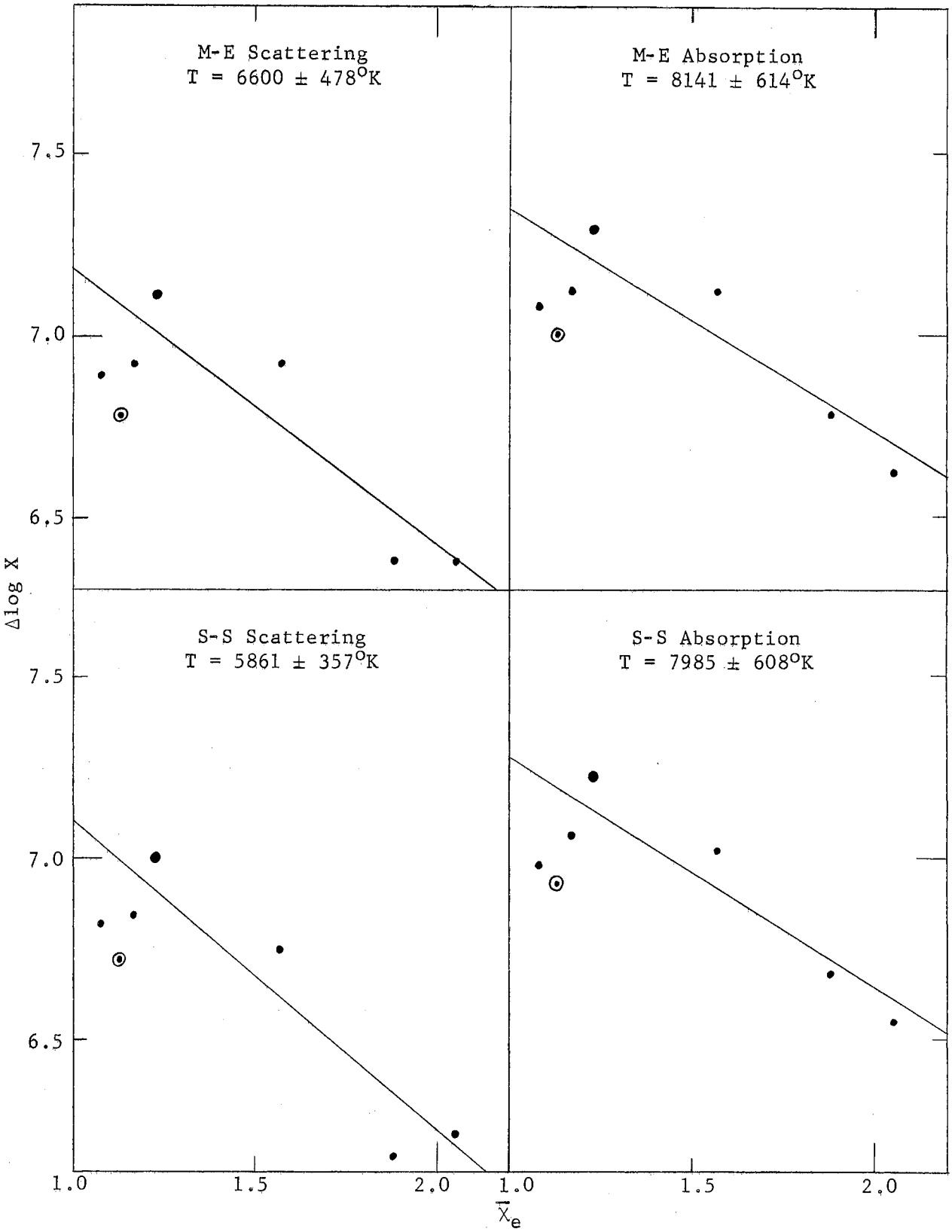

Figure 24. Excitation Temperatures Derived From Ti II Lines.

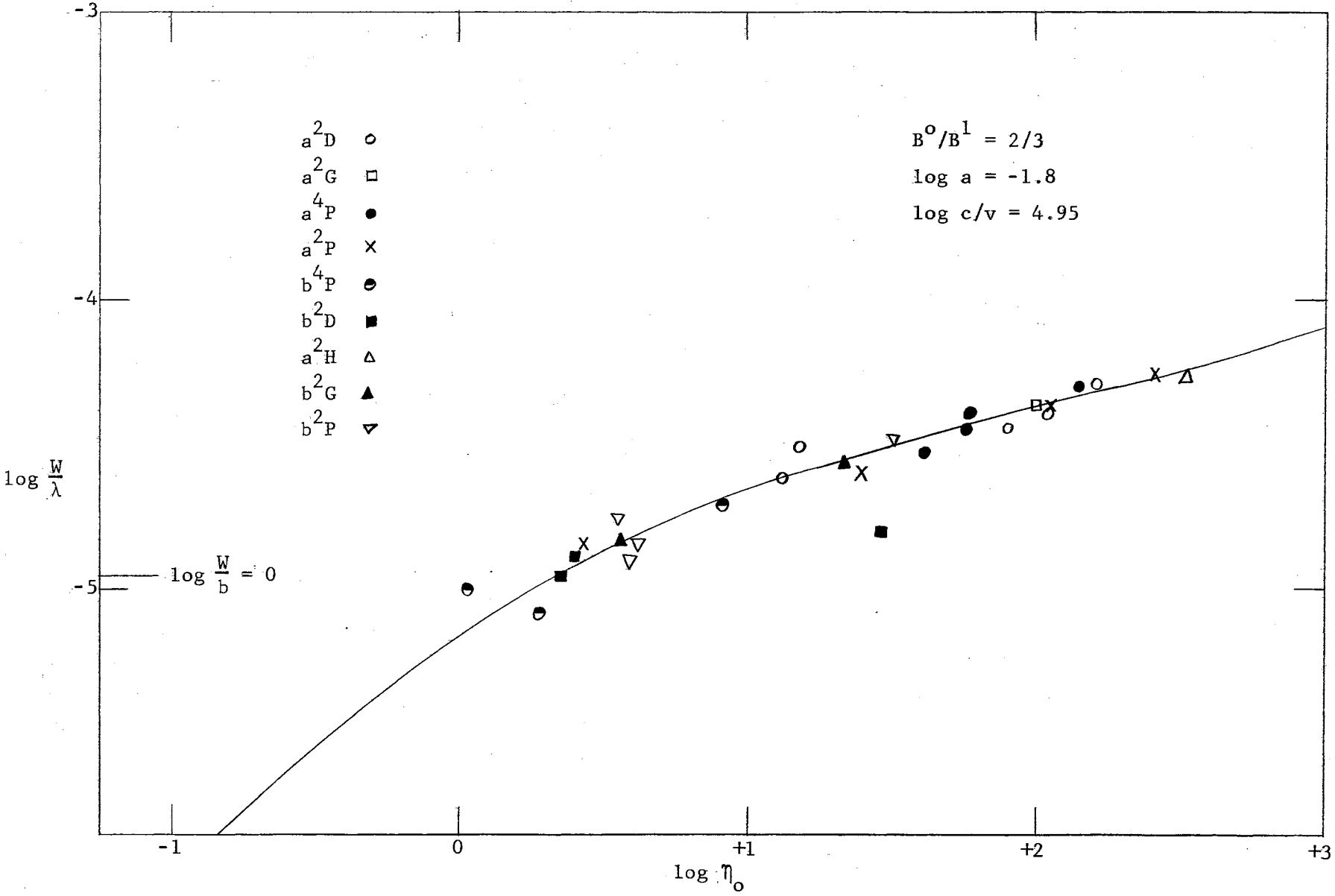

Figure 25. Milne-Eddington Pure Scattering Curve of Growth for Ti II.

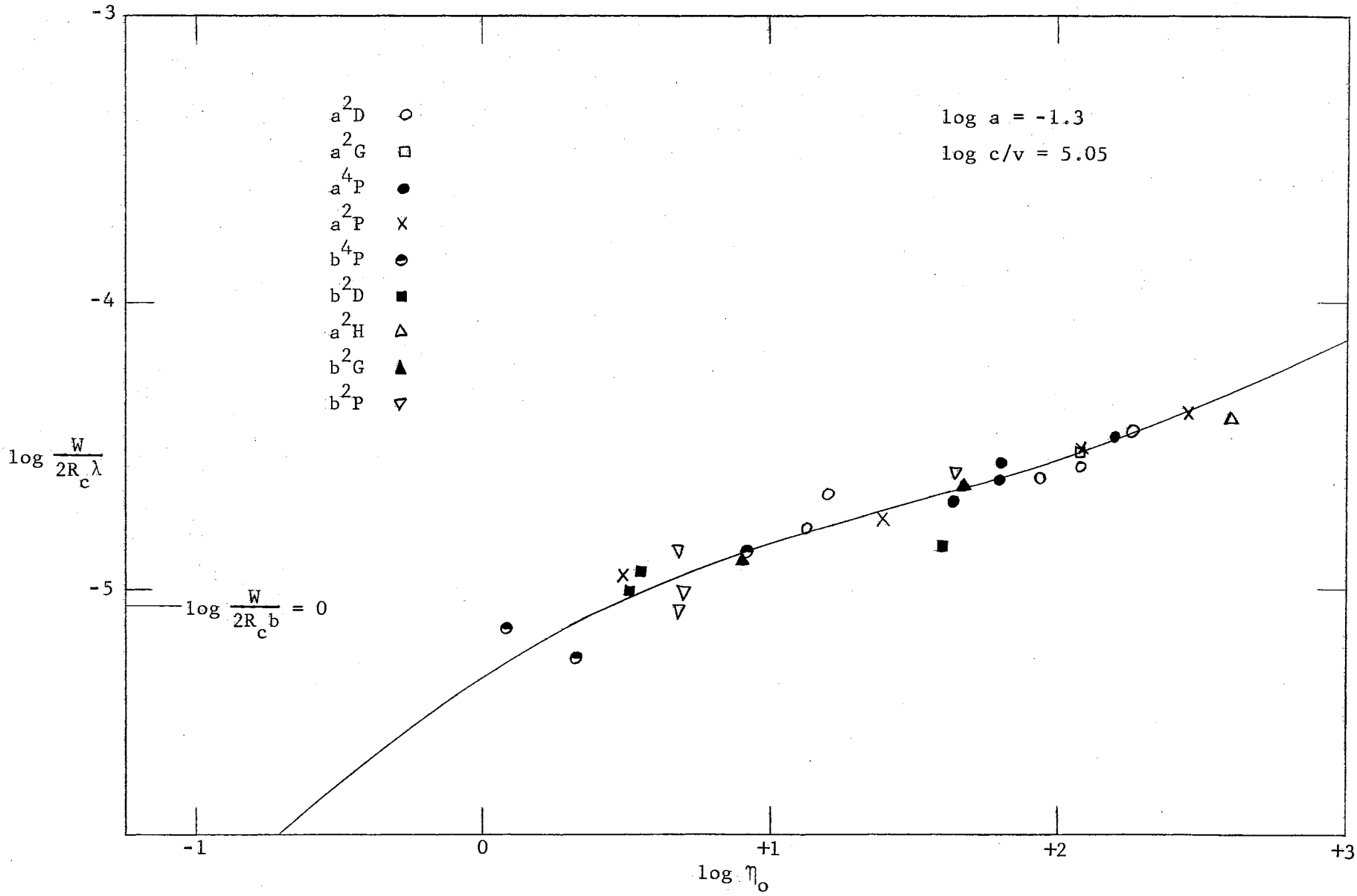

Figure 26. Milne-Eddington Pure Absorption Curve of Growth for Ti II.

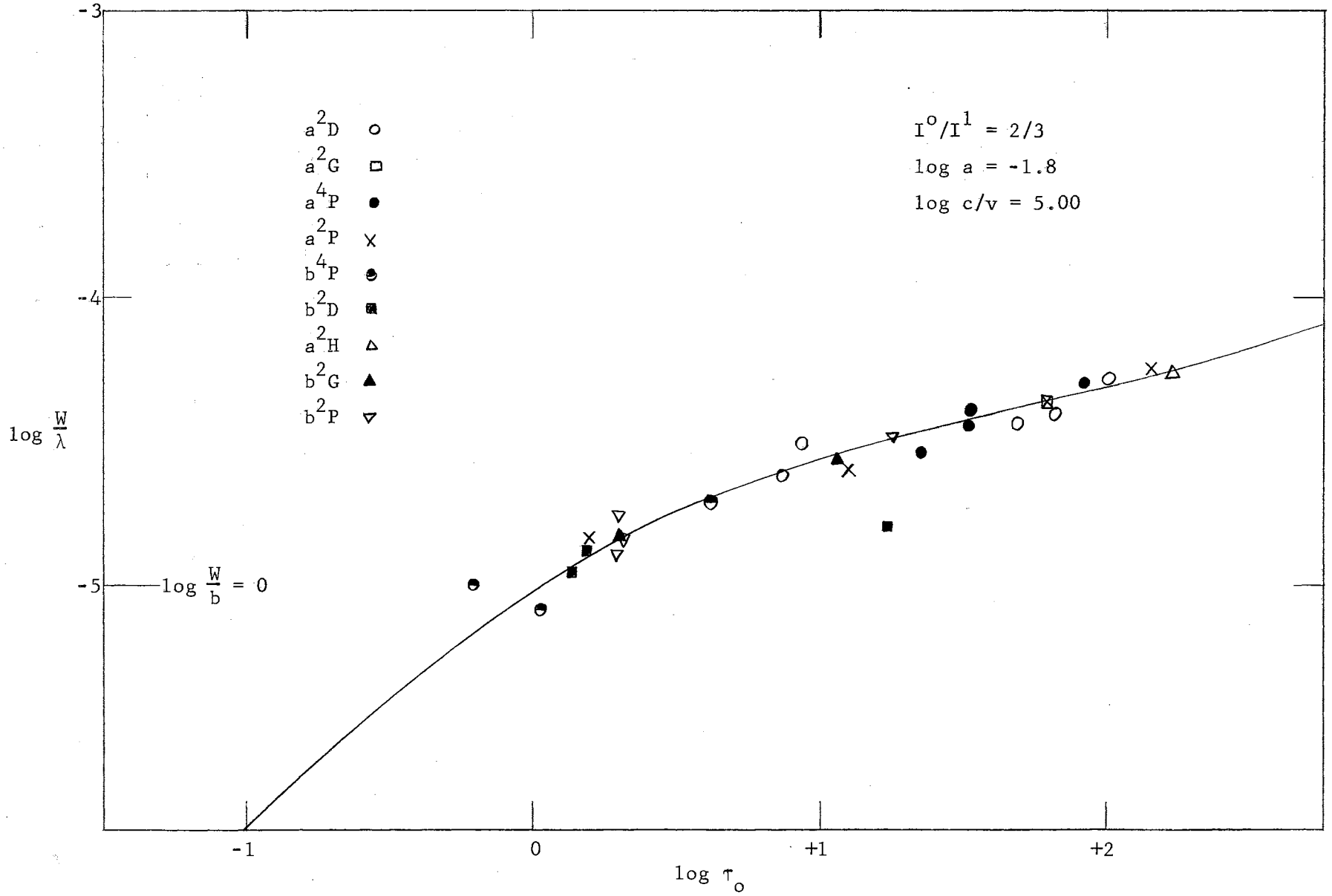

Figure 27. Schuster-Schwarzschild Pure Scattering Curve of Growth for Ti II.

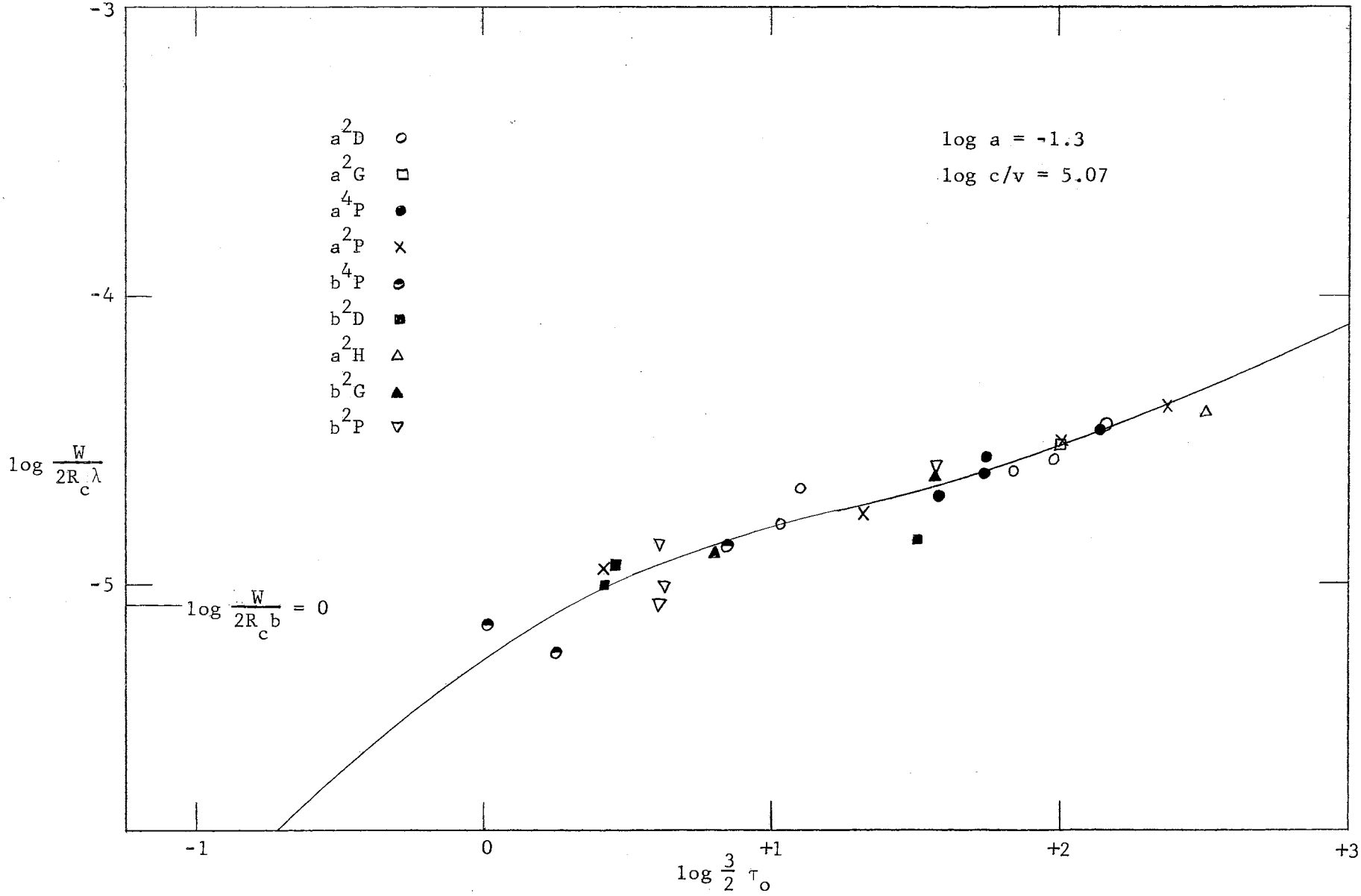

Figure 28. Schuster-Schwarzschild Pure Absorption Curve of Growth for Ti II.

Results for Cr I

Cr I-NBS

The results for Cr I-NBS are given in Table X. The a^5D plot was used to determine log c/v. The scatter of the points in the a^5D plot was quite large, making the determination of log c/v rather uncertain. Also, the points representing the two weakest lines of the a^5D term were separated a large distance from the other points on the plot. Hence, these two weak lines exerted considerable influence in the determination of log c/v. Since the possible effects of blending are most serious for weak lines, this influence leads to uncertainty in the values of log c/v.

An attempt was made to determine the values of log a by comparing plots of Δlog X versus $\overline{\chi}_e$ from fittings on theoretical curves with various values of log a to see which gave the best straight lines. The values of log a decided upon in this manner, and listed in Table X, are very uncertain due to the large scatter of the points.

Figures 29, 30, 31, 32, and 33 present the plots illustrating the least squares determinations of the excitation temperatures and the curves of growth obtained for each of the four models.

TABLE X

CURVE OF GROWTH DATA DERIVED FROM Cr I-NBS LINES

				M-E Model				S-S Model			
				Scattering		Absorption		Scattering		Absorption	
	log c/v			4.70		4.65		4.95		4.80	
	log a			-1.8		-1.8		-1.4		-1.8	
Term	$\overline{\chi}_e$	No. of Lines	Weight	Δlog X	Shift	Δlog X	Shift	Δlog X	Shift	Δlog X	Shift
a^7S	0.00	3	1	5.81	5.81	5.63	5.63	6.22	6.22	5.89	5.89
a^5S	0.94	3	1	5.40	6.17	5.45	6.21	5.63	6.41	5.56	6.33
a^5D	0.99	21	3	5.33	6.14	5.22	6.02	5.50	6.32	5.37	6.19
a^5G	2.53	3	1	3.90	5.96	3.80	5.84	4.07	6.17	3.94	6.02
a^5P	2.70	5	1	3.99	6.19	3.87	6.05	4.11	6.35	4.05	6.27
z^7P^o	2.89	3	1	4.15	6.51	4.16	6.50	4.32	6.72	4.25	6.63
a^3H	2.98	2	1	3.79	6.22	3.68	6.09	3.97	6.44	3.79	6.25
b^5D	3.00	4	2	3.55	6.00	3.46	5.88	3.73	6.22	3.58	6.05
a^3G	3.08	6	2	3.62	6.13	3.52	6.01	3.78	6.34	3.64	6.18
a^3F	3.11	2	1	3.79	6.32	3.72	6.23	3.95	6.53	3.84	6.40
z^7F^o	3.14	3	1	3.43	5.99	3.38	5.92	3.62	6.23	3.52	6.11
b^3P	3.35	1	0	4.28	7.01	4.24	6.95	4.38	7.16	4.35	7.11
z^7D^o	3.38	1	0	3.79	6.54	3.72	6.45	3.89	6.70	3.83	6.62

TABLE X (Continued)

				M-E Model				S-S Model			
				Scattering		Absorption		Scattering		Absorption	
Term	$\bar{\chi}_e$	No. of Lines	Weight	Δlog X	Shift	Δlog X	Shift	Δlog X	Shift	Δlog X	Shift
a^3D	3.54	1	0	3.35	6.24	3.28	6.14	3.50	6.44	3.40	6.32
a^3I	3.83	4	1	2.76	5.88	2.65	5.74	2.96	6.14	2.78	5.94
a^5F	3.87	2	1	2.93	6.08	2.82	5.95	3.12	6.33	2.95	6.14
b^3F	4.09	1	0	3.53	6.86	3.43	6.73	3.72	7.11	3.57	6.94
θ				0.815		0.808		0.830		0.824	
Excitation Temperature (°K)				6187 ± 292		6239 ± 352		6071 ± 305		6114 ± 305	
log u				1.11		1.12		1.10		1.10	
Weighted Shift				6.11		6.00		6.33		6.18	
Abundance	log $N/\rho\bar{\mu}$			14.82		14.77					
	log NH							14.78		14.60	
Δlog η				2.35							

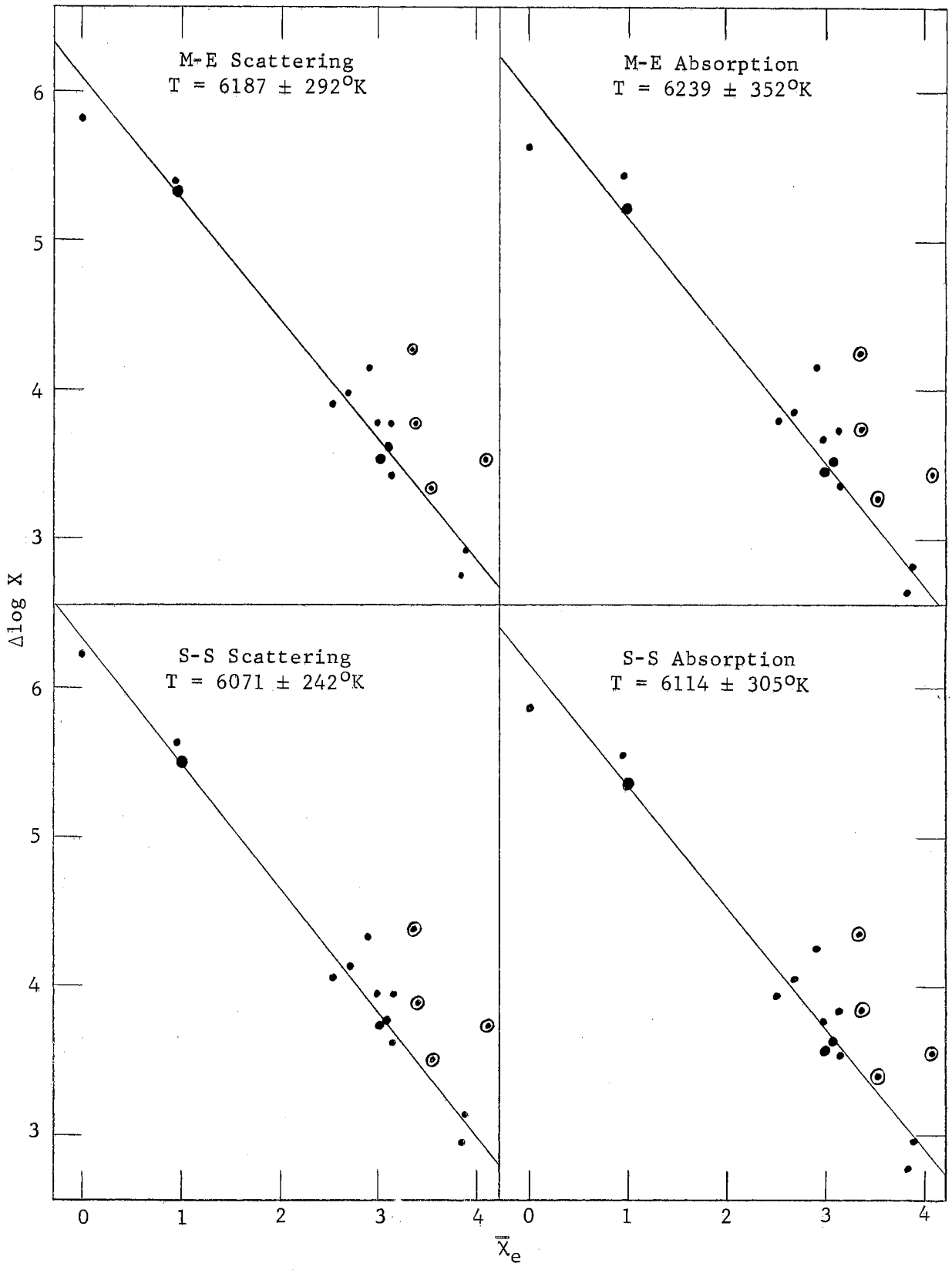

Figure 29. Excitation Temperatures Derived From Cr I-NBS Lines.

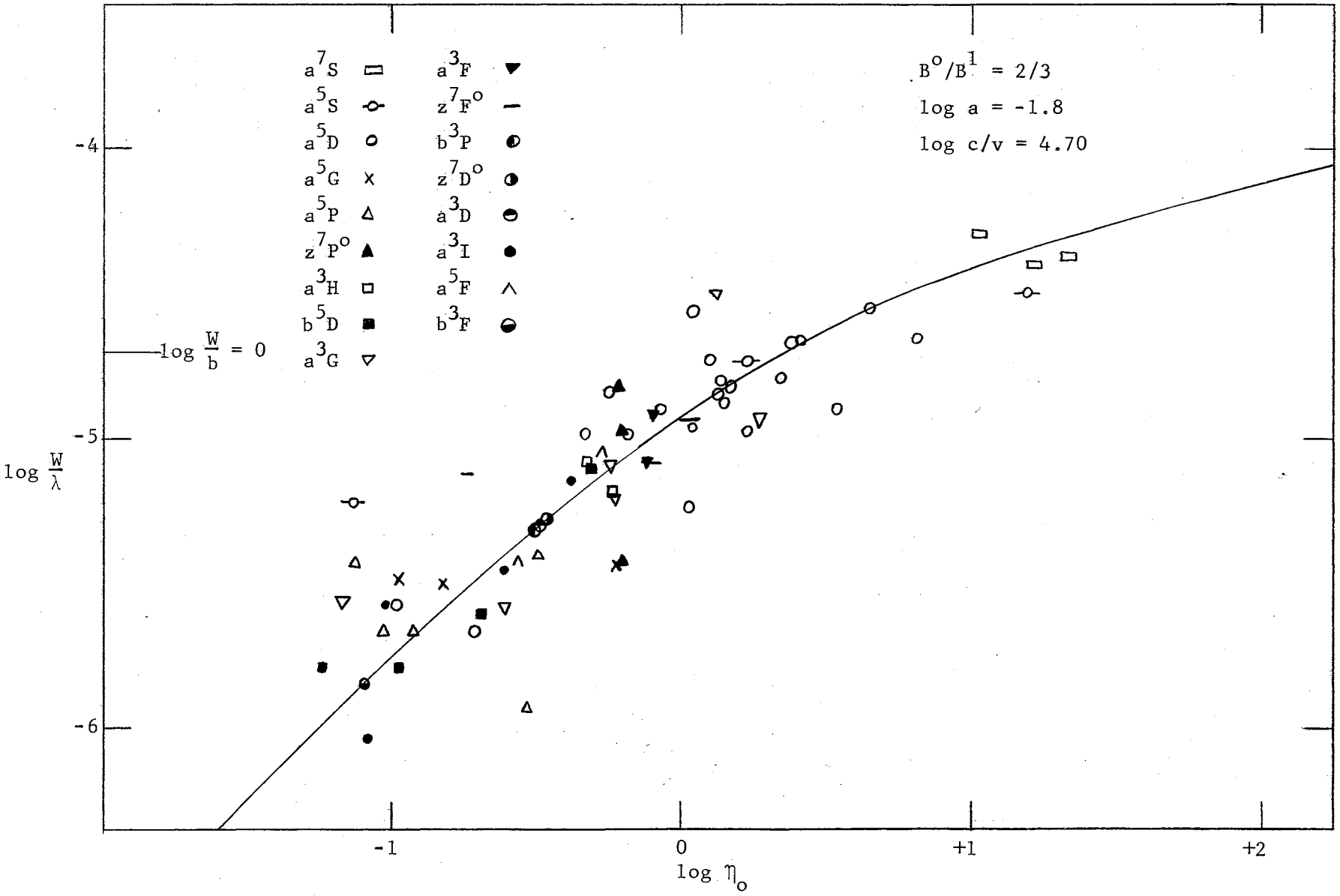

Figure 30. Milne-Eddington Pure Scattering Curve of Growth for Cr I-NBS.

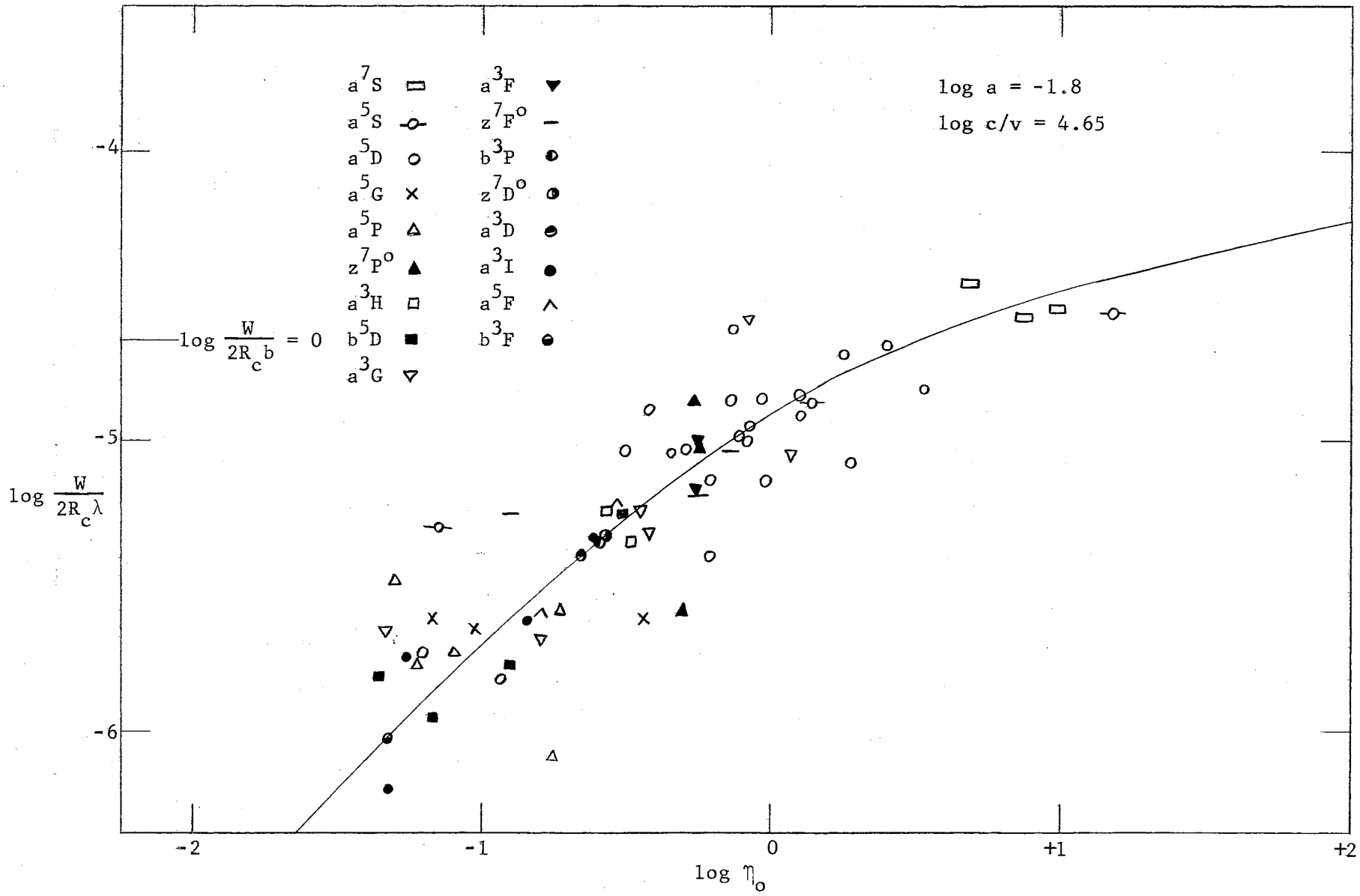

Figure 31. Milne-Eddington Pure Absorption Curve of Growth for Cr I-NBS.

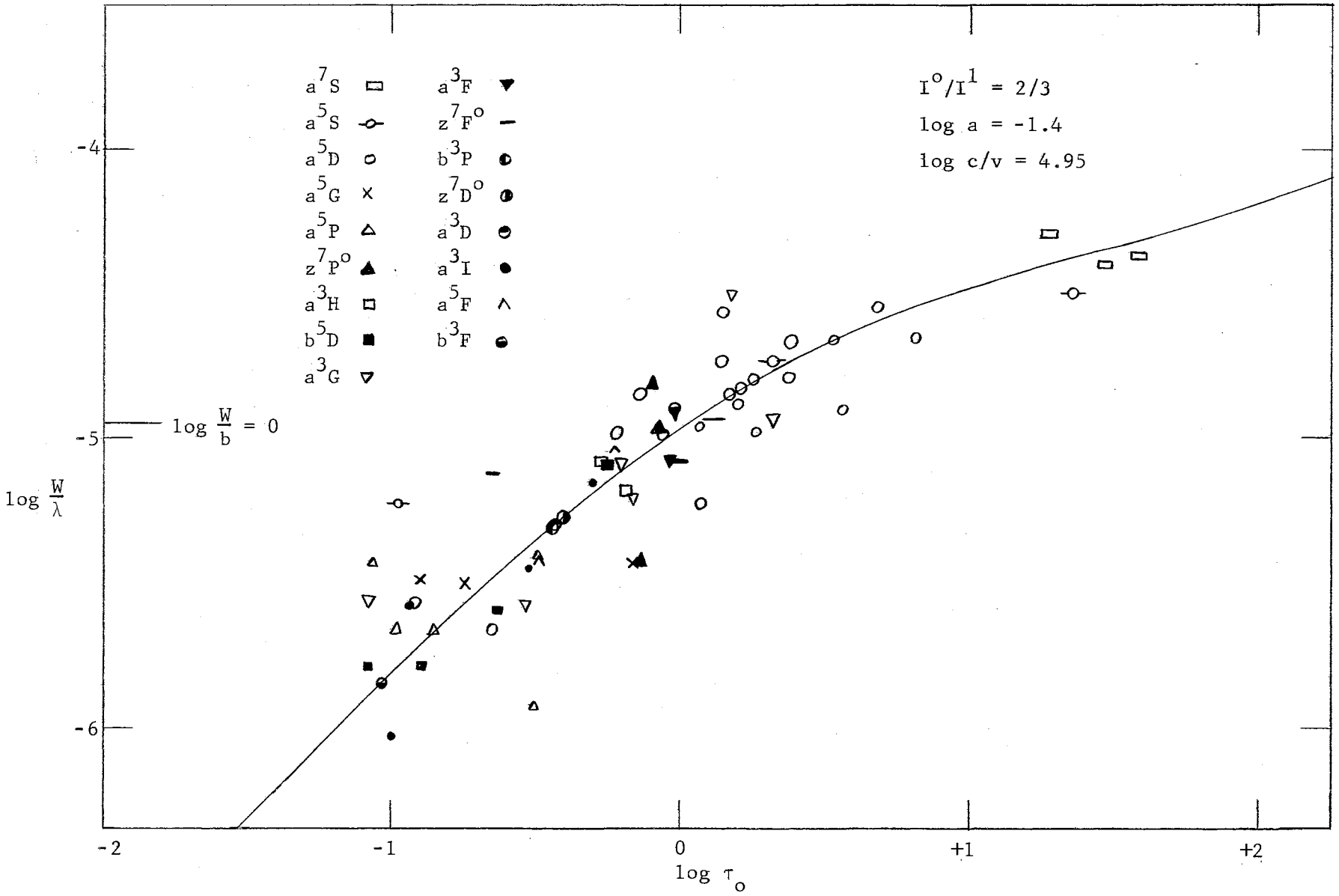

Figure 32. Schuster-Schwarzschild Pure Scattering Curve of Growth for Cr I-NBS.

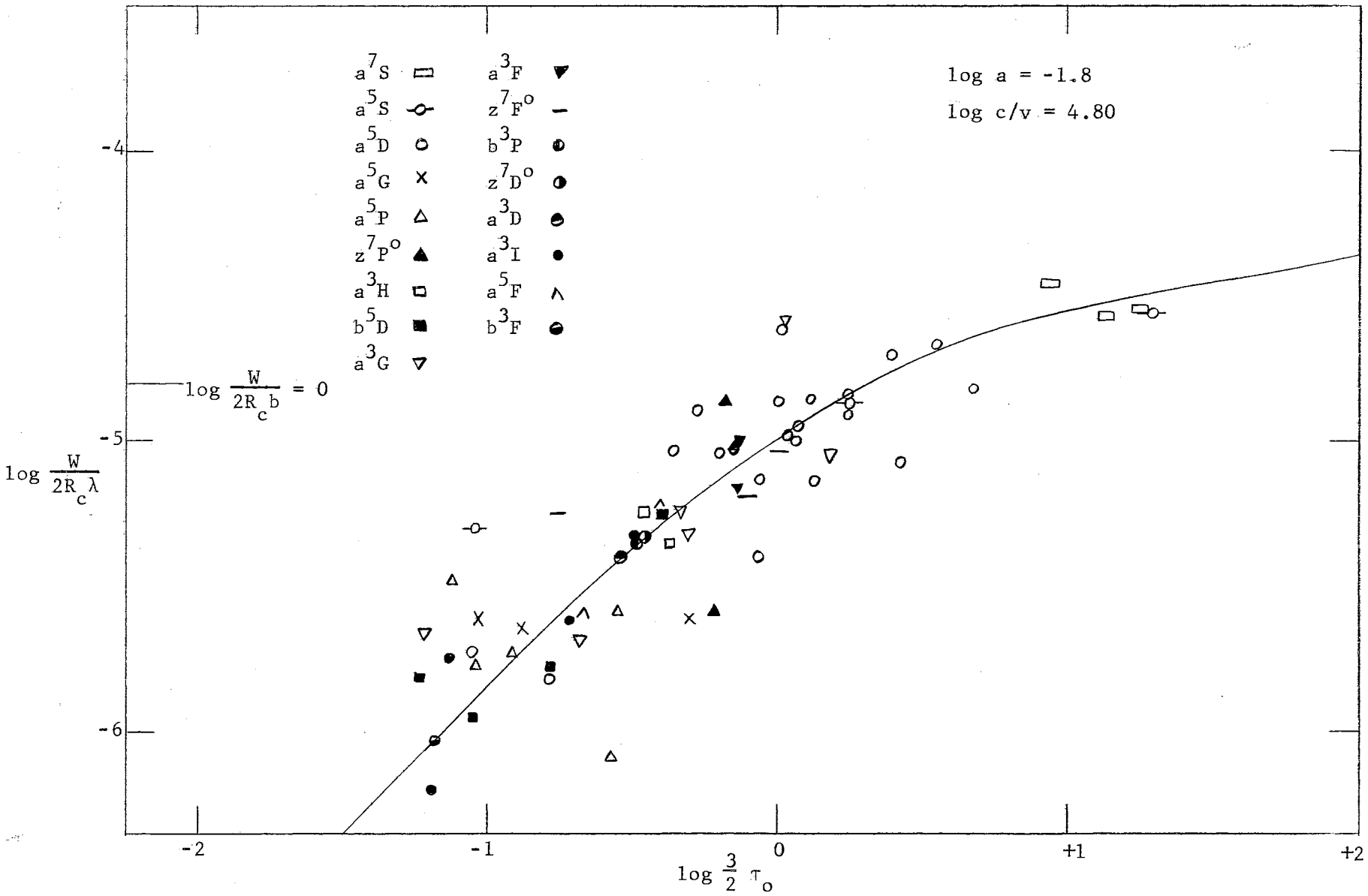

Figure 33. Schuster-Schwarzschild Pure Absorption Curve of Growth for Cr I-NBS.

Cr I-Hill

The Cr I-Hill data are presented in Table XI. The values of log c/v were determined from the a^5D plot. The values of log a were determined in the same manner as for Cr I-NBS, and are also quite uncertain.

Hill's f-values are on a relative scale, and to obtain a value of Δlog gf for use in the abundance calculations the absolute f-values of Bell et al. (1958a) were employed. These measurements are regarded as highly accurate. The value obtained for Δlog gf was -3.42.

Figure 34 presents the plots of the data and least squares straight lines used in finding the excitation temperatures. The curves of growth for Cr I-Hill are reproduced in Figures 35, 36, 37, and 38.

TABLE XI

CURVE OF GROWTH DATA DERIVED FROM Cr I-HILL LINES

				M-E Model				S-S Model			
				Scattering		Absorption		Scattering		Absorption	
		log c/v		5.05		5.00		5.10		5.05	
		log a		-1.8		-1.8		-1.8		-1.8	
Term	$\overline{\chi}_e$	No. of Lines	Weight	Δlog X	Shift	Δlog X	Shift	Δlog X	Shift	Δlog X	Shift
a^7S	0.00	3	1	3.76	3.76	3.78	3.78	3.68	3.68	3.82	3.82
a^5S	0.94	2	1	2.80	3.87	2.95	4.04	2.67	3.73	2.90	3.98
a^5D	0.99	15	3	2.67	3.79	2.65	3.80	2.49	3.60	2.57	3.71
a^5G	2.53	1	0	0.18	3.05	0.03	2.97	0.11	2.95	0.03	2.95
a^5P	2.70	2	0	0.01	3.07	-0.12	3.02	-0.05	2.98	-0.09	3.02
z^7P^o	2.89	3	2	0.53	3.80	0.49	3.85	0.36	3.61	0.45	3.78
a^3H	2.98	2	1	0.42	3.80	0.28	3.75	0.33	3.68	0.28	3.72
b^5D	3.00	1	0	0.36	3.76	0.22	3.71	0.25	3.62	0.20	3.66
a^3G	3.08	3	1	0.22	3.71	0.10	3.68	0.14	3.60	0.10	3.65
a^3F	3.11	2	1	0.55	4.07	0.54	4.16	0.41	3.91	0.47	4.06
z^7F^o	3.17	2	1	-0.03	3.56	-0.10	3.59	-0.16	3.40	-0.15	3.51
		θ		1.133		1.163		1.124		1.153	
Excitation Temperature (^oK)				4449 ± 146		4335 ± 182		4484 ± 151		4370 ± 182	

TABLE XI (Continued)

		M-E Model		S-S Model	
		Scattering	Absorption	Scattering	Absorption
log u		0.98	0.97	0.98	0.98
Weighted Shift		3.79	3.83	3.64	3.77
Abundance	log $N/\rho\bar{\kappa}$	15.44	15.52		
	log NH			15.24	15.24
Δlog η			2.35		

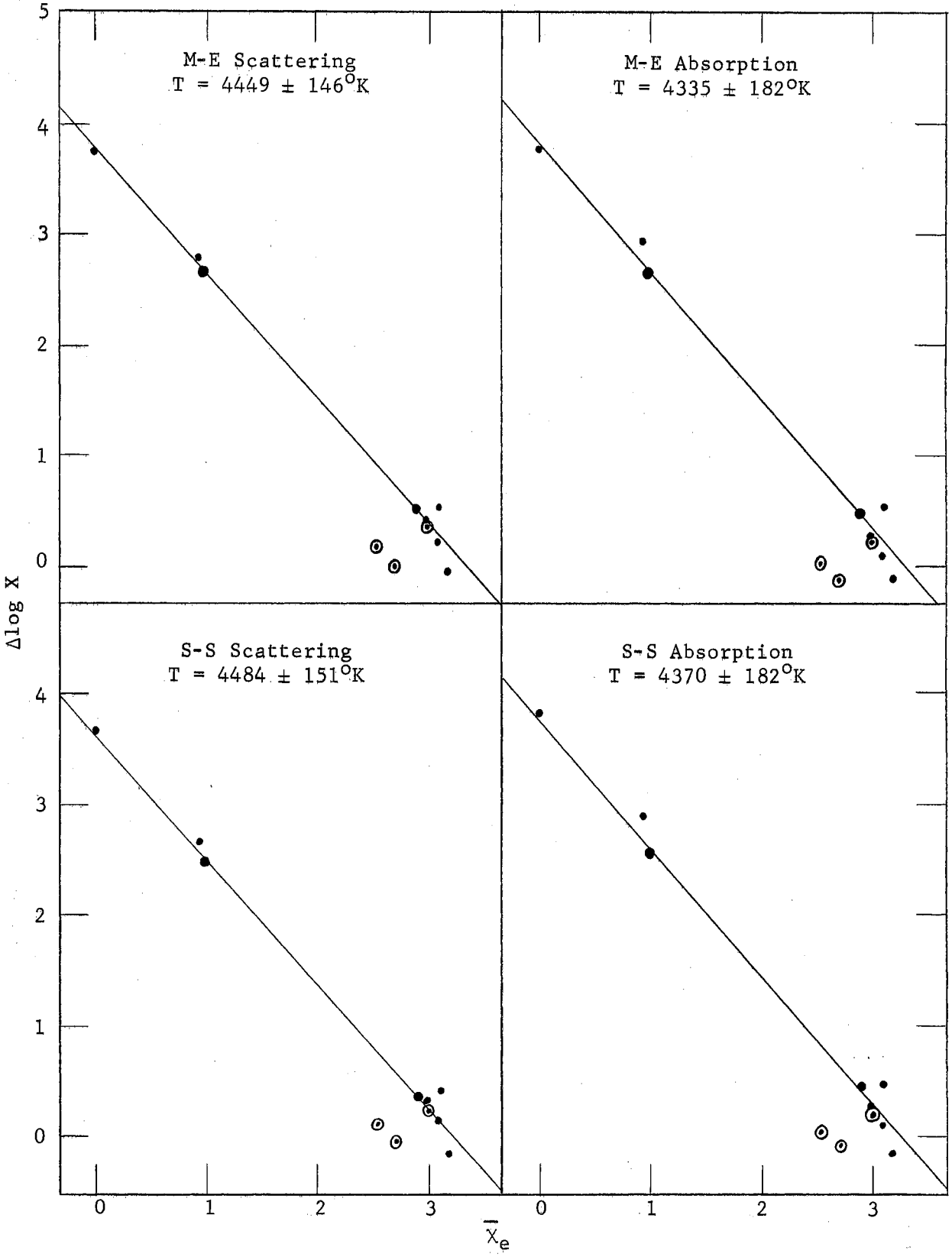

Figure 34. Excitation Temperatures Derived From Cr I-Hill Lines.

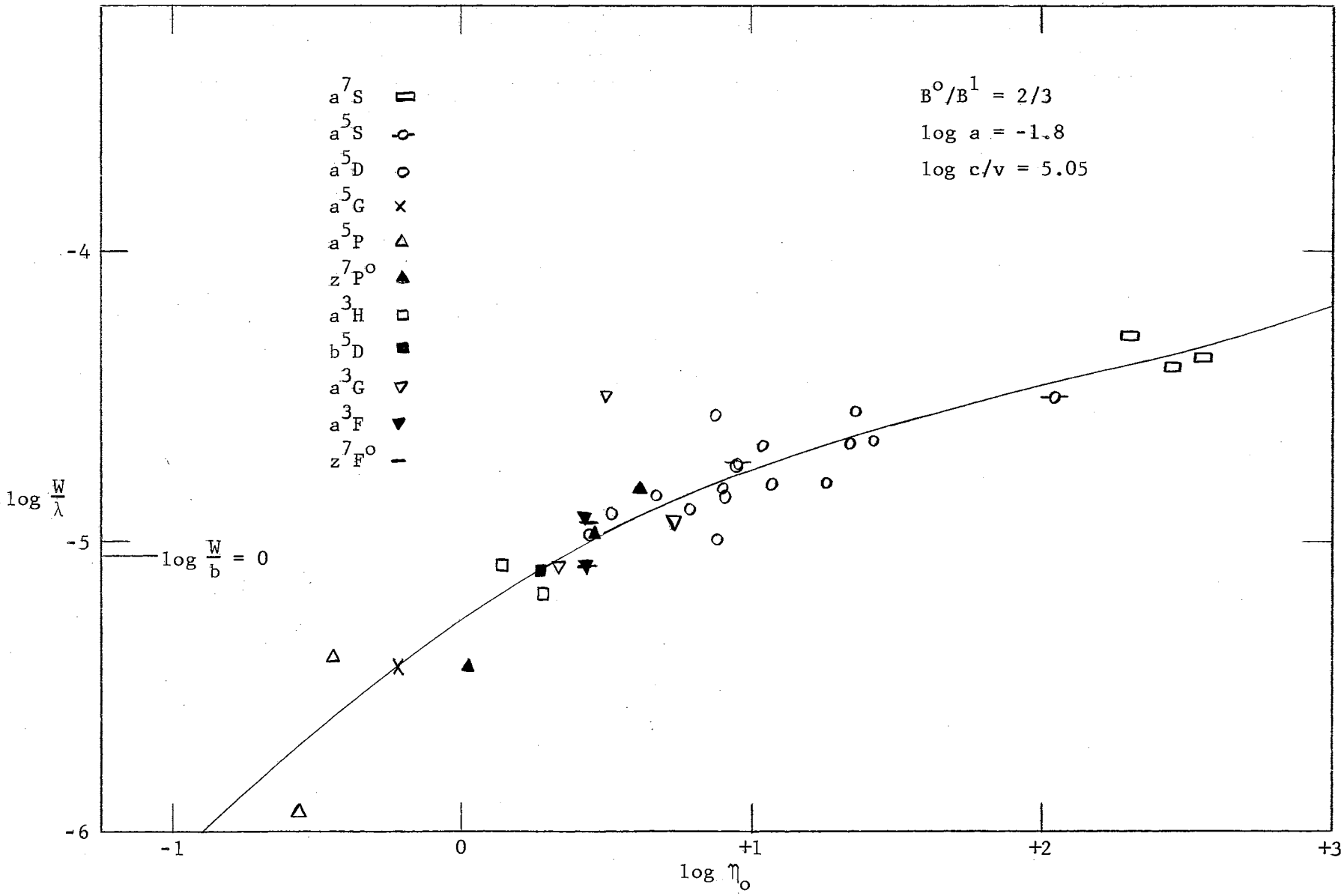

Figure 35. Milne-Eddington Pure Scattering Curve of Growth for Cr I-Hill.

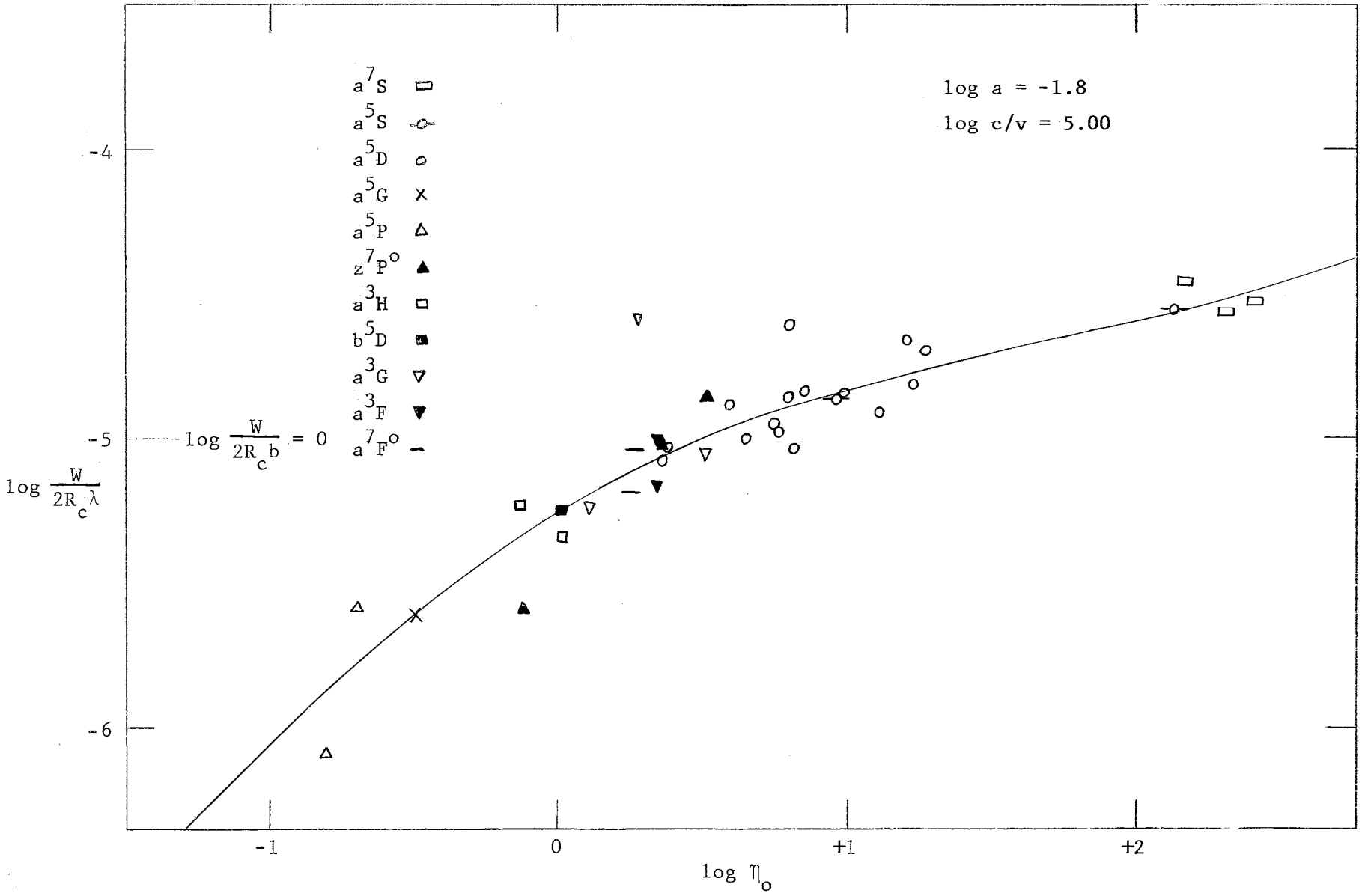

Figure 36. Milne-Eddington Pure Absorption Curve of Growth for Cr I-Hill.

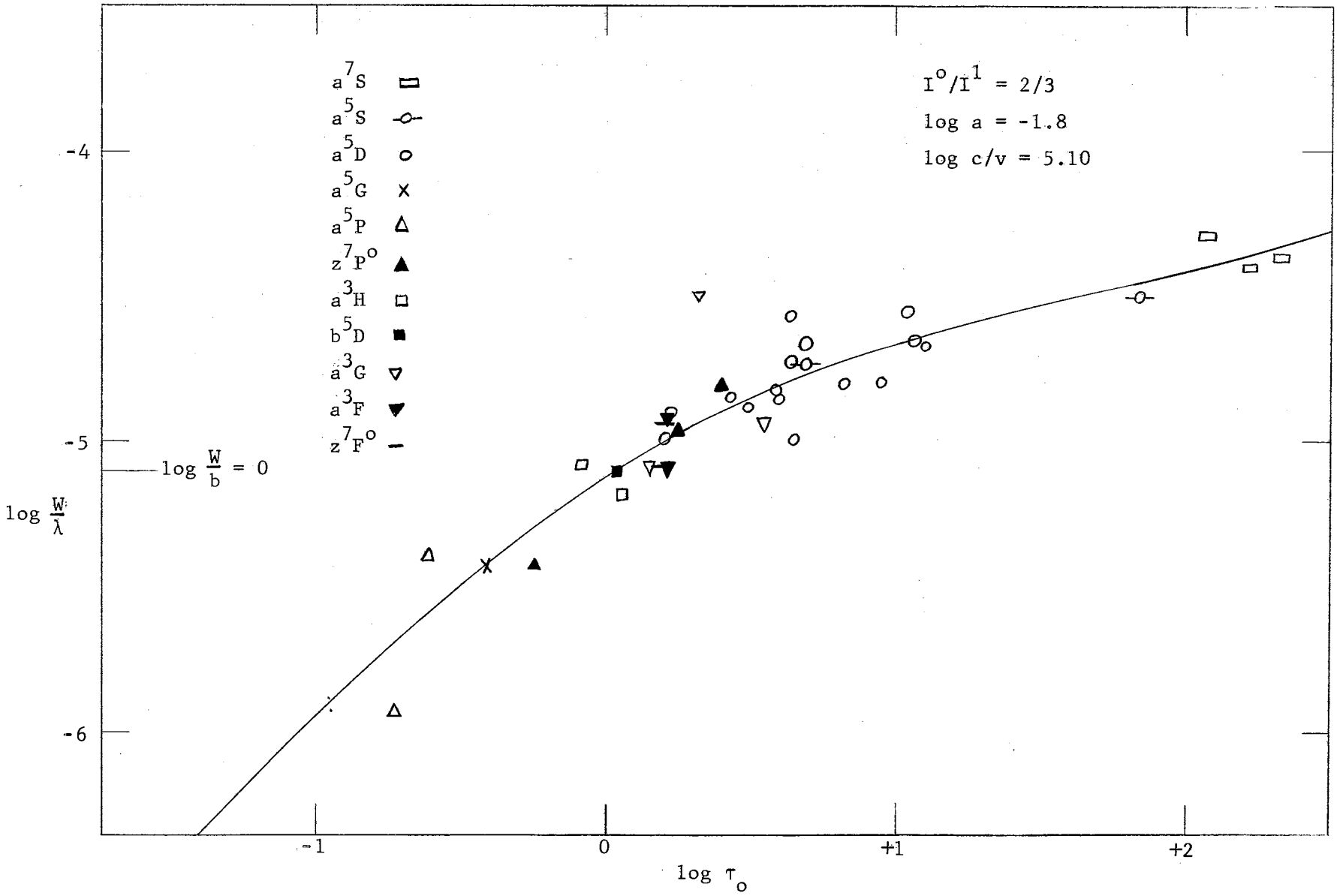

Figure 37. Schuster-Schwarzschild Pure Scattering Curve of Growth for Cr I-Hill.

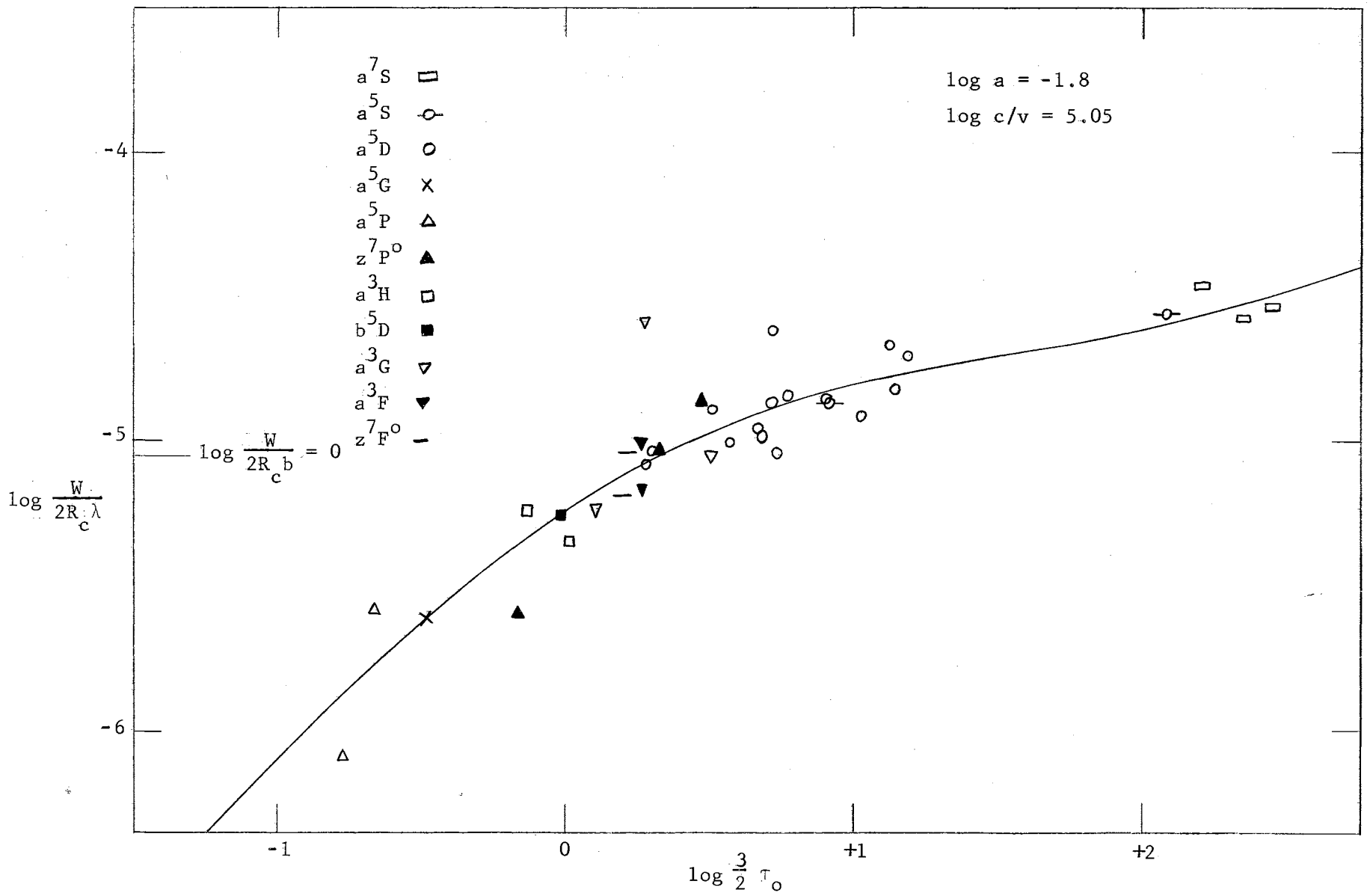

Figure 38. Schuster-Schwarzschild Pure Absorption Curve of Growth for Cr I-Hill.

Results for Mn I

The NBS f-values were employed for Mn I. Table XII gives the results obtained from the curve of growth analysis. The values of log c/v were adopted from those determined for Fe I-NBS. The values of log a were taken to be those that gave the best straight line relations between Δlog X and $\overline{\chi}_e$.

The plots illustrating the determinations of the excitation temperatures are shown in Figure 39. The curves of growth are shown in Figures 40, 41, 42, and 43.

TABLE XII

CURVE OF GROWTH DATA DERIVED FROM Mn I-LINES

				M-E Model				S-S Model			
				Scattering		Absorption		Scattering		Absorption	
log c/v				(5.06)		(5.00)		(5.07)		(5.05)	
log a				-1.4		-1.3		-1.4		-1.3	
Term	$\overline{\chi}_e$	No. of Lines	Weight	Δlog X	Shift	Δlog X	Shift	Δlog X	Shift	Δlog X	Shift
a^6S	0.00	3	1	7.38	7.38	7.22	7.22	7.22	7.22	7.24	7.24
a^6D	2.15	5	2	5.10	7.41	4.94	7.22	4.93	7.25	4.90	7.20
z^8P^o	2.29	3	0	5.75	8.21	5.84	8.27	5.58	8.05	5.93	8.38
a^4D	2.92	9	2	4.22	7.36	4.10	7.20	4.04	7.18	4.08	7.20
z^6P^o	3.06	2	1	4.20	7.49	4.05	7.29	4.06	7.36	4.05	7.32
θ				1.074		1.060		1.077		1.069	
Excitation Temperature (^oK)				4693 ± 130		4752 ± 95		4678 ± 164		4714 ± 124	
log u				0.82		0.82		0.82		0.82	
Weighted Shift				7.40		7.23		7.24		7.23	
Abundance	log $N/\rho\overline{\chi}$			15.46		15.35					
	log NH							15.29		15.12	
Δlog γ						2.05					

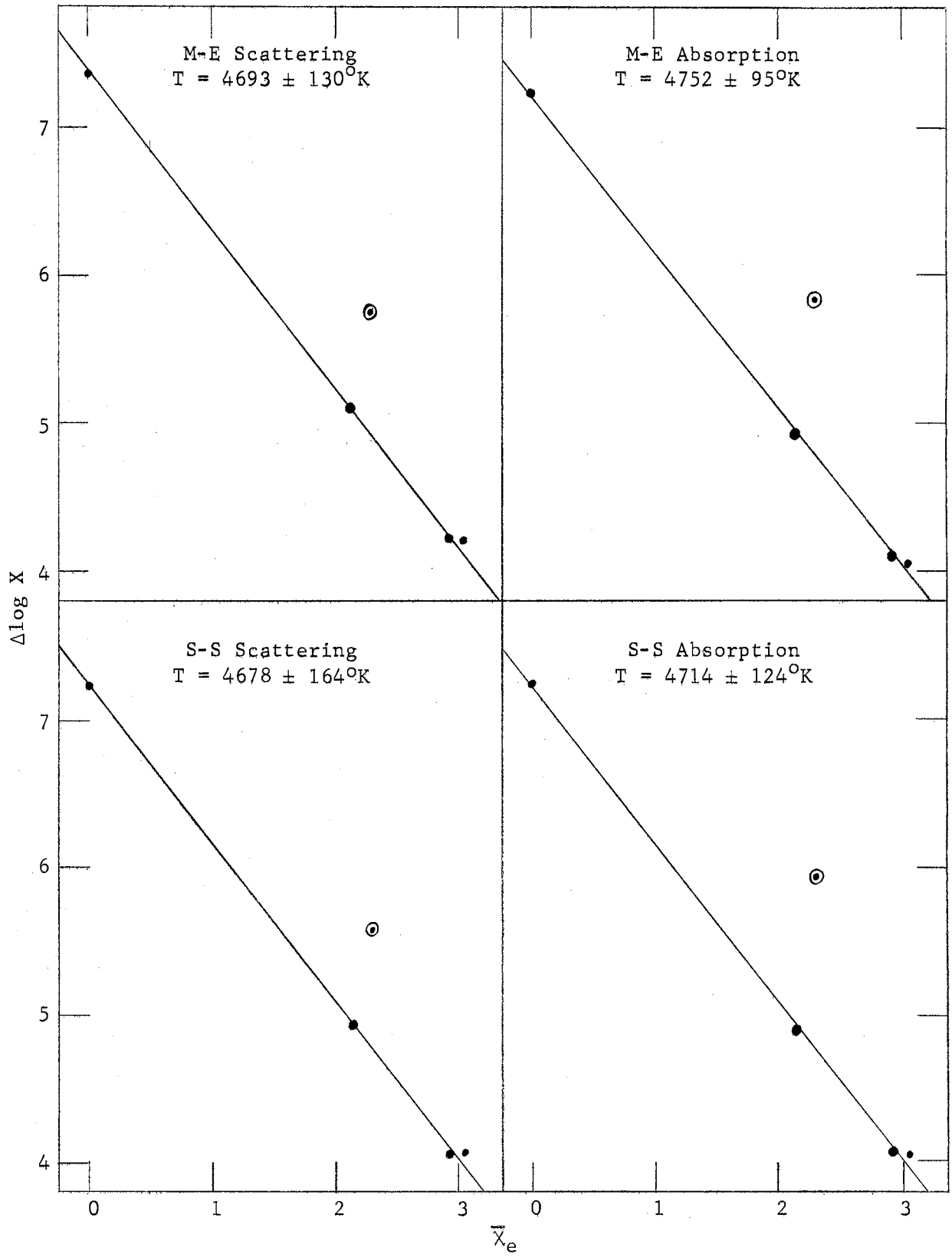

Figure 39. Excitation Temperatures Derived From Mn I Lines.

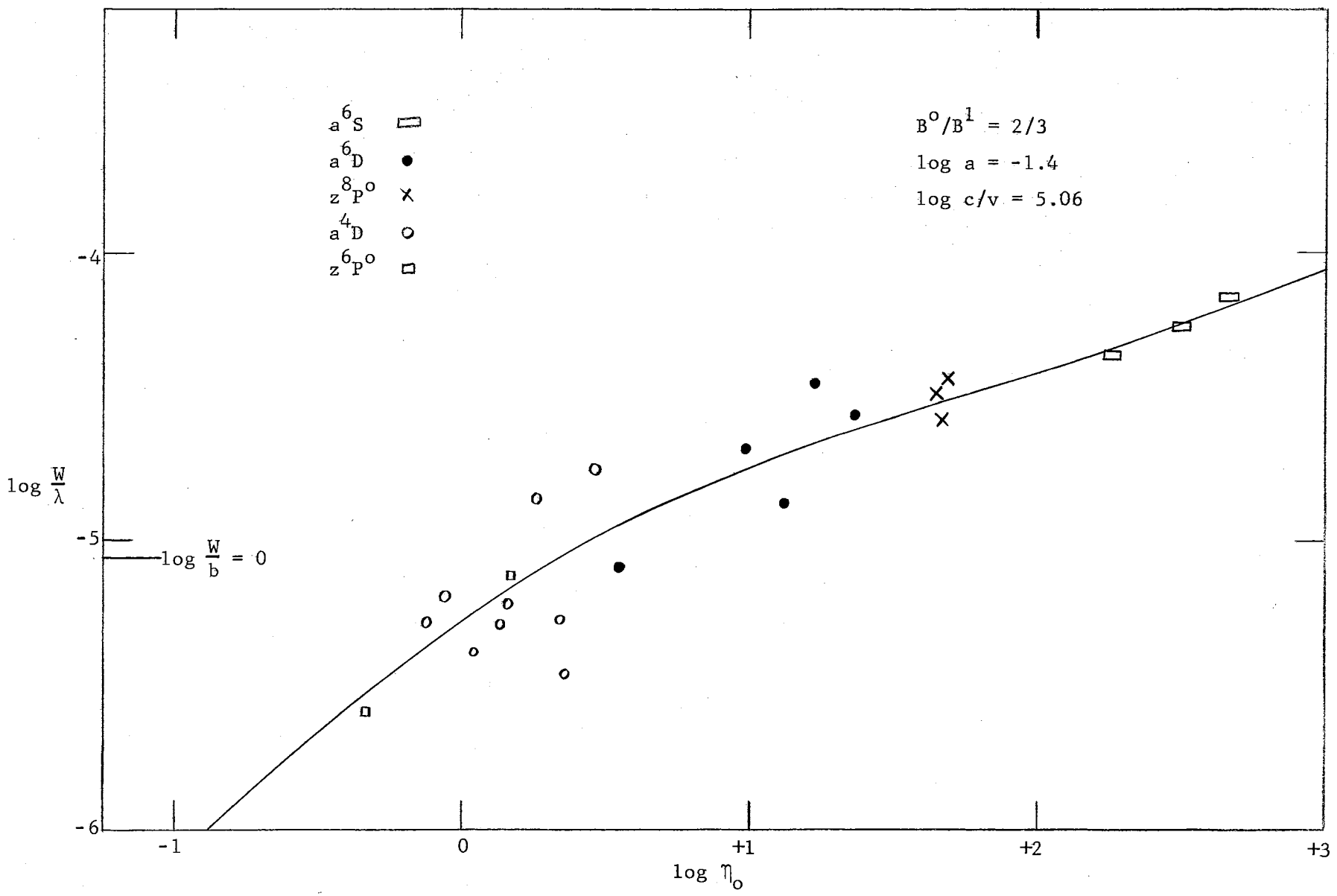

Figure 40. Milne-Eddington Pure Scattering Curve of Growth for Mn I.

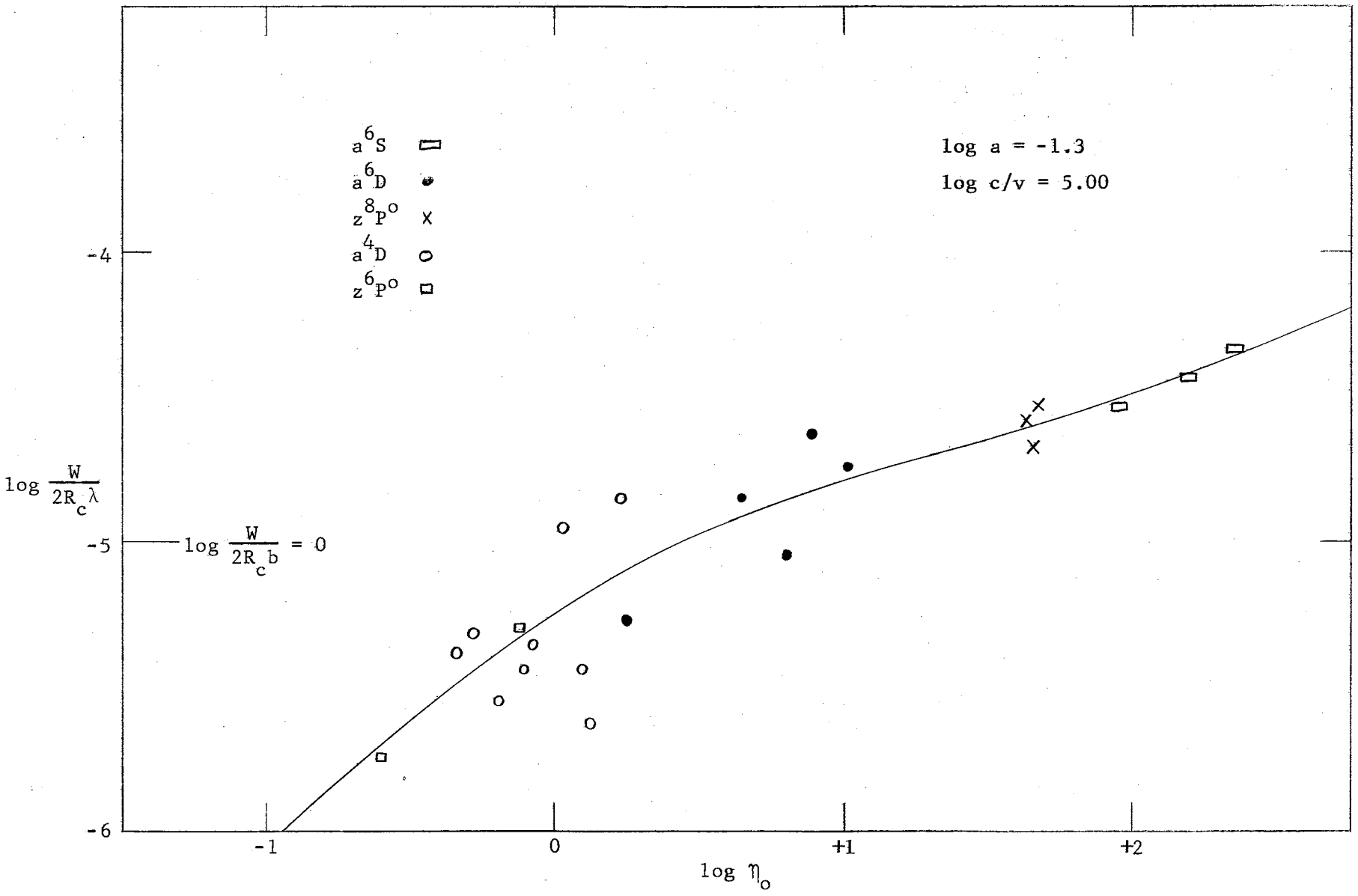

Figure 41. Milne-Eddington Pure Absorption Curve of Growth for Mn I.

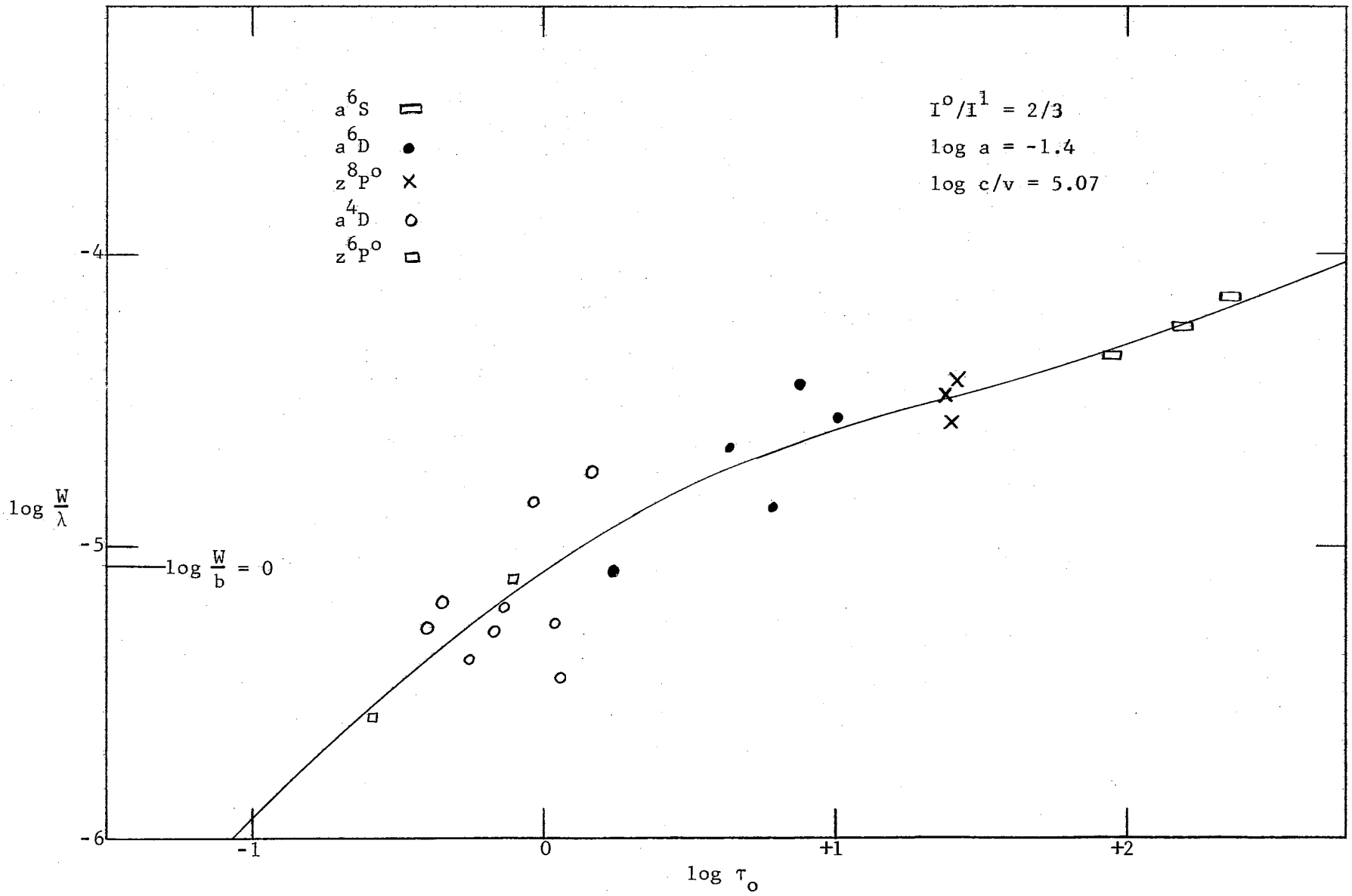

Figure 42. Schuster-Schwarzschild Pure Scattering Curve of Growth for Mn I.

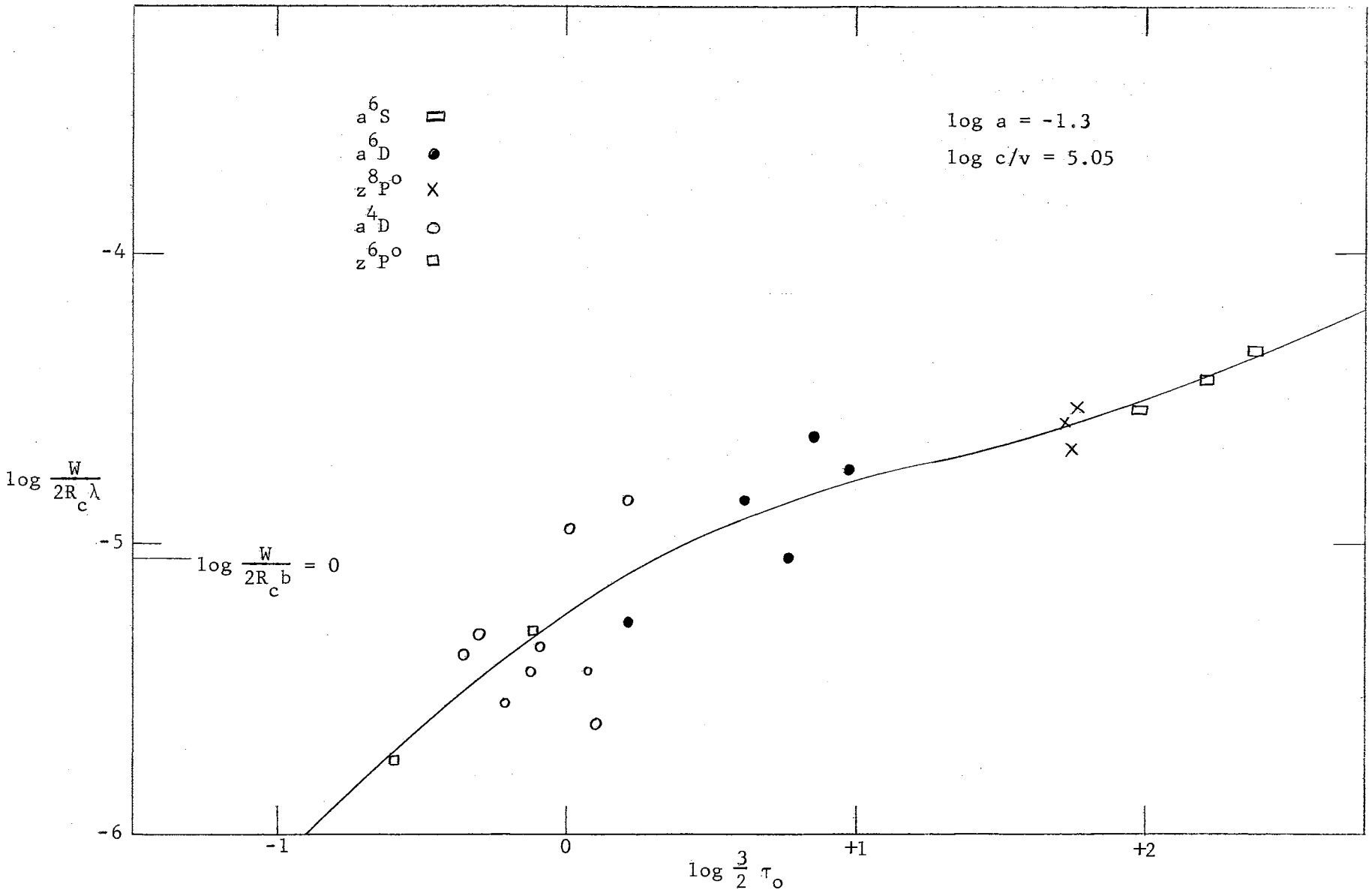

Figure 43. Schuster-Schwarzschild Pure Absorption Curve of Growth for Mn I.

Results for Fe I

Fe I-NBS

The results for Fe I-NBS are presented in Table XIII. The values of log c/v and log a were determined from the a^5P and a^3F plots. The a^5P plot fit around the knee of the curve of growth and the a^3F plot determined the damping and transition portions of the curve.

Figures 44, 45, 46, 47, and 48 give the excitation temperature plots and the curves of growth.

TABLE XIII

CURVE OF GROWTH DATA DERIVED FROM Fe I-NBS LINES

				M-E Model				S-S Model			
				Scattering		Absorption		Scattering		Absorption	
log c/v				5.06		5.00		5.07		5.05	
log a				-1.8		-1.8		-1.4		-1.8	
Term	$\bar{\chi}_e$	No. of Lines	Weight	Δlog X	Shift	Δlog X	Shift	Δlog X	Shift	Δlog X	Shift
a^5D	0.03	5	1	9.12	9.15	9.17	9.20	8.69	8.72	9.22	9.25
a^5F	0.95	12	2	8.24	9.16	8.58	9.45	7.72	8.61	8.63	9.52
a^3F	1.53	18	4	7.27	8.75	7.23	8.63	6.77	8.21	7.25	8.68
a^5P	2.19	8	3	6.55	8.67	6.62	8.62	6.19	8.25	6.60	8.65
a^3P	2.27	2	1	6.77	8.96	7.05	9.12	6.30	8.44	7.01	9.13
a^3H	2.41	4	1	6.50	8.83	6.84	9.04	6.07	8.34	6.80	9.06
z^7D^o	2.44	9	1	6.23	8.59	6.25	8.48	5.83	8.13	6.28	8.56
b^3F	2.58	3	1	6.27	8.76	6.58	8.94	5.80	8.23	6.53	8.94
b^3P	2.83	8	1	5.81	8.54	5.74	8.32	5.42	8.08	5.70	8.35
z^7F^o	2.85	8	1	6.54	9.29	6.75	9.35	6.05	8.73	6.80	9.47
z^7P^o	2.98	6	1	5.90	8.78	6.20	8.92	5.42	8.22	6.25	9.04
a^1G	3.03	2	1	5.82	8.75	5.73	8.50	5.45	8.30	5.69	8.53
z^5D^o	3.22	5	1	5.72	8.83	6.04	8.98	5.25	8.28	6.05	9.06

TABLE XIII (Continued)

				M-E Model				S-S Model			
				Scattering		Absorption		Scattering		Absorption	
Term	$\overline{\chi}_e$	No. of Lines	Weight	Δlog X	Shift	Δlog X	Shift	Δlog X	Shift	Δlog X	Shift
z^5F^o	3.37	8	1	5.77	9.03	5.97	9.05	5.32	8.49	6.04	9.19
a^1H	3.56	1	0	5.33	8.77	5.30	8.55	4.93	8.28	5.33	8.66
z^5P^o	3.62	3	1	5.40	8.90	5.80	9.11	4.96	8.37	5.69	9.08
z^3F^o	3.86	1	0	6.00	9.73	6.31	9.83	5.56	9.19	6.35	9.96
z^3D^o	3.87	1	0	4.80	8.54	6.12	9.65	5.38	9.02	6.15	9.77
y^5F^o	4.16	1	0	5.17	9.19	5.52	9.32	4.72	8.63	5.55	9.44
z^3P^o	4.19	1	0	5.20	9.25	5.48	9.31	4.78	8.72	5.40	9.32
z^5G^o	4.35	5	1	4.83	9.03	5.04	9.01	4.38	8.47	5.00	9.07
z^3G^o	4.41	3	1	4.94	9.20	5.18	9.21	4.48	8.63	5.14	9.27
y^3F^o	4.53	1	0	4.45	8.83	4.58	8.72	4.10	8.36	4.45	8.69
θ				0.966		0.913		0.941		0.936	
Excitation Temperature (^oK)				5219 ± 279		5522 ± 511		5358 ± 263		5383 ± 501	
log u				1.46		1.48		1.47		1.47	
Weighted Shift				8.87		8.89		8.36		8.94	
Abundance	log $N/\rho\overline{\pi}$			17.57		17.67					
	log NH							17.06		17.48	
Δlog η				1.79							

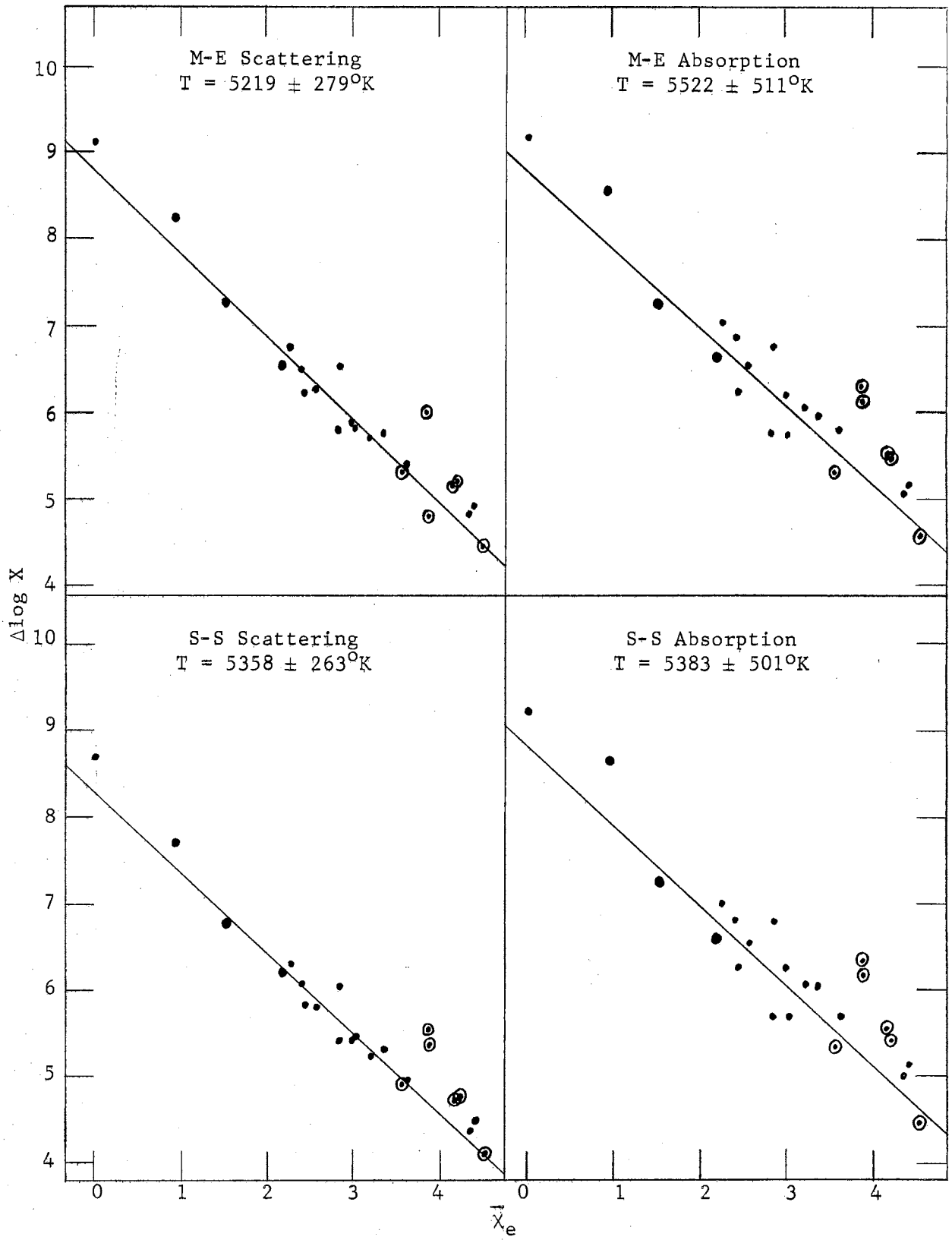

Figure 44. Excitation Temperatures Derived From Fe I-NBS Lines.

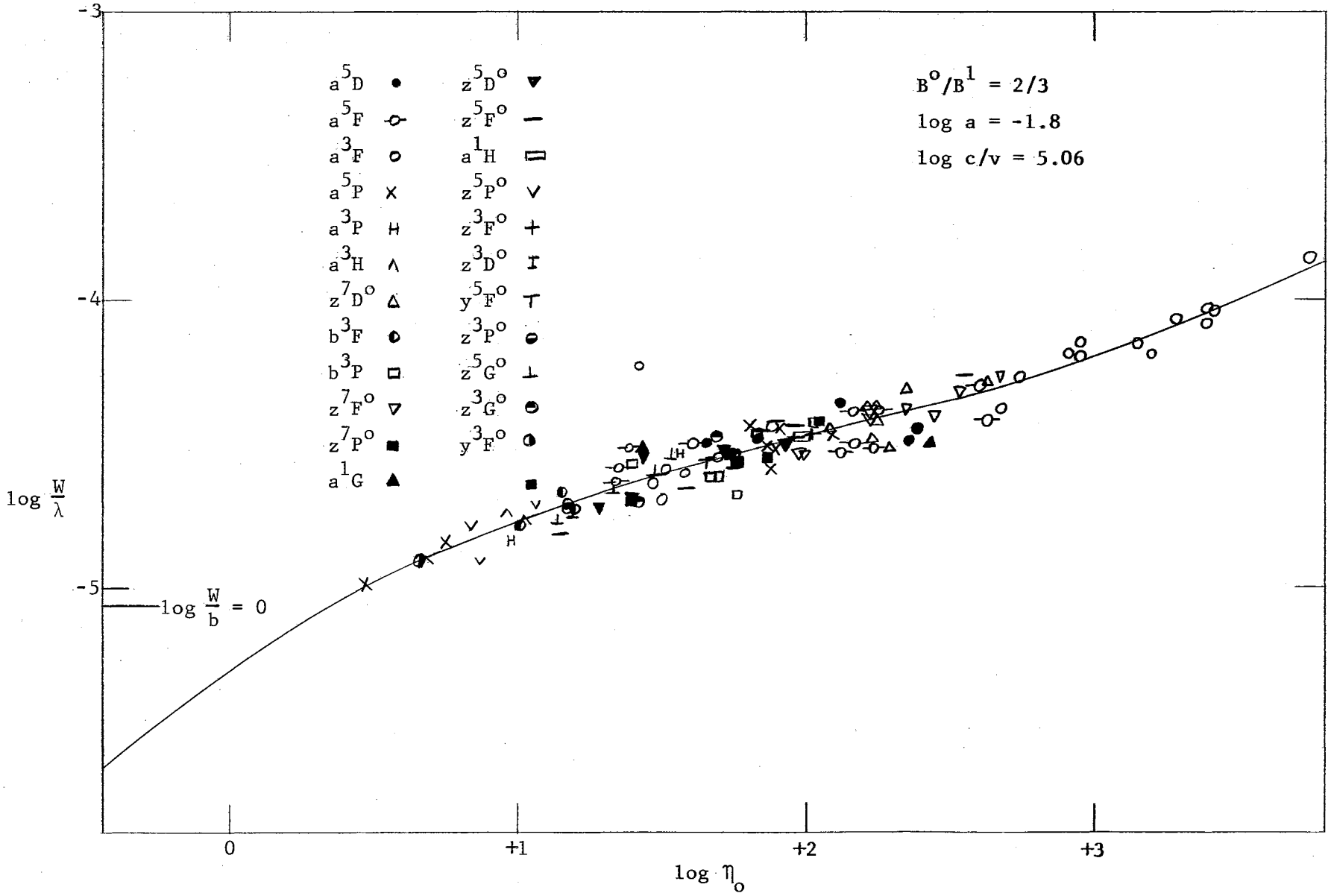

Figure 45. Milne-Eddington Pure Scattering Curve of Growth for Fe I-NBS.

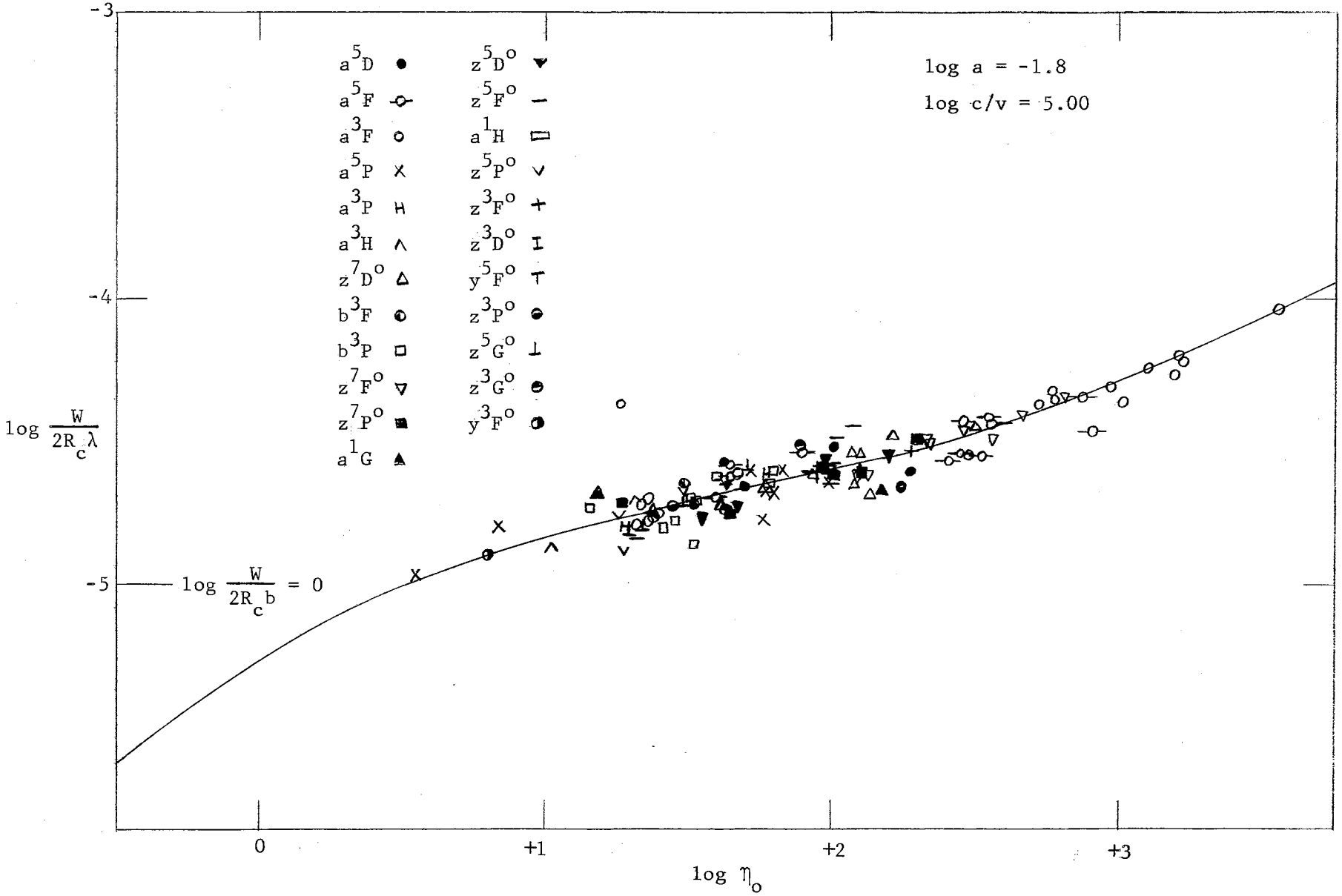

Figure 46. Milne-Eddington Pure Absorption Curve of Growth for Fe I-NBS.

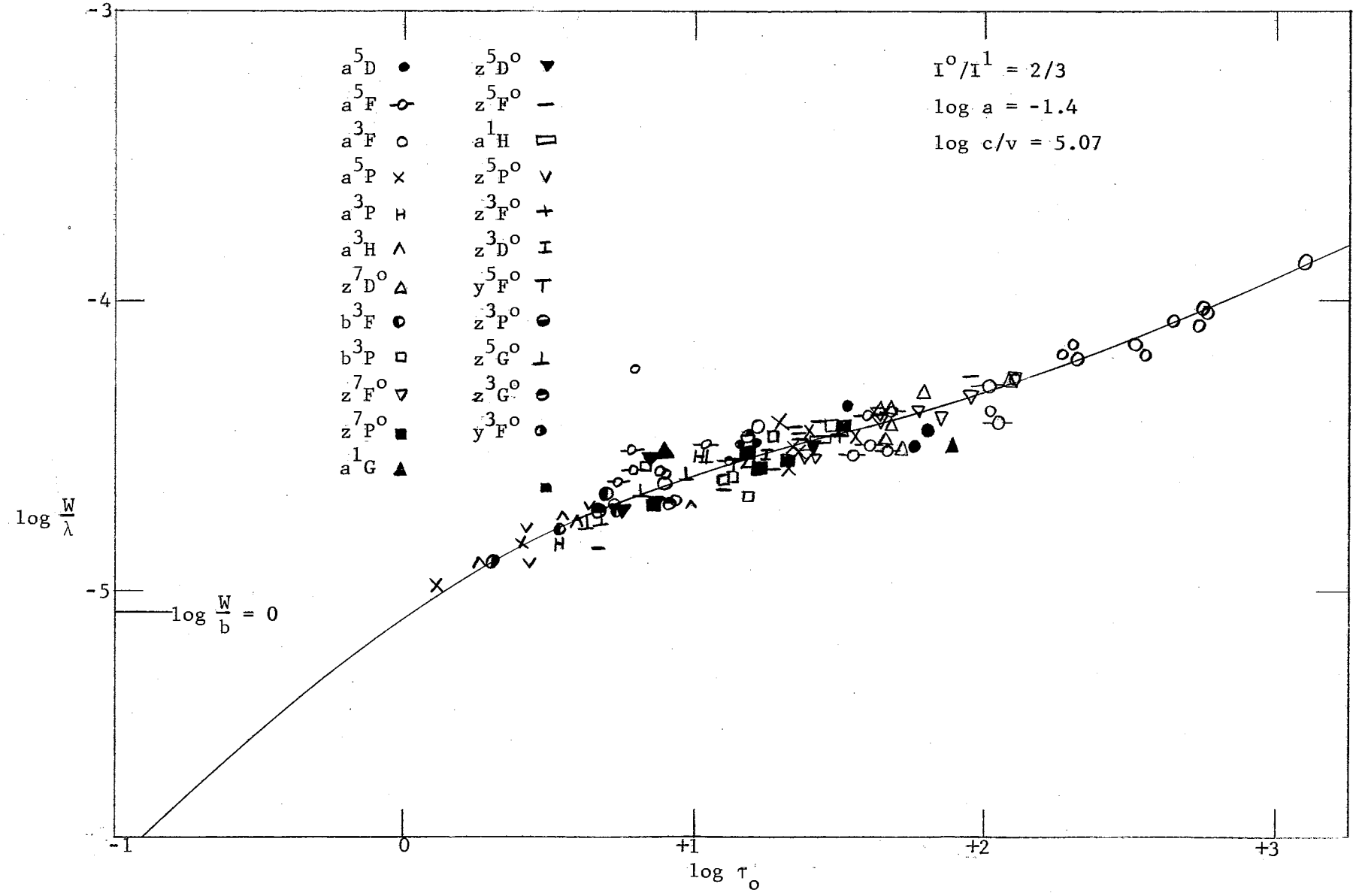

Figure 47. Schuster-Schwarzschild Pure Scattering Curve of Growth for Fe I-NBS.

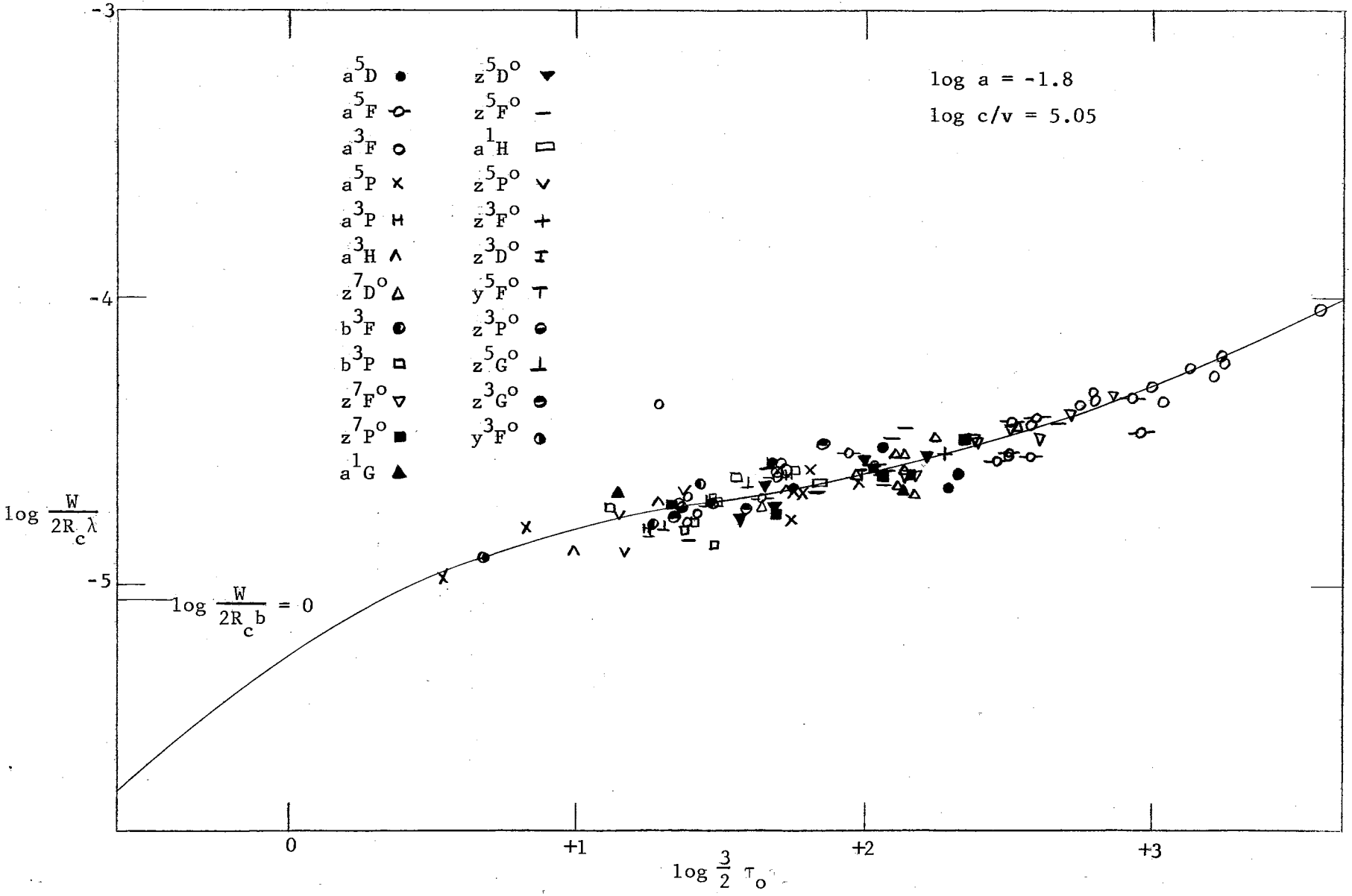

Figure 48. Schuster-Schwarschild Pure Absorption Curve of Growth for Fe I-NBS.

Fe I-King

Table XIV contains the results obtained for Fe I-King. The values of log c/v and log a were determined from the a^5D and a^3F plots.

The reliable absolute f-values of Bell et al. (1958b) were used to obtain a value of Δlog gf equal to -3.27 for use in the abundance determinations.

Excitation temperature data are plotted in Figure 49. The curves of growth are shown in Figures 50, 51, 52, and 53.

TABLE XIV

CURVE OF GROWTH DATA DERIVED FROM Fe I-KING LINES

				M-E Model				S-S Model			
				Scattering		Absorption		Scattering		Absorption	
log c/v				4.97		4.90		5.05		4.95	
log a				-1.4		-1.3		-1.4		-1.3	
Term	$\overline{\chi}_e$	No. of Lines	Weight	Δlog X	Shift	Δlog X	Shift	Δlog X	Shift	Δlog X	Shift
a^5D	0.05	9	2	5.43	5.50	5.27	5.34	5.46	5.52	5.24	5.31
a^5F	0.95	7	1	4.06	5.34	4.20	5.48	3.99	5.27	4.23	5.49
a^3F	1.54	14	2	3.43	5.50	3.25	5.33	3.46	5.54	3.25	5.30
θ				1.347		1.351		1.350		1.330	
Excitation Temperature (^oK)				3741 ± 165		3730 ± 153		3732 ± 267		3790 ± 201	
log u				1.38		1.38		1.38		1.38	
Weighted Shift				5.47		5.36		5.48		5.35	
Abundance	$\log N/\rho\overline{\kappa}$			17.45		17.41					
	log NH							17.38		17.17	
Δlog η							1.79				

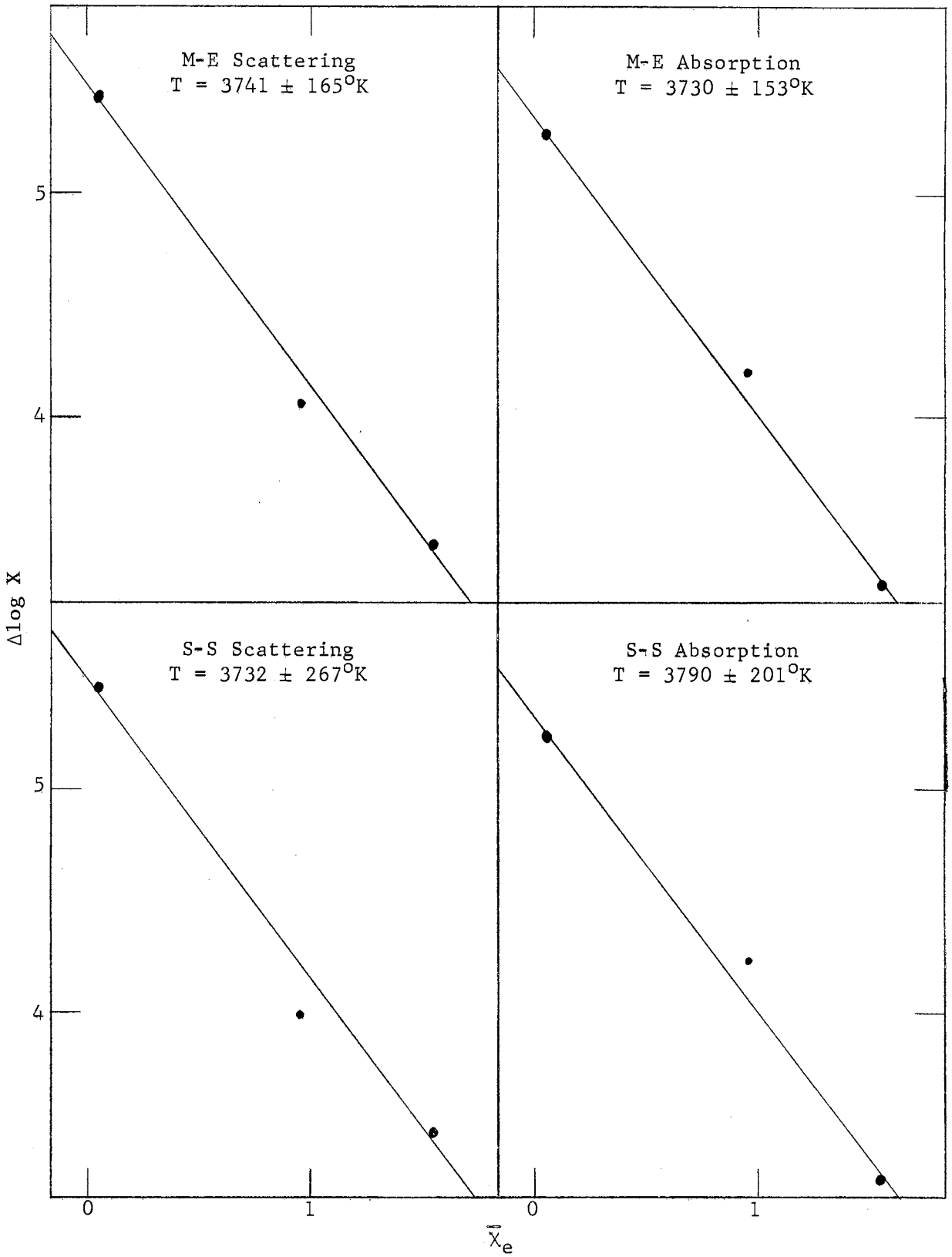

Figure 49. Excitation Temperatures Derived From Fe I-King Lines.

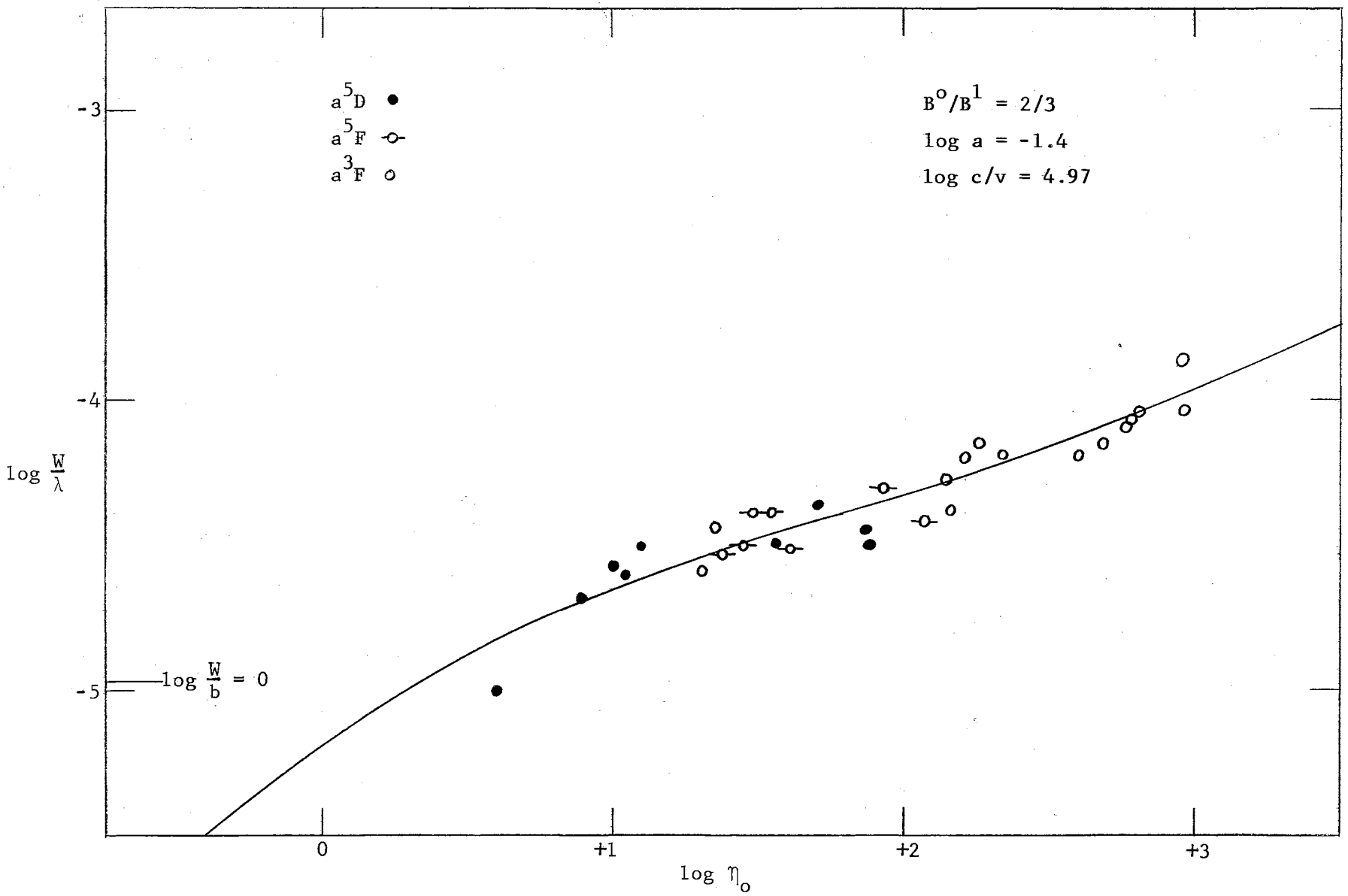

Figure 50. Milne-Eddington Pure Scattering Curve of Growth for Fe I-King.

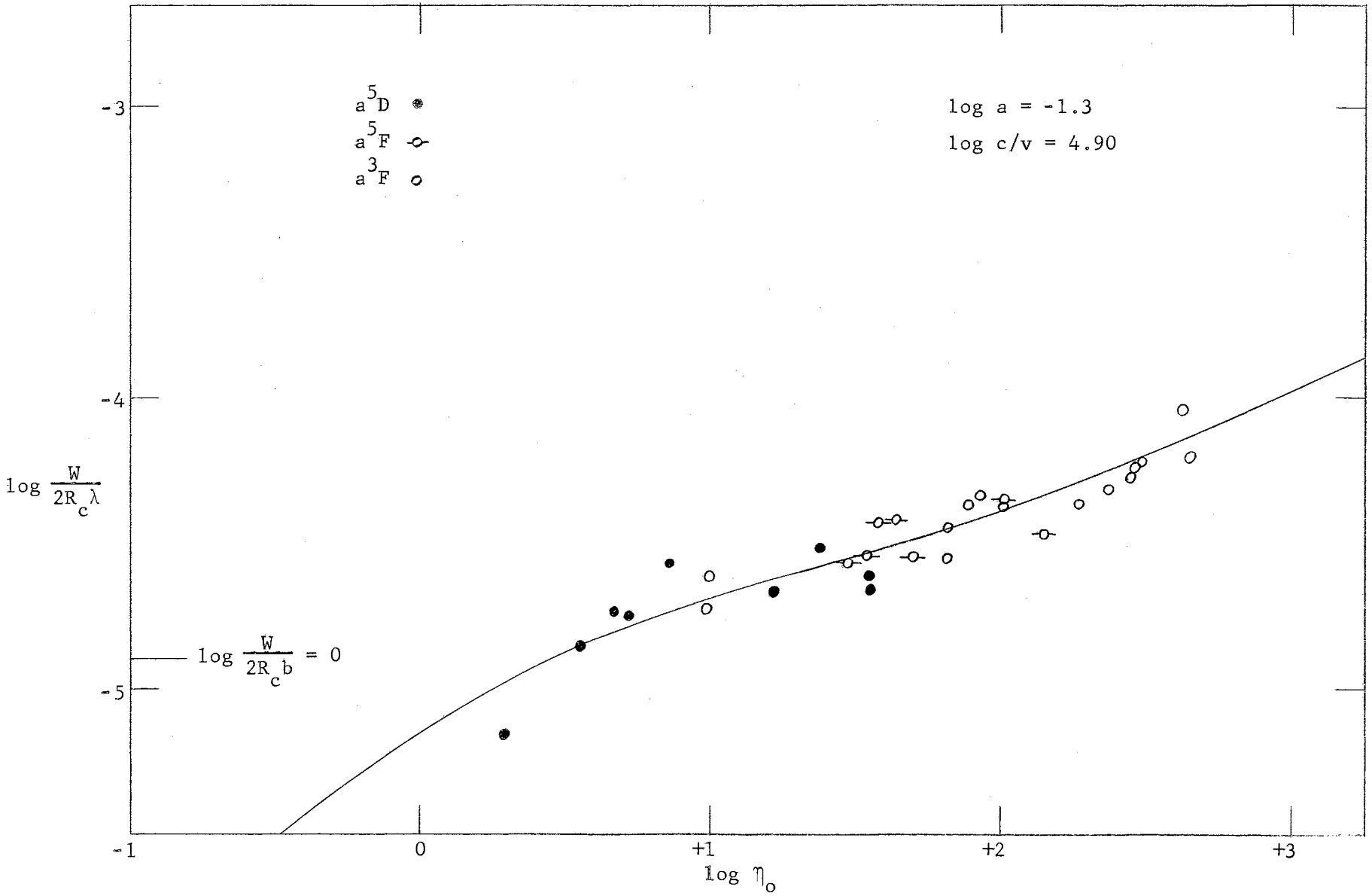

Figure 51. Milne-Eddington Pure Absorption Curve of Growth for Fe I-King.

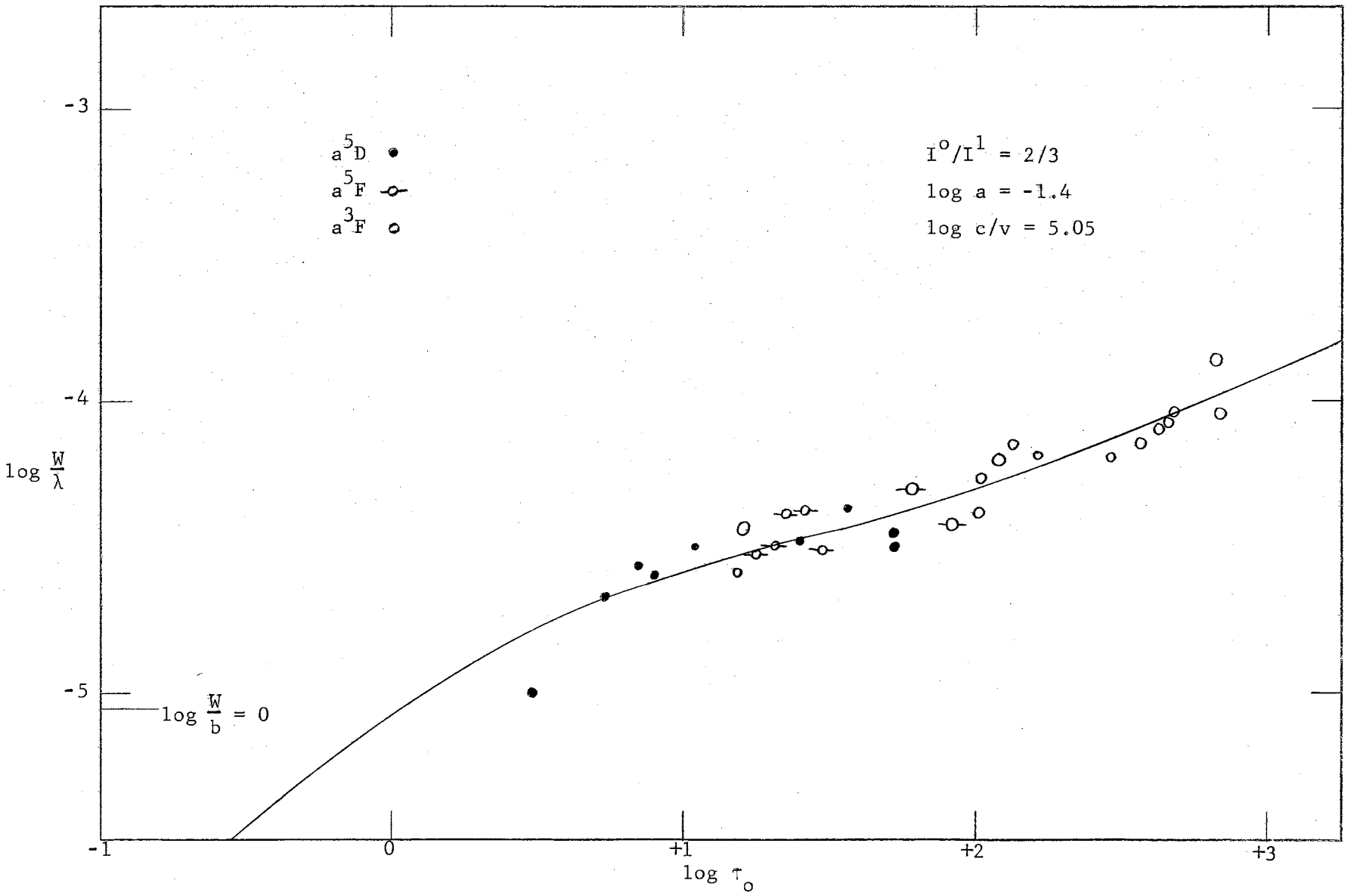

Figure 52. Schuster-Schwarzschild Pure Scattering Curve of Growth for Fe I-King.

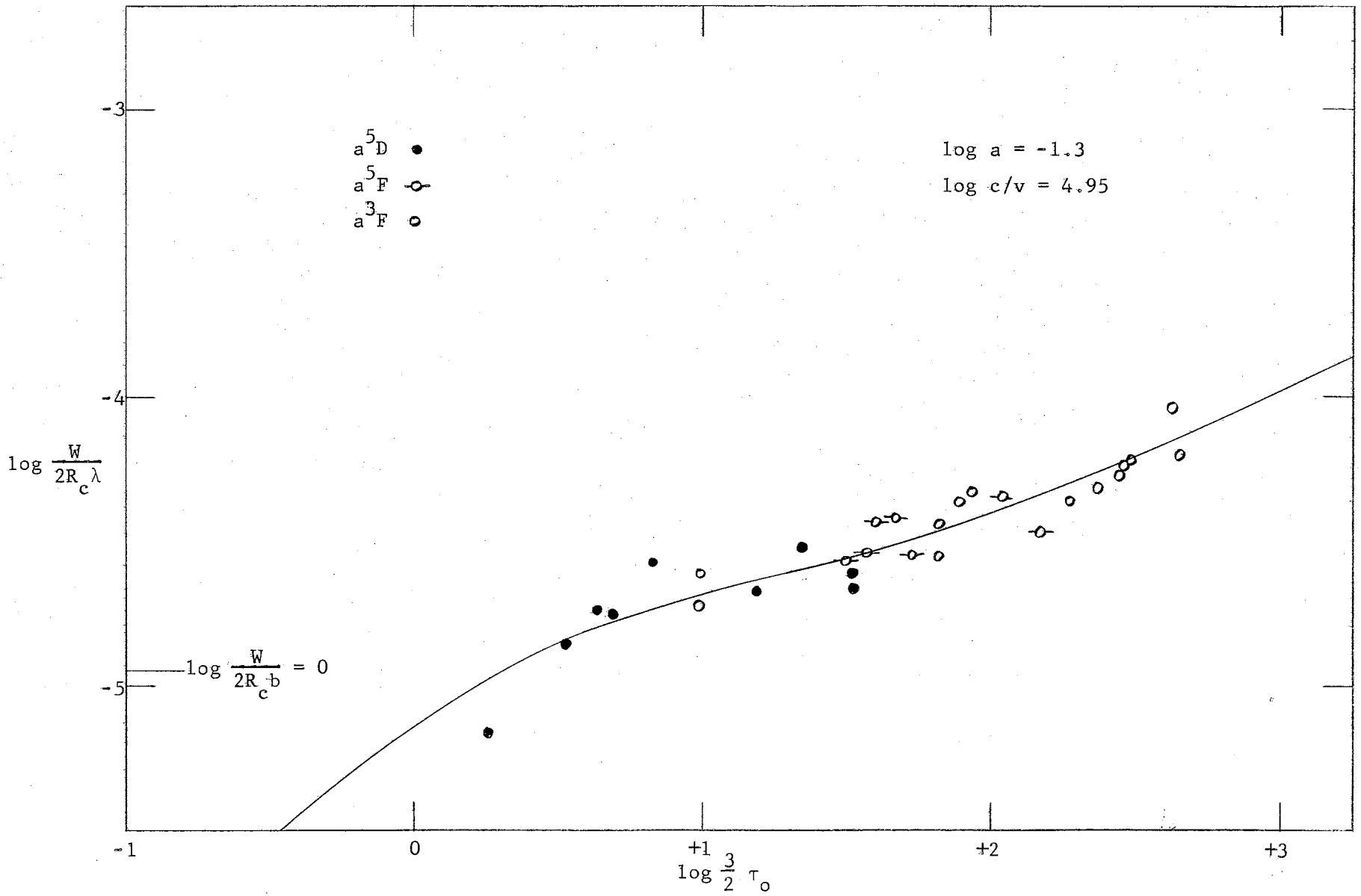

Figure 53. Schuster-Schwarzschild Pure Absorption Curve of Growth for Fe I-King.

Fe I-Carter

Table XV presents the results obtained for Fe I-Carter. The values of log c/v were taken to be the same as the values obtained for Fe I-King. Values of log a could not be determined because of the absence of strong lines. In Table XV, the listed values of log a indicate the theoretical curves used in the analysis.

Carter's f-values were intended to be on an absolute scale. However, the absolute scale used by Carter is now believed to be incorrect, and for the purposes of this investigation the scale was regarded as relative. Carter first determined his f-values on a relative scale, that of the Kings (1938), then converted to the absolute scale of R. B. King (1942). Later, as discussed in the paper by Bell et al. (1958b), it was necessary to revise King's absolute scale because of improved vapor pressure data. Due to this revision, a correction is required in the absolute scale used by Carter. This was taken into account in the calculation of abundances by applying a value of Δlog gf equal to 0.46.

The excitation temperature plots and the curves of growth are shown in Figures 54, 55, 56, 57, and 58.

TABLE XV

CURVE OF GROWTH DATA DERIVED FROM Fe I-CARTER LINES

				M-E Model				S-S Model			
				Scattering		Absorption		Scattering		Absorption	
	log c/v			(4.97)		(4.90)		(5.05)		(4.95)	
	log a			(-1.4)		(-1.3)		(-1.4)		(-1.3)	
Term	$\overline{\chi}_e$	No. of Lines	Weight	Δlog X	Shift	Δlog X	Shift	Δlog X	Shift	Δlog X	Shift
a^5D	0.11	1	1	9.33	9.46	9.28	9.41	9.22	9.34	9.24	9.36
a^3F	1.56	4	2	7.49	9.27	7.53	9.32	7.38	9.10	7.50	9.25
a^5P	2.19	6	3	6.60	9.10	6.41	8.92	6.62	9.03	6.42	8.88
z^7D^o	2.44	6	2	6.13	8.91	5.97	8.77	6.19	8.88	6.00	8.74
b^3P	2.84	2	0	5.35	8.59	5.19	8.45	5.34	8.47	5.15	8.34
z^7P^o	2.99	4	2	5.81	9.22	5.90	9.33	5.72	9.01	5.92	9.28
c^3P	3.06	1	0	5.23	8.72	5.08	8.59	5.21	8.58	5.05	8.49
z^5D^o	3.20	1	1	5.54	9.19	5.66	9.33	5.44	8.96	5.70	9.29
z^5F^o	3.35	3	2	5.58	9.40	5.42	9.26	5.65	9.34	5.46	9.22
a^1H	3.56	1	1	5.01	9.07	4.85	8.93	5.04	8.96	4.82	8.82
	θ			1.140		1.147		1.101		1.123	
Excitation Temperature (^oK)				4420 ± 310		4394 ± 447		4578 ± 306		4487 ± 456	

TABLE XV (Continued)

		M-E Model		S-S Model	
		Scattering	Absorption	Scattering	Absorption
log u		1.42	1.42	1.43	1.42
Weighted Shift		9.19	9.13	9.07	9.08
Abundance	log $N/\rho\bar{\kappa}$	17.94	17.95		
	log NH			17.75	17.67
$\Delta \log \gamma$			1.79		

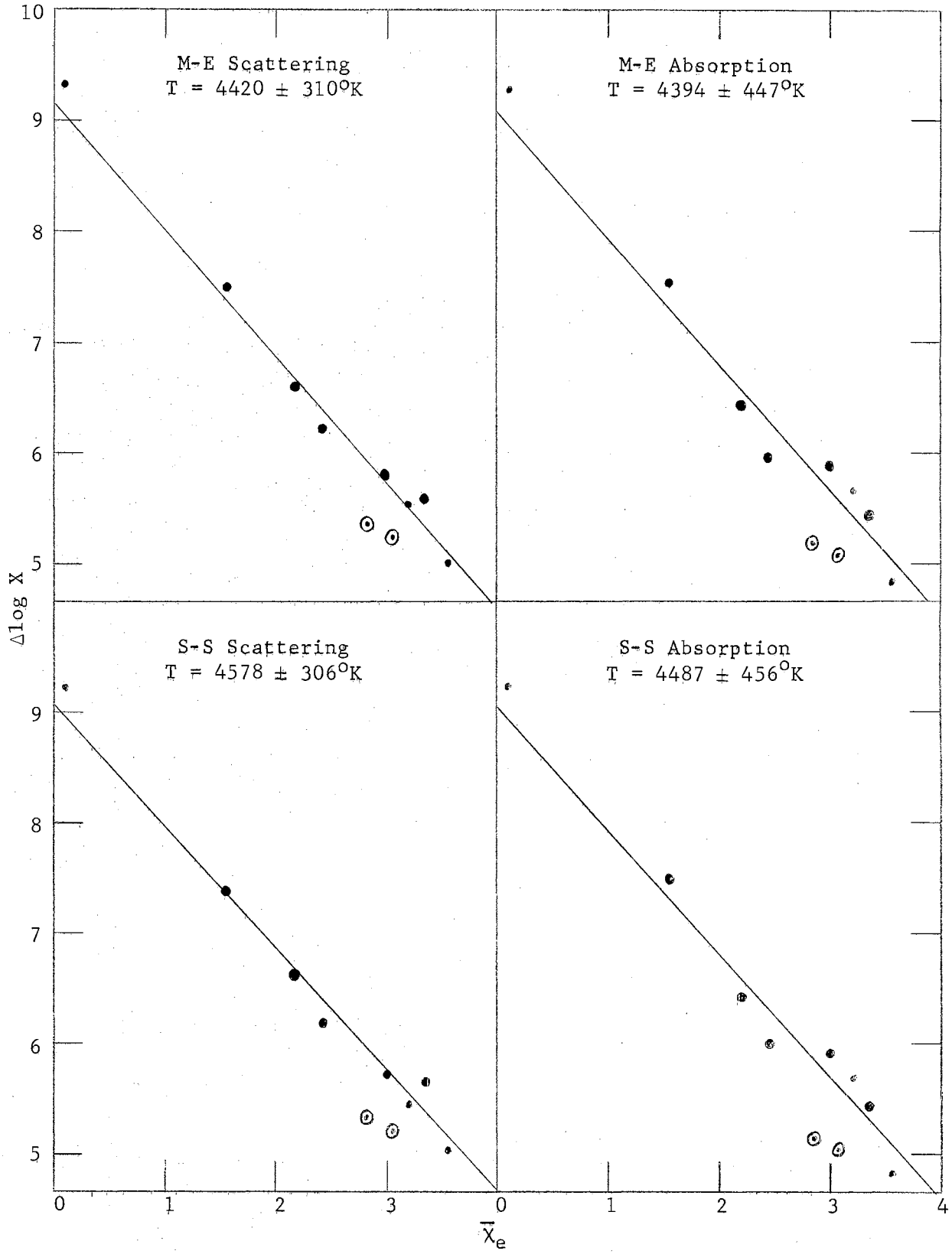

Figure 54. Excitation Temperatures Derived From Fe I-Carter Lines.

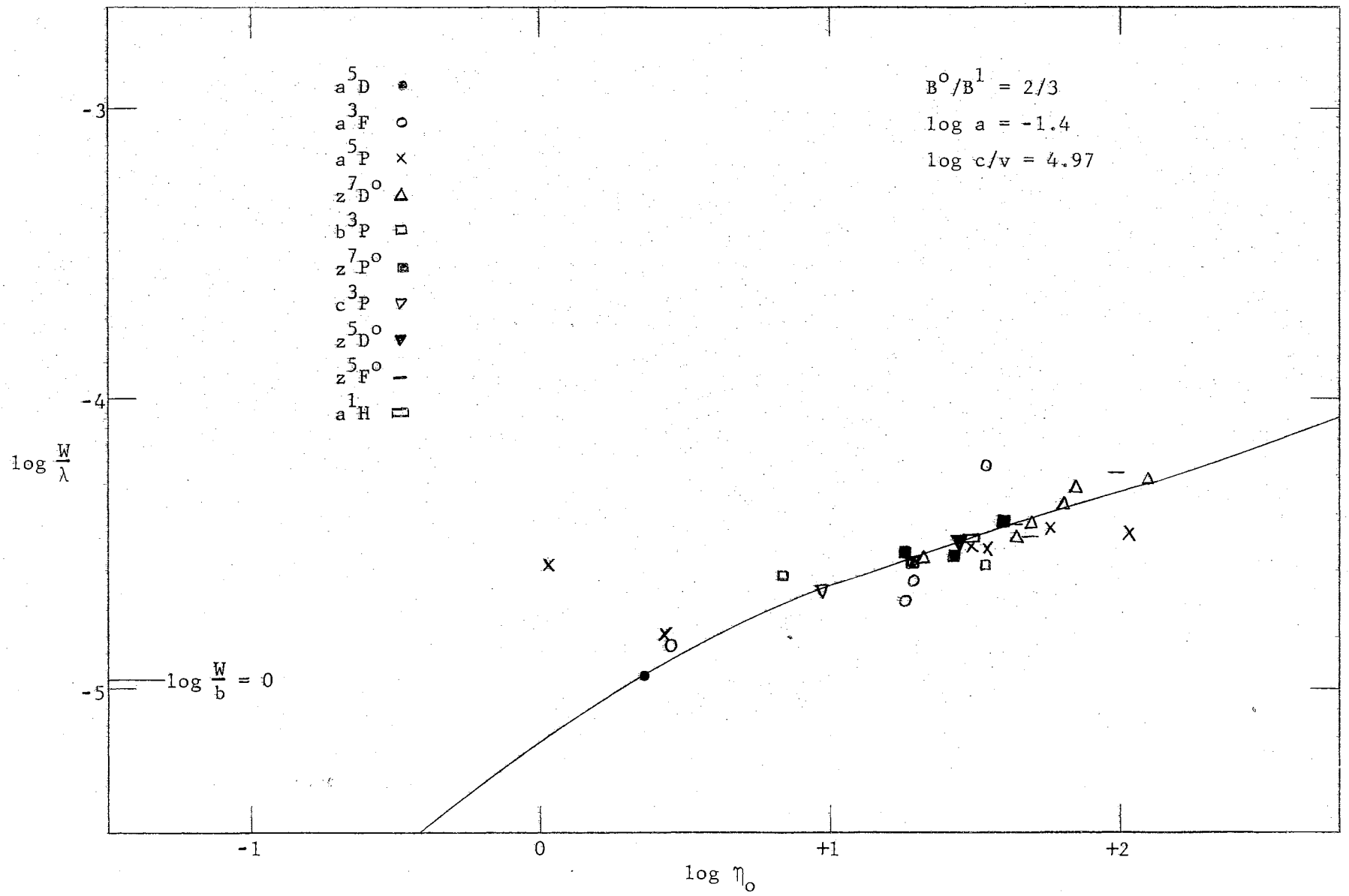

Figure 55. Milne-Eddington Pure Scattering Curve of Growth for Fe I-Carter.

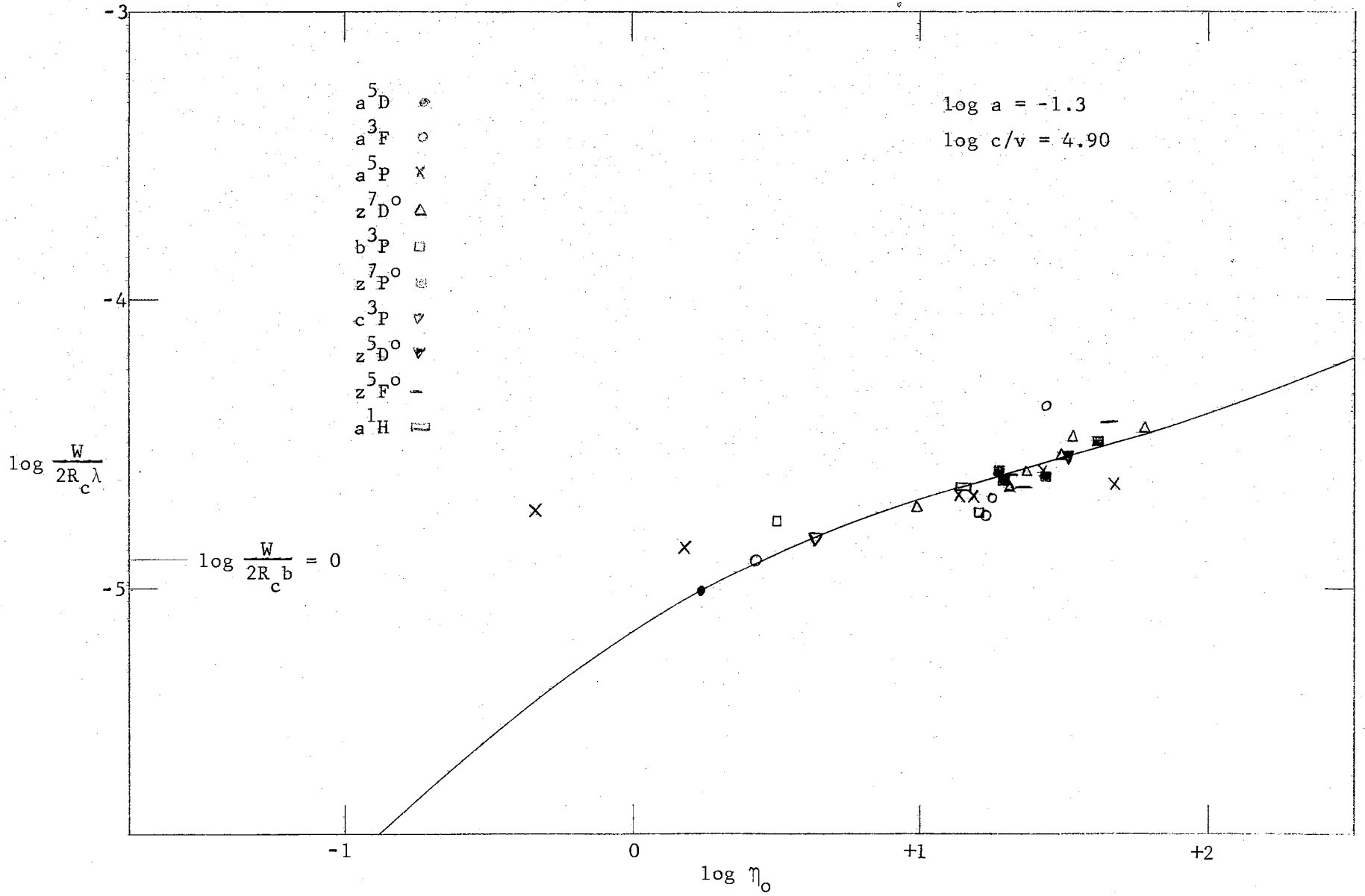

Figure 56. Milne-Eddington Pure Absorption Curve of Growth for Fe I-Carter.

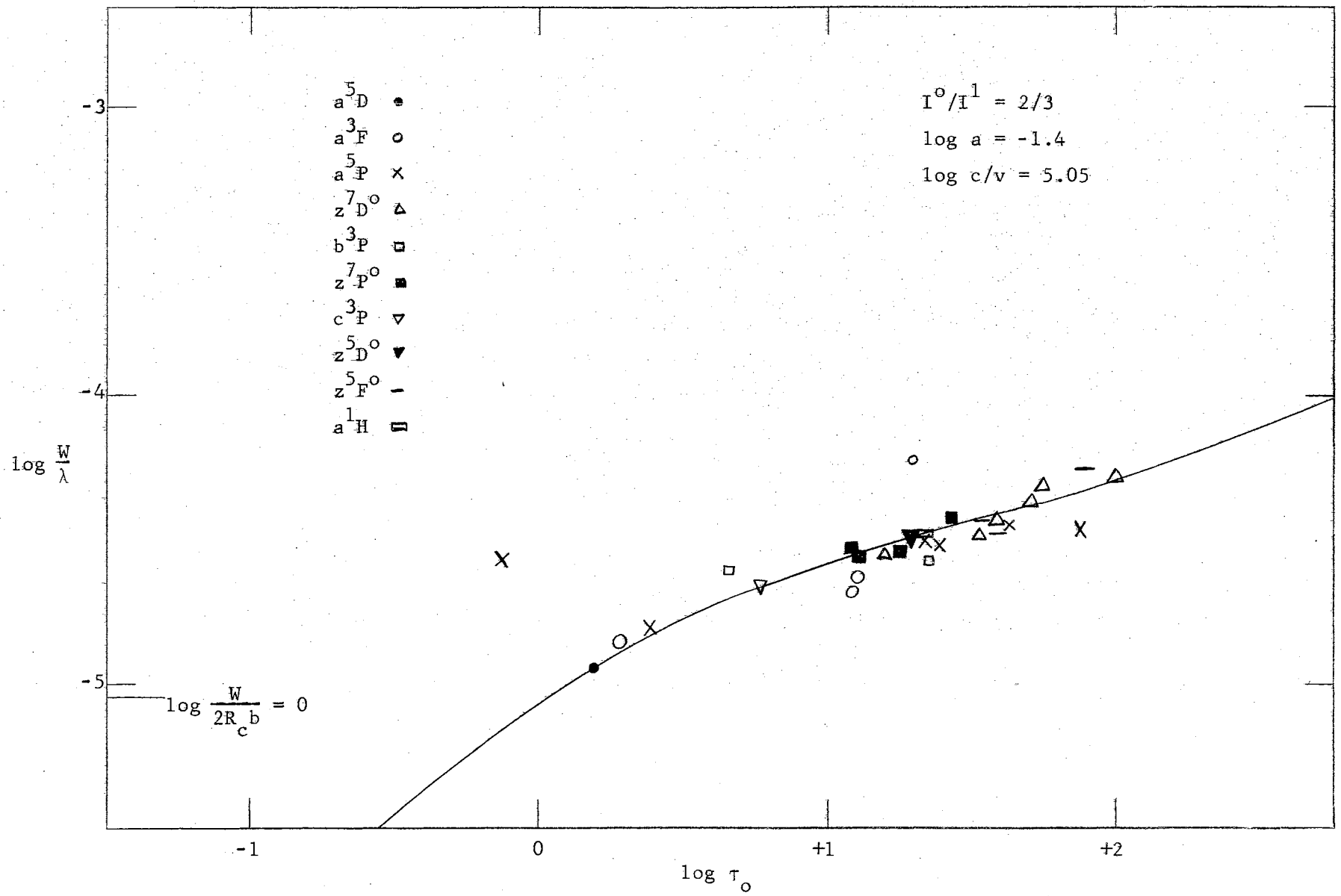

Figure 57. Schuster-Schwarzschild Pure Scattering Curve of Growth for Fe I-Carter.

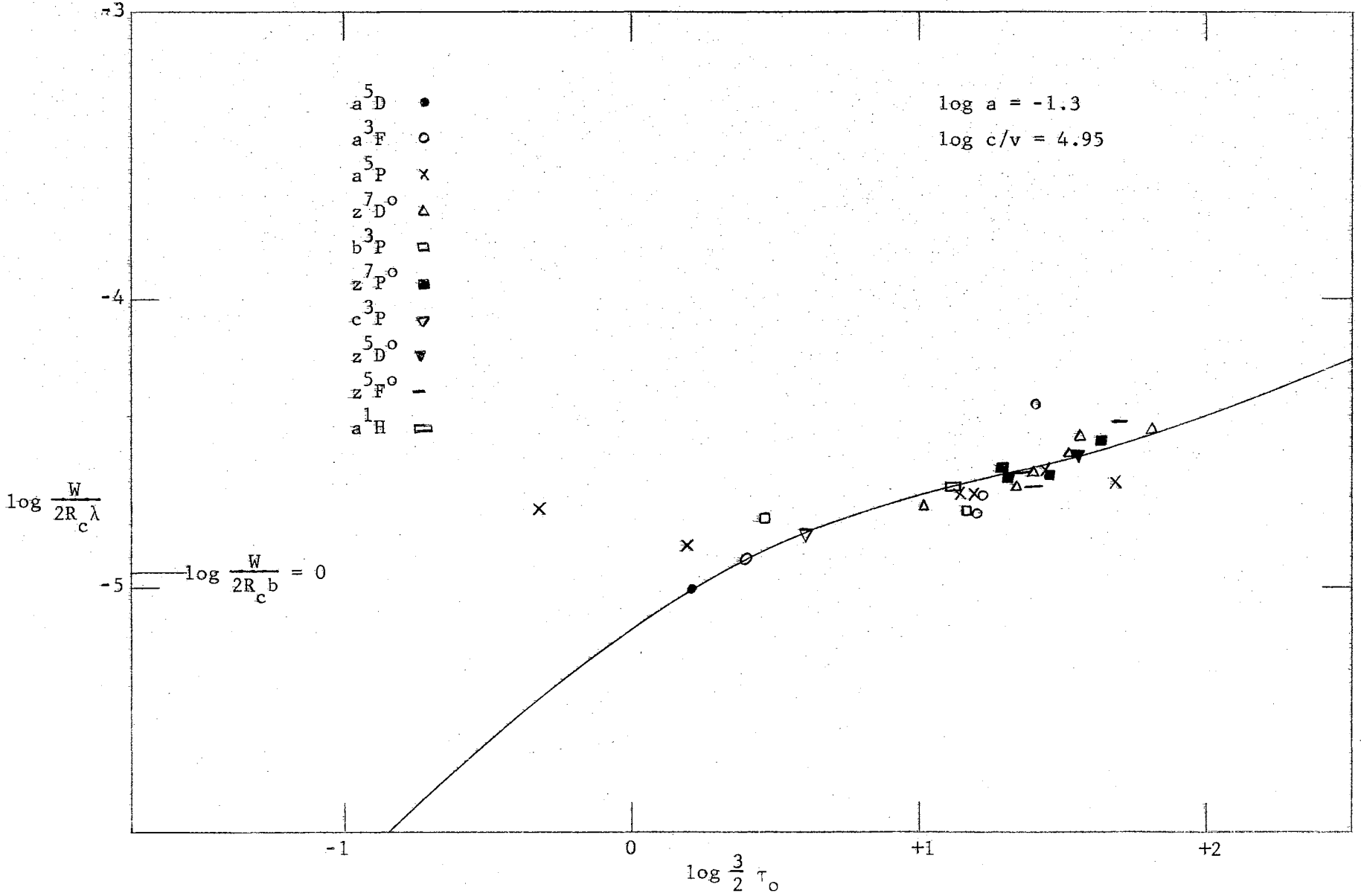

Figure 58. Schuster-Schwarzschild Pure Absorption Curve of Growth for Fe I-Carter.

Results for Co I

For Co I the NBS f-values were used. Table XVI presents the results obtained. The values of log q/v were adopted from those obtained for Fe I-NBS. Because of the absence of strong lines it was not possible to determine values of log a. The values listed in Table XVI merely indicate the theoretical curves used in the analysis.

The excitation temperature data are plotted in Figure 59. The curves of growth are shown in Figures 60, 61, 62, and 63.

TABLE XVI

CURVE OF GROWTH DATA DERIVED FROM Co I LINES

				M-E Model				S-S Model			
				Scattering		Absorption		Scattering		Absorption	
log c/v				(5.06)		(5.00)		(5.07)		(5.05)	
log a				(-1.8)		(-1.8)		(-1.4)		(-1.8)	
Term	$\overline{\chi}_e$	No. of Lines	Weight	Δlog X	Shift	Δlog X	Shift	Δlog X	Shift	Δlog X	Shift
b^4F	0.43	2	2	6.63	7.05	6.48	6.89	6.47	6.89	6.51	6.92
a^2F	0.96	3	2	5.80	6.74	5.60	6.52	5.48	6.41	5.55	6.47
a^4P	1.73	1	1	5.18	6.88	5.10	6.76	5.00	6.67	5.11	6.77
z^6F^o	3.11	1	1	4.31	7.36	4.16	7.15	4.16	7.17	4.16	7.14
z^6D^o	3.22	1	1	3.66	6.82	3.55	6.65	3.52	6.64	3.55	6.63
z^4F^o	3.50	1	1	3.18	6.61	3.10	6.47	3.00	6.39	3.11	6.46
y^4G^o	4.01	2	2	3.01	6.94	2.90	6.76	2.81	6.69	2.91	6.75
z^2G^o	4.04	1	0	4.10	8.06	4.06	7.95	3.85	7.76	4.02	7.89
θ				0.980		0.962		0.968		0.958	
Excitation Temperature (^oK)				5142 ± 425		5241 ± 458		5204 ± 551		5259 ± 517	
log u				1.50		1.51		1.50		1.51	
Weighted Shift				6.91		6.74		6.69		6.73	

TABLE XVI (Continued)

		M-E Model		S-S Model	
		Scattering	Absorption	Scattering	Absorption
Abundance	log $N/\rho\bar{\mu}$	15.63	15.55		
	log NH			15.40	15.29
Δlog η			1.58		

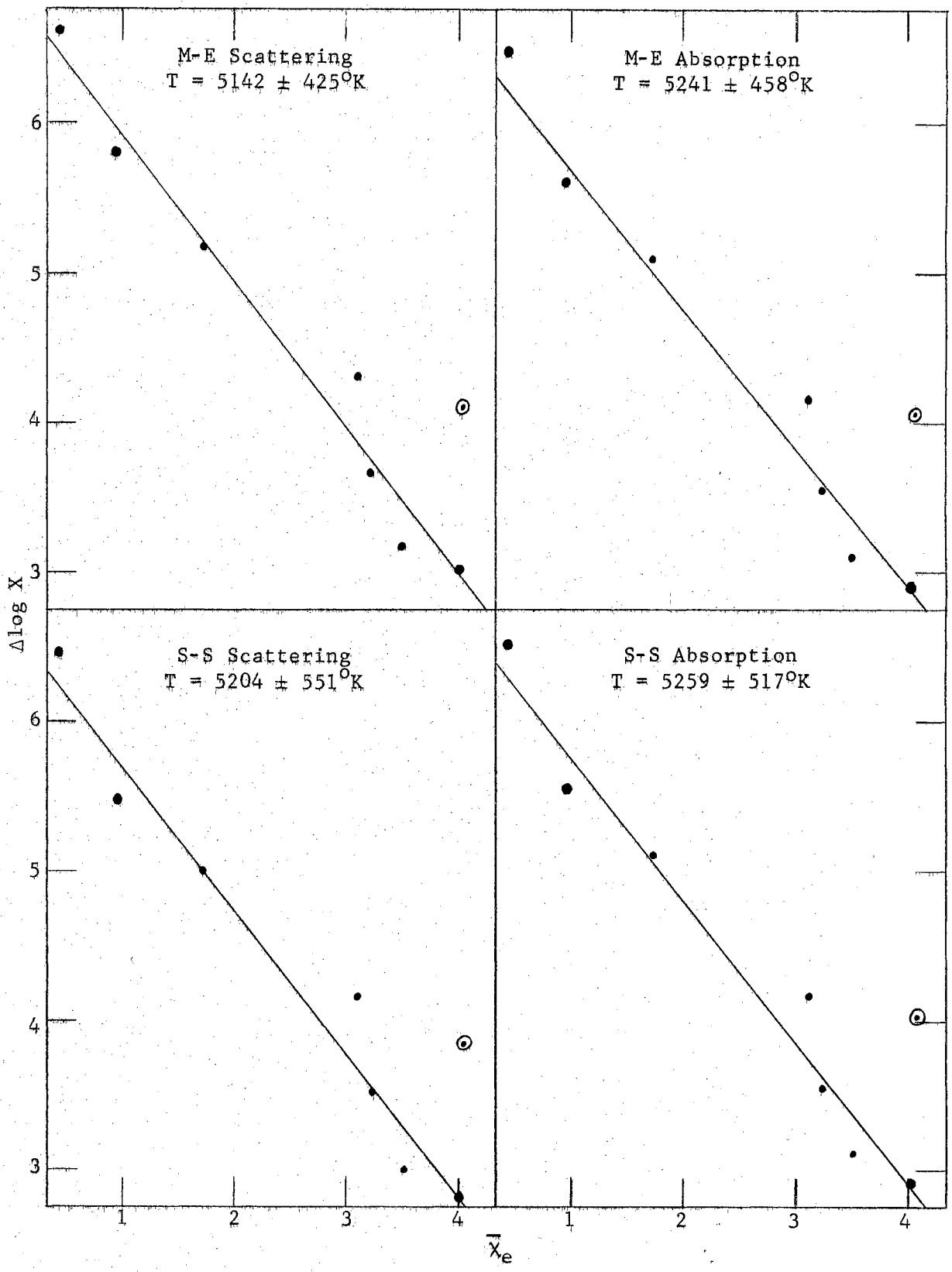

Figure 59. Excitation Temperatures Derived From Co I Lines.

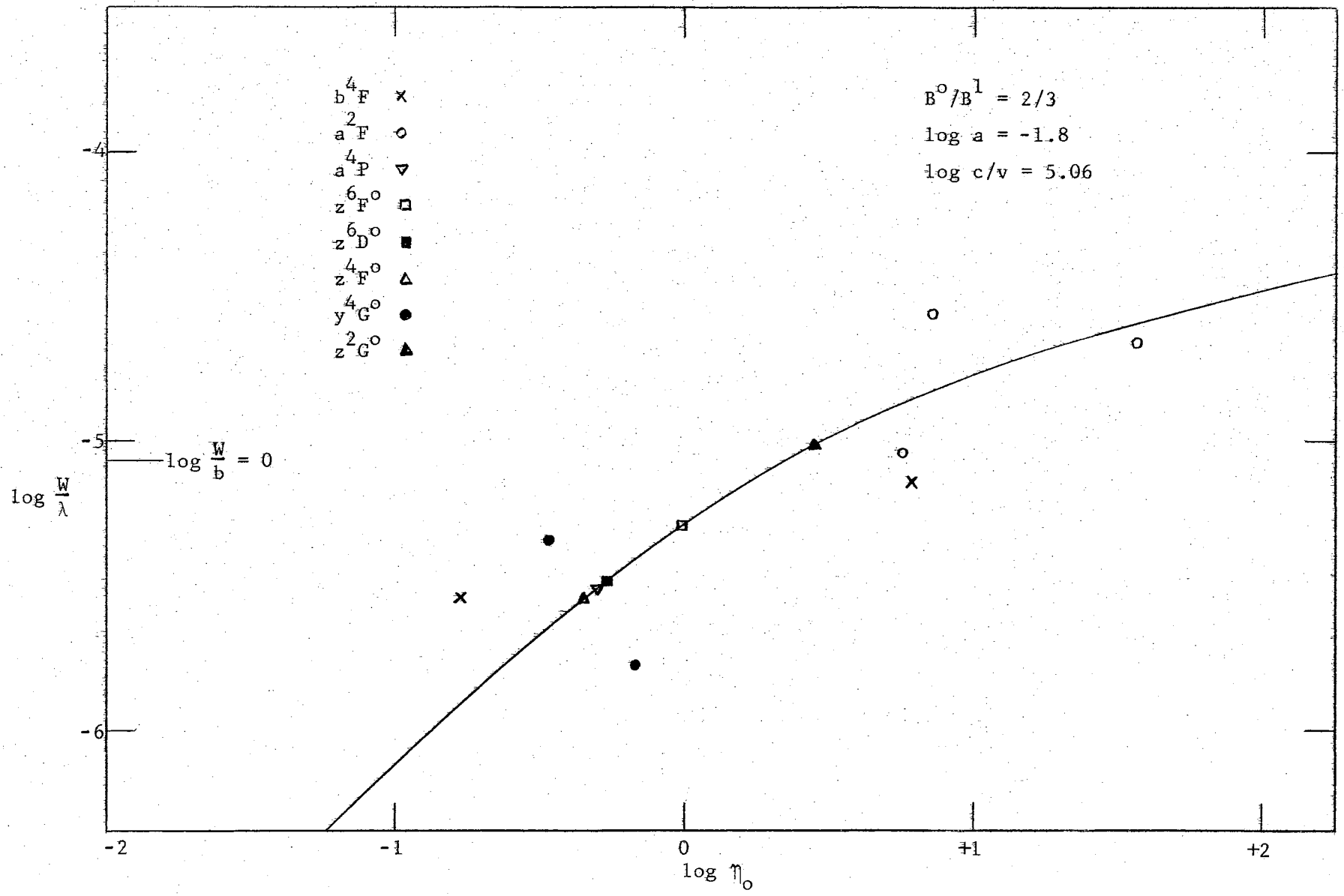

Figure 60. Milne-Eddington Pure Scattering Curve of Growth for Co I.

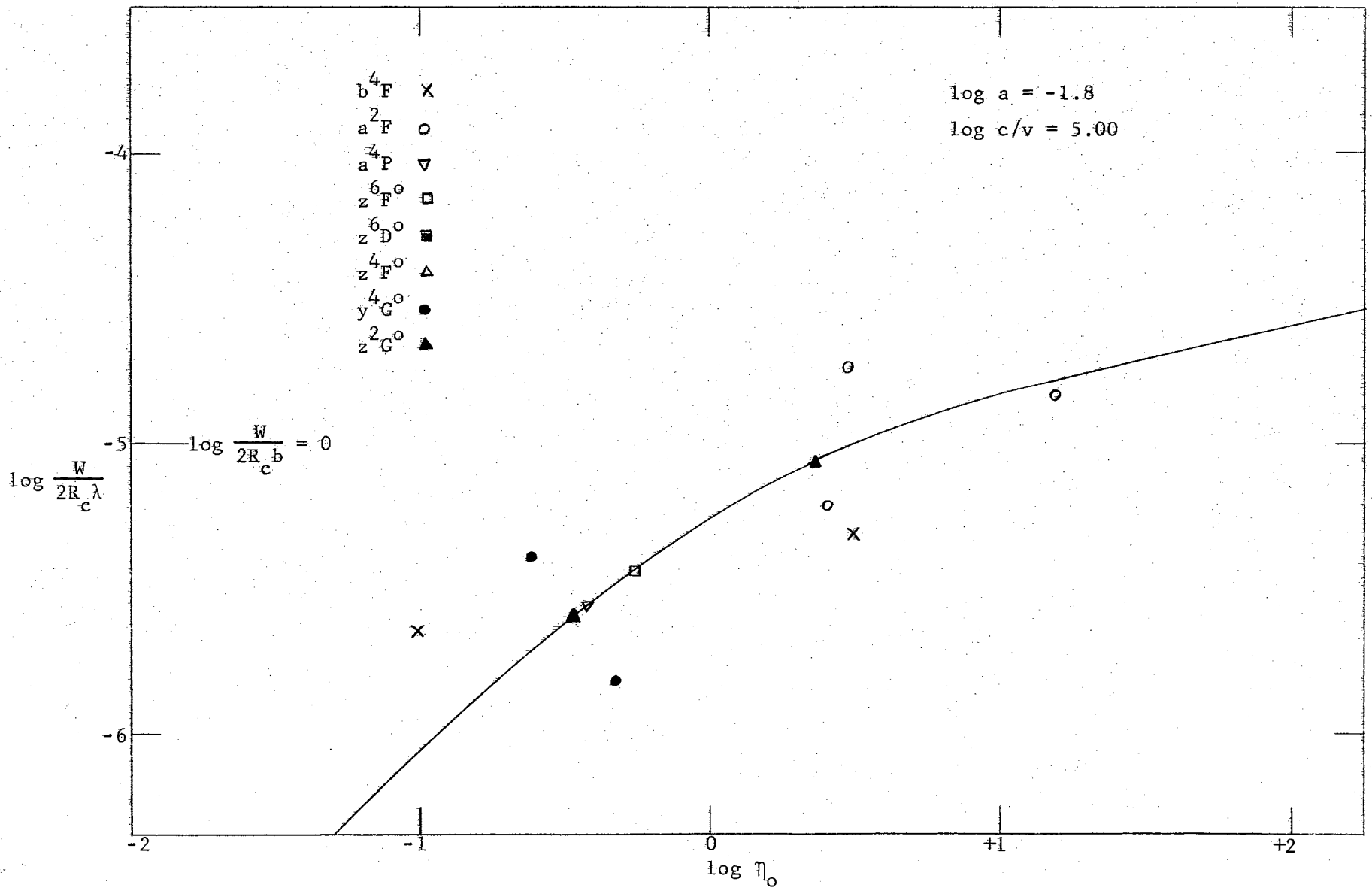

Figure 61. Milne-Eddington Pure Absorption Curve of Growth for Co I.

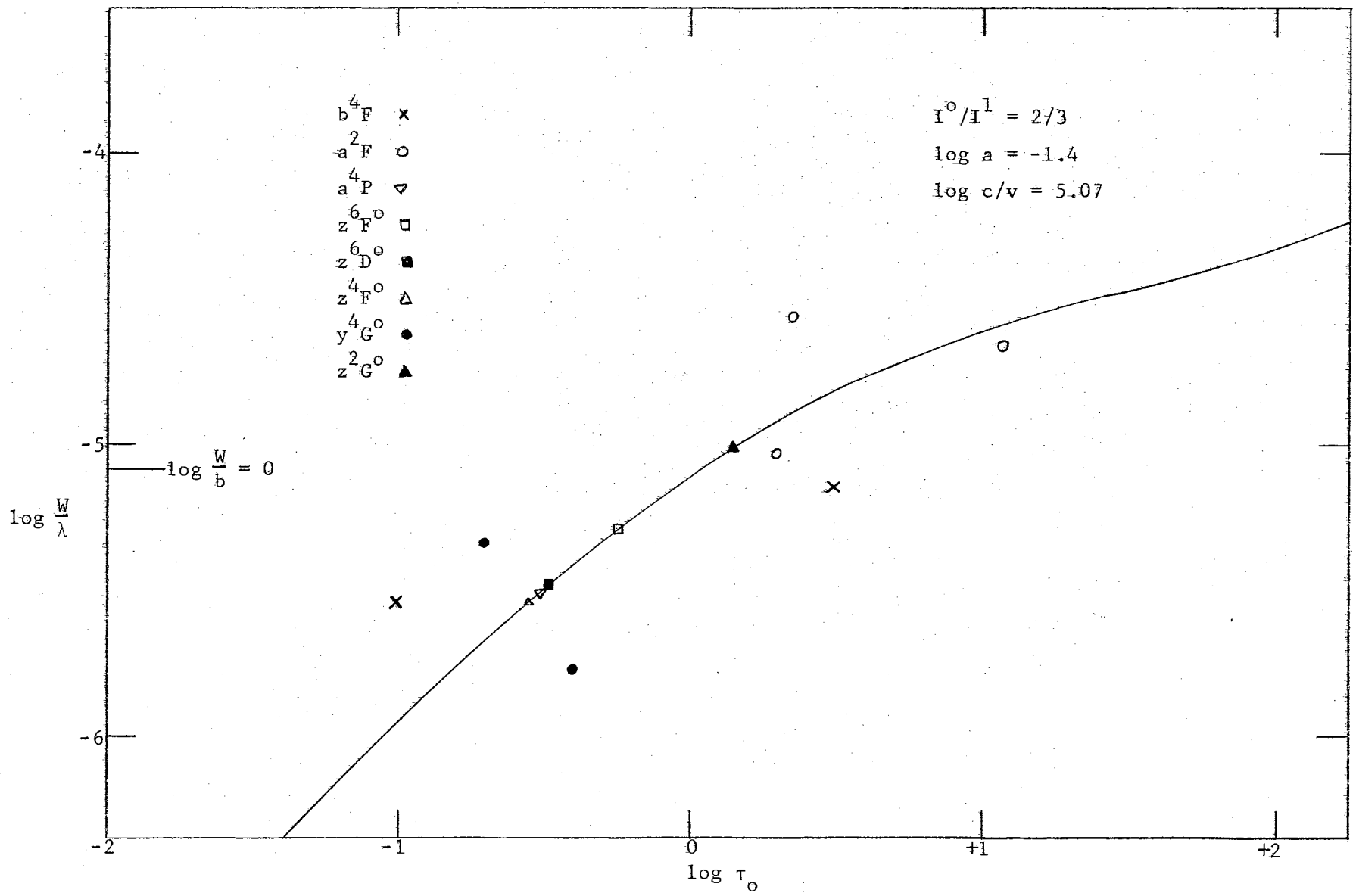

Figure 62. Schuster-Schwarzschild Pure Scattering Curve of Growth for Co I.

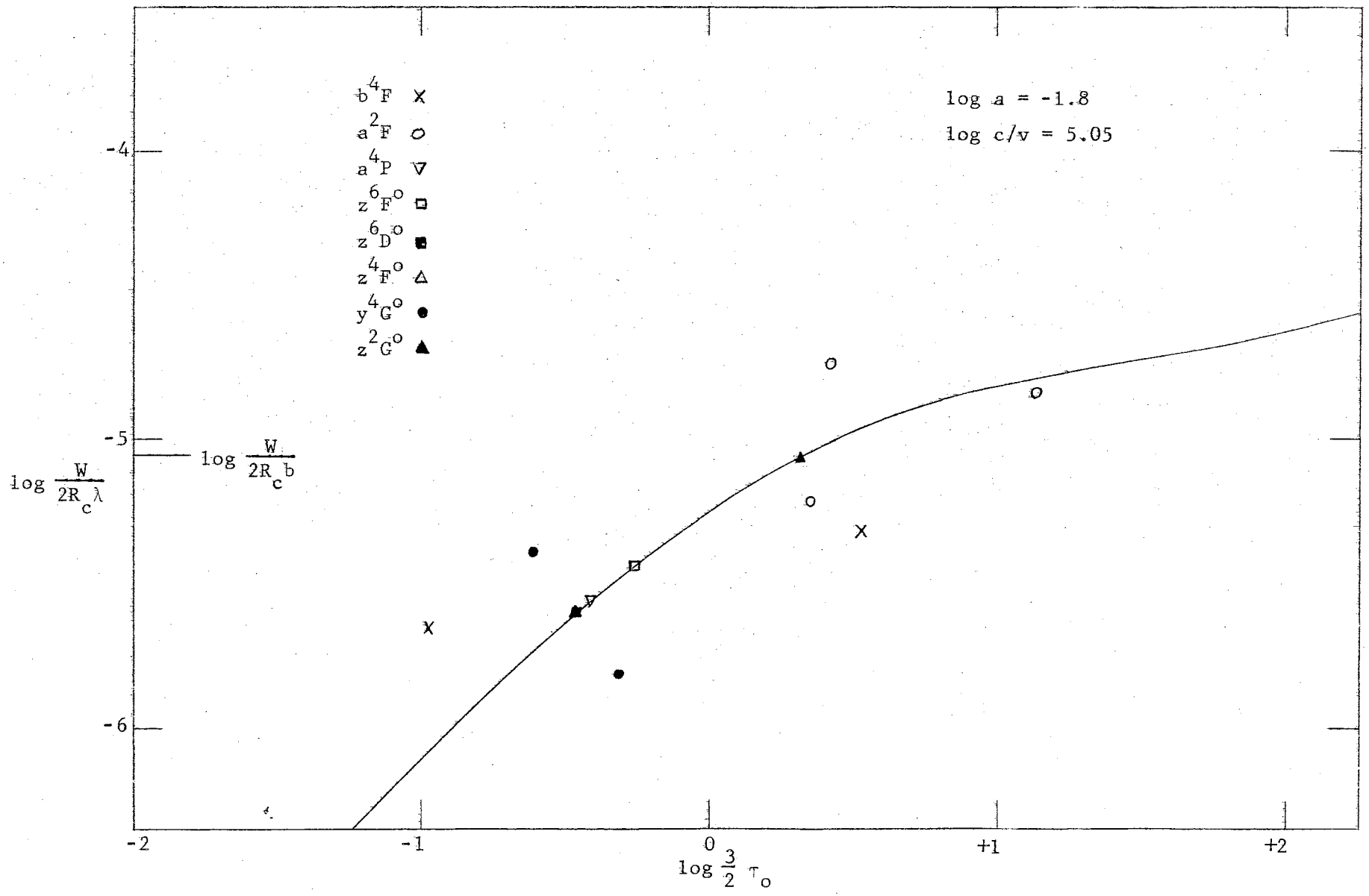

Figure 63. Schuster-Schwarzschild Pure Absorption Curve of Growth for Co I.

Results for Ni I

The f-values used here were those of the NBS. Table XVII gives the results obtained for Ni I. The values of log c/v listed in the table were adopted from the values obtained for Fe I-NBS. Because of the absence of strong lines, values of log a could not be determined, and the values listed in Table XVII merely refer to the theoretical curves used in the analysis.

Figures 64, 65, 66, 67, and 68 present the excitation temperature plots and the curves of growth obtained for each of the four models.

TABLE XVII

CURVE OF GROWTH DATA DERIVED FROM Ni I LINES

				M-E Model				S-S Model			
				Scattering		Absorption		Scattering		Absorption	
log c/v				(5.06)		(5.00)		(5.07)		(5.05)	
log a				(-1.4)		(-1.8)		(-1.4)		(-1.8)	
Term	$\overline{\chi}_e$	No. of Lines	Weight	Δlog X	Shift	Δlog X	Shift	Δlog X	Shift	Δlog X	Shift
$b\,^1D$	1.67	1	1	6.49	7.97	6.42	7.82	6.25	7.75	6.40	7.84
$a\,^3P$	1.94	1	1	5.80	7.52	5.71	7.34	5.56	7.30	5.69	7.36
$z\,^5D^o$	3.42	2	2	4.51	7.54	4.42	7.29	4.30	7.36	4.33	7.28
$z\,^5G^o$	3.48	7	3	4.37	7.45	4.32	7.24	4.14	7.26	4.22	7.22
$z\,^3P^o$	3.53	2	2	4.73	7.86	4.71	7.67	4.40	7.56	4.59	7.64
$z\,^5F^o$	3.60	5	3	4.58	7.77	4.61	7.63	4.34	7.57	4.51	7.62
$z\,^3F^o$	3.67	4	1	4.53	7.78	4.71	7.79	4.18	7.47	4.61	7.78
$z\,^3D^o$	3.67	4	2	4.59	7.84	4.69	7.77	4.33	7.62	4.57	7.74
$z\,^1F^o$	3.83	1	1	4.10	7.49	4.13	7.34	3.82	7.25	4.03	7.34
$z\,^3G^o$	3.85	3	2	4.28	7.69	4.23	7.46	4.03	7.48	4.17	7.49
$z\,^1D^o$	3.88	2	2	4.24	7.68	4.21	7.47	4.00	7.48	4.16	7.51
θ				0.886		0.839		0.896		0.863	
Excitation Temperature (^oK)				5686 ± 437		6004 ± 619		5625 ± 383		5840 ± 574	

TABLE XVII (Continued)

		M-E Model		S-S Model	
		Scattering	Absorption	Scattering	Absorption
log u		1.50	1.52	1.50	1.51
Weighted Shift		7.68	7.51	7.46	7.51
Abundance	log $N/\rho\bar{\kappa}$	16.42	16.33		
	log NH			16.19	16.09
Δlog η			1.42		

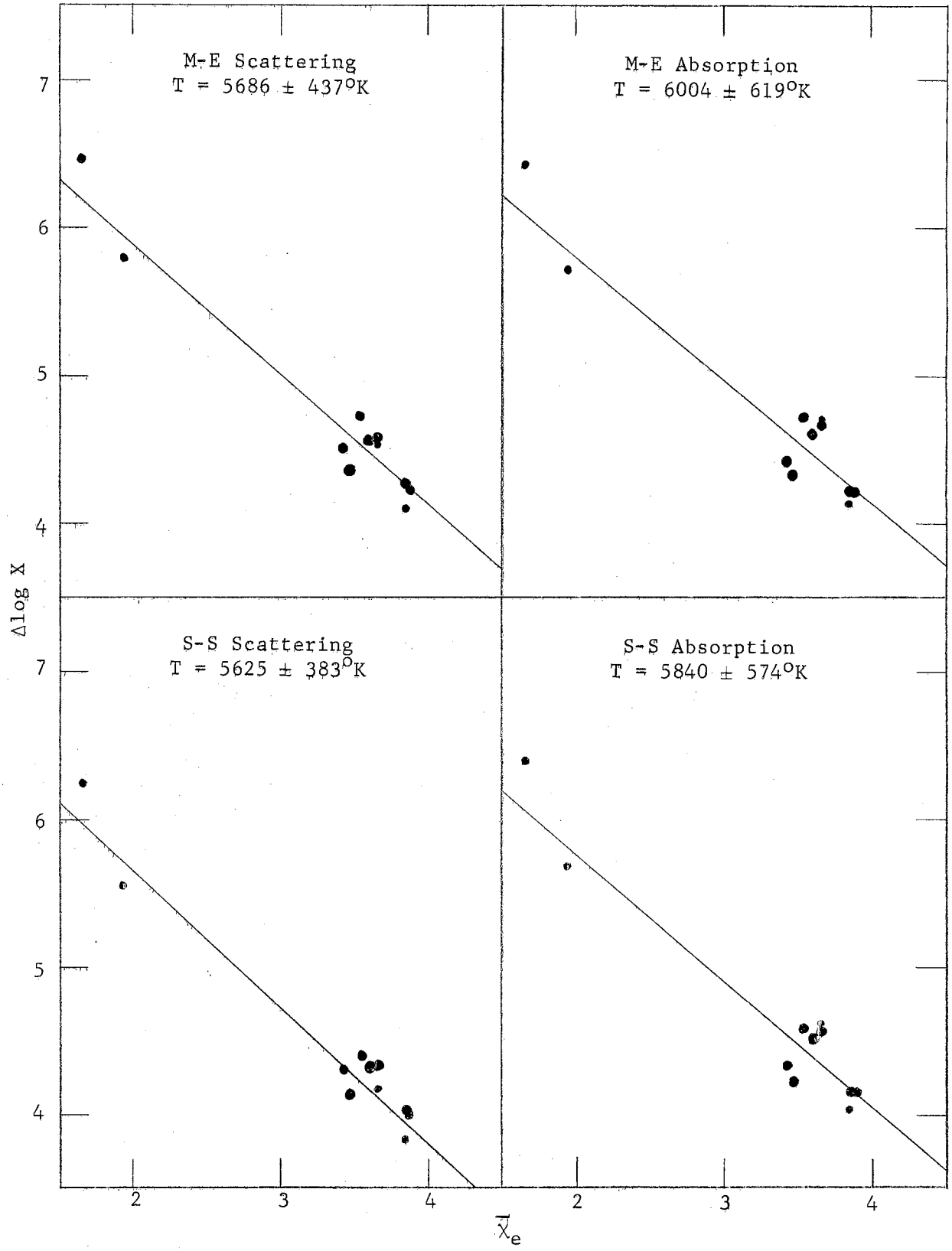

Figure 64. Excitation Temperatures Derived From Ni I Lines.

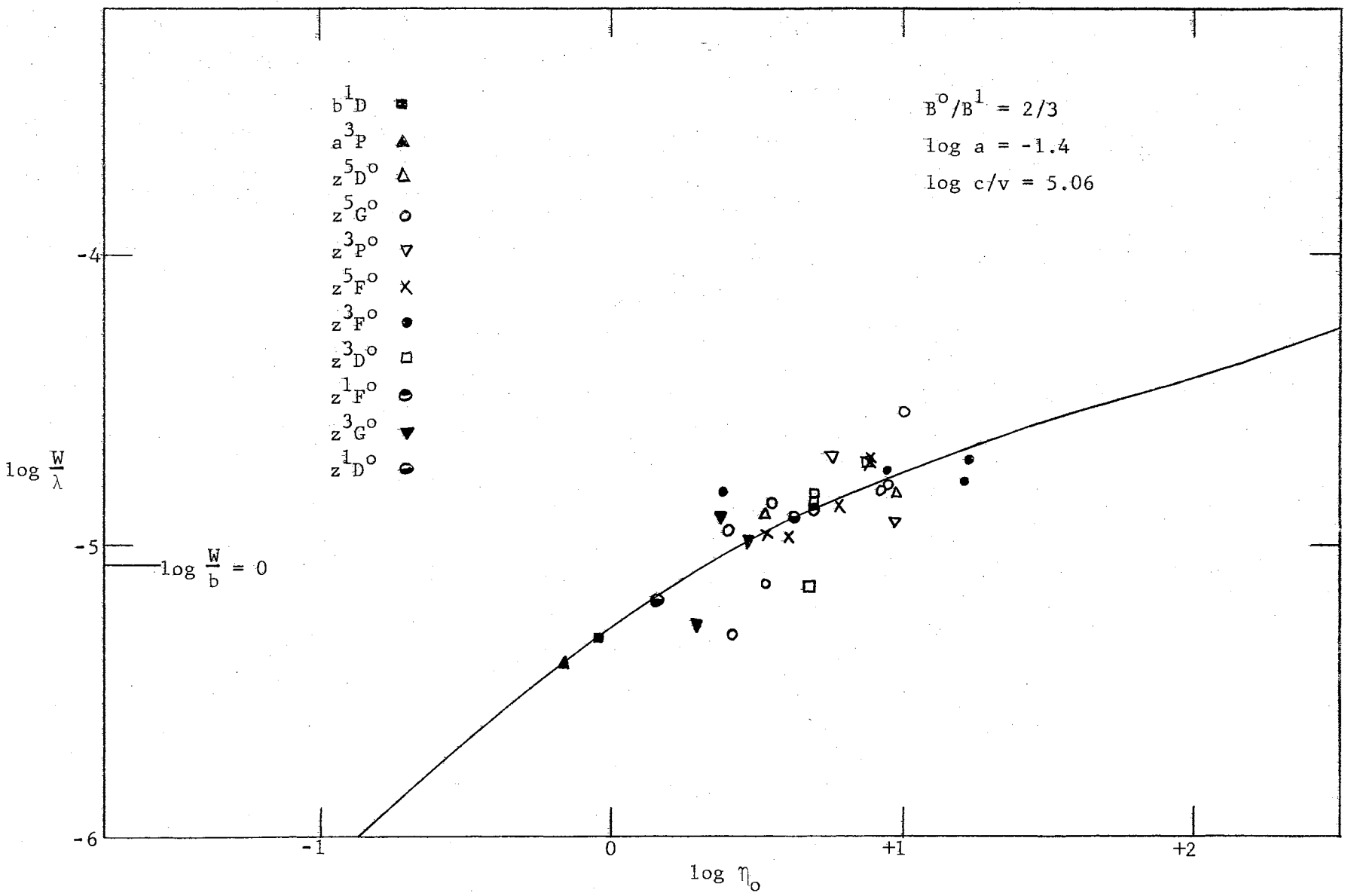

Figure 65. Milne-Eddington Pure Scattering Curve of Growth for Ni I.

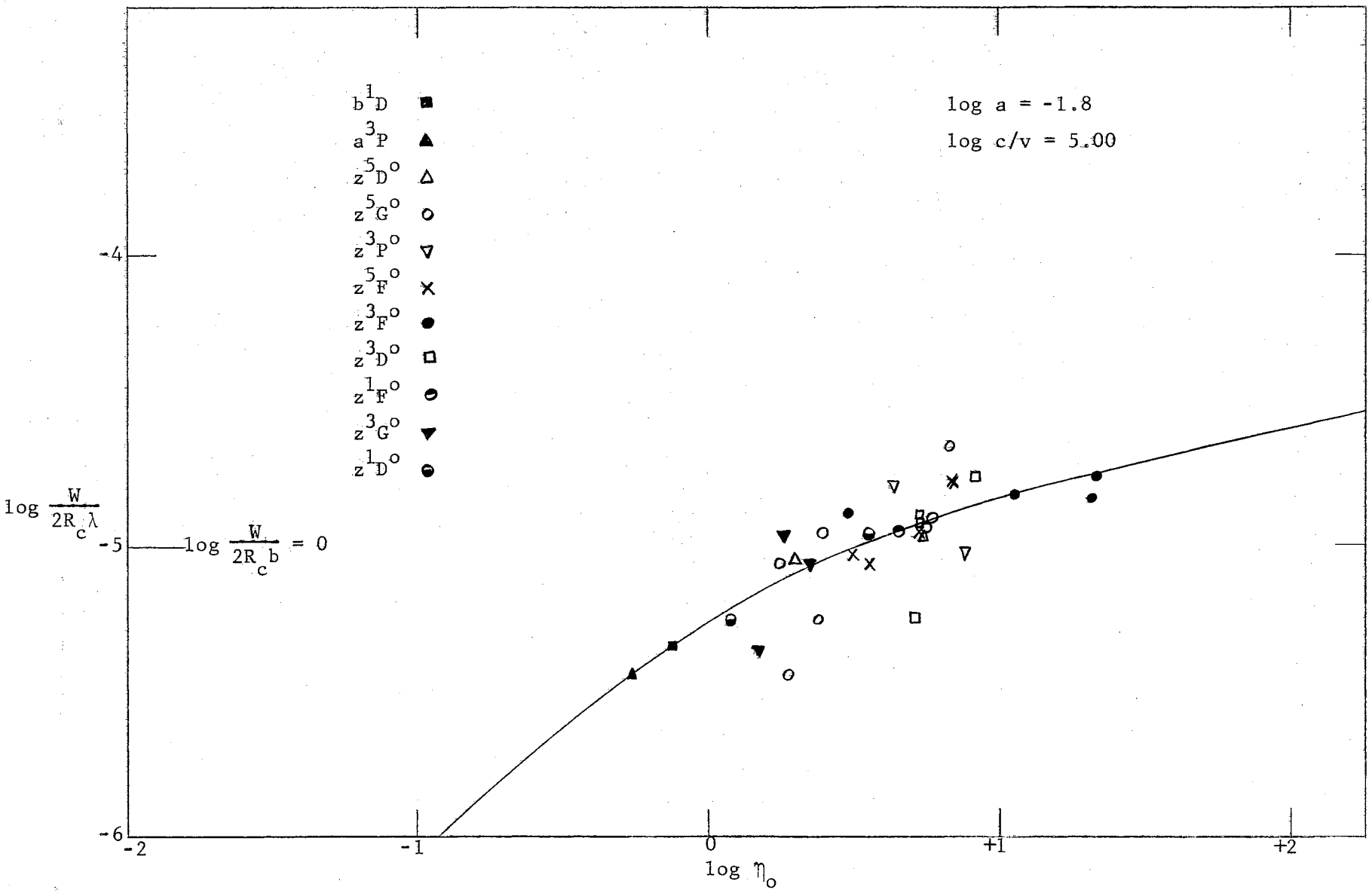

Figure 66. Milne-Eddington Pure Absorption Curve of Growth for Ni I.

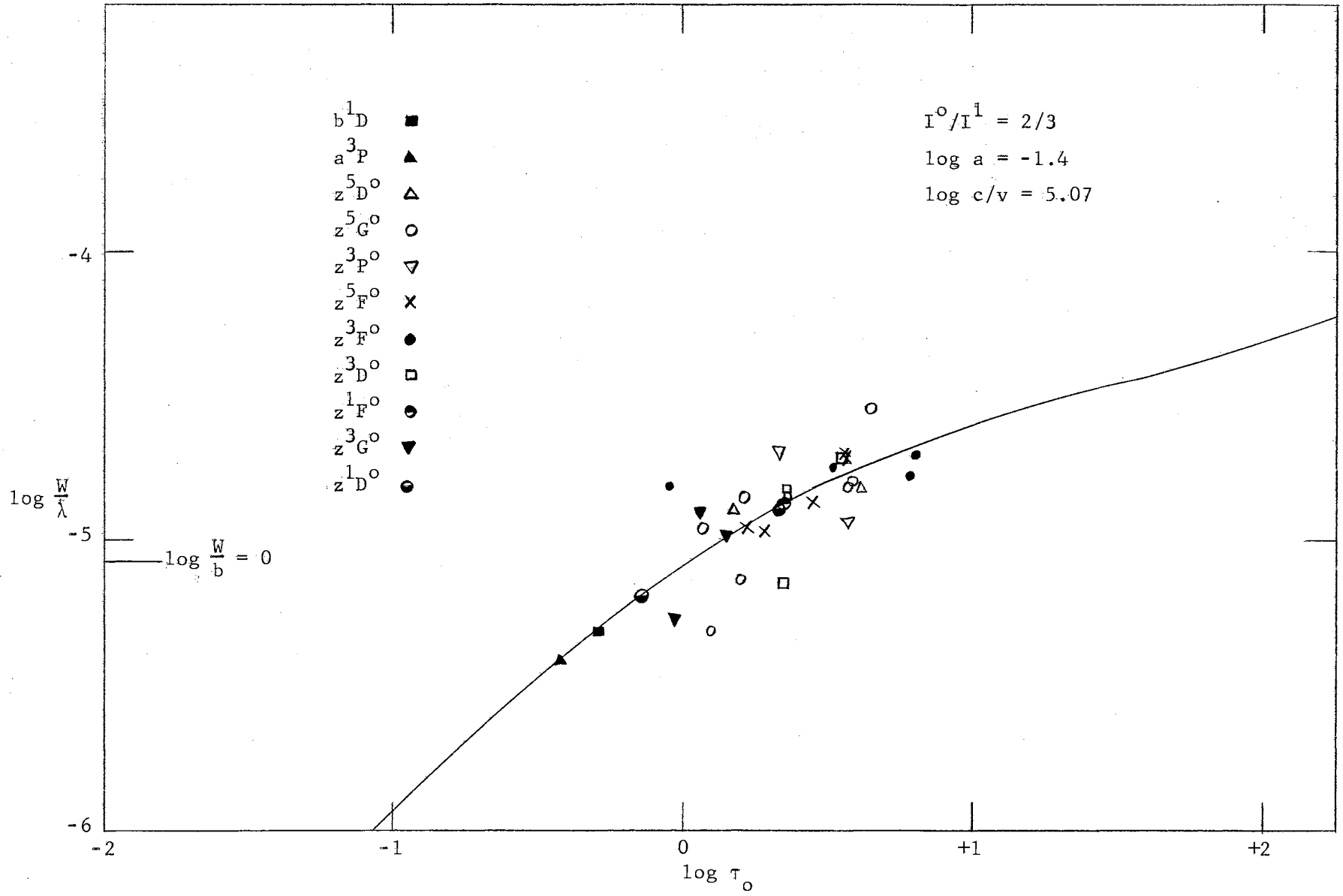

Figure 67. Schuster-Schwarzschild Pure Scattering Curve of Growth for Ni I.

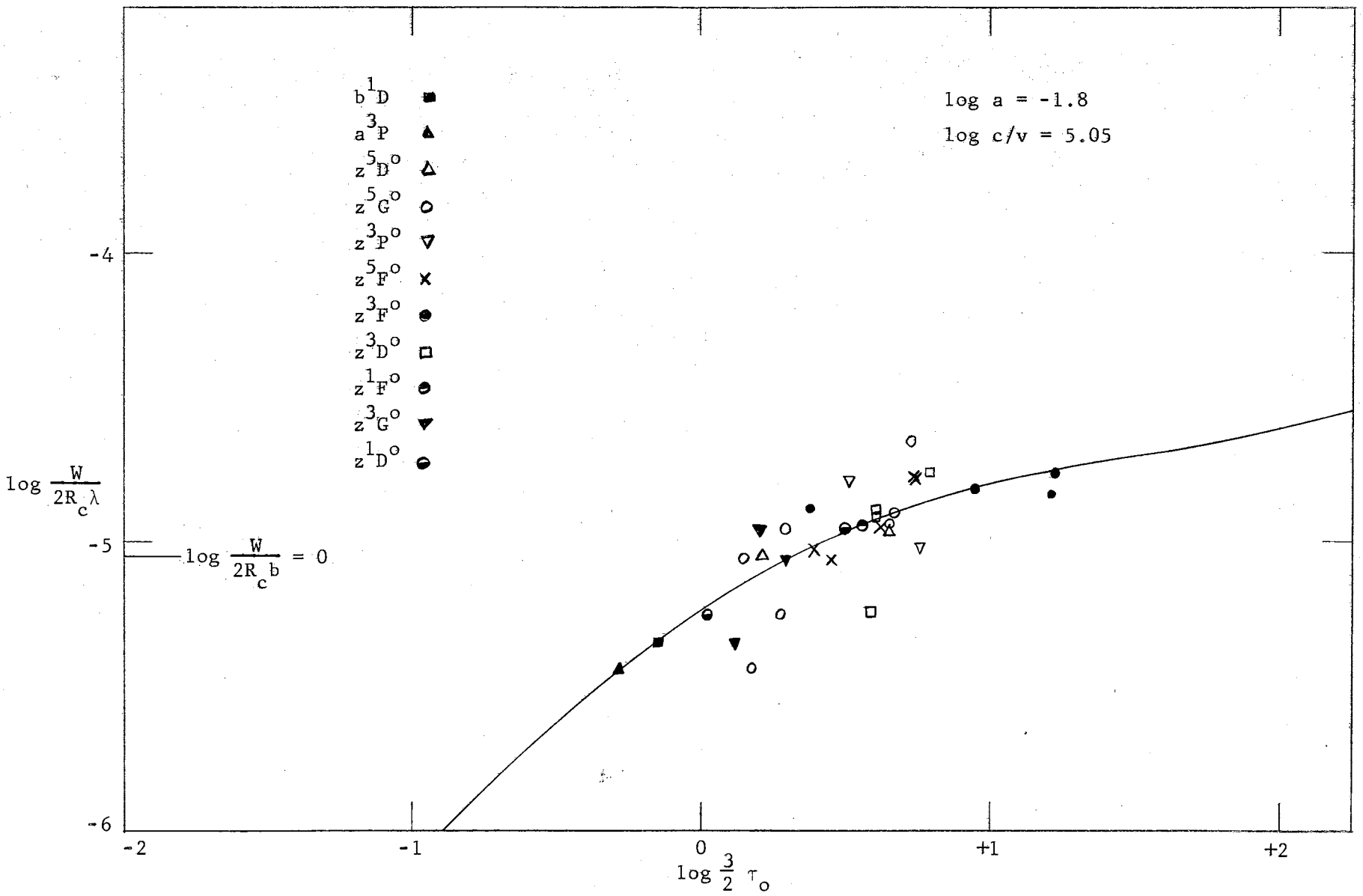

Figure 68. Schuster-Schwarzschild Pure Absorption Curve of Growth for Ni I.

CHAPTER V

SUMMARY AND CONCLUSIONS

The results of this investigation are summarized in Table XVIII. Values of log c/v, or log a, or both could not be determined from the observed curves of growth for some of the sets of lines. In such cases, values of log c/v and log a were adopted, as discussed in Chapter IV, for use in the analysis. In Table XVIII such values are enclosed in parentheses to indicate that they are not definitive results of this investigation. For titanium no value of $\Delta \log \eta$ is given since the abundances listed for Ti II also represent, to the limit of the accuracy attained in this study, the total abundances obtained for titanium.

The results obtained from the Fe I-NBS lines are regarded as the most reliable; more lines were available here than for any other set, and the observed curves of growth for Fe I-NBS were very well defined. A curve of growth analysis is a statistical procedure, and the Fe I-NBS data must be considered as best from a statistical point of view.

The excitation temperatures found from the Ti II lines are very uncertain, as evidenced by the four very different values obtained from the application of the four idealized models. As discussed in Chapter IV in the presentation of the results for Ti II, the responsibility for this uncertainty lies in the small range of χ_e represented by the Ti II lines. In such a situation, small changes in the values of $\Delta \log X$ can result in a relatively large change in the slope of the best straight

TABLE XVIII

SUMMARY OF THE RESULTS

	log c/v	log a	Excitation Temperature (°K)	log $N/\rho\bar{\kappa}$	log NH	$\Delta \log \eta$
M-E Scattering	(5.06)	-1.8	4825 ± 34	15.53		
M-E Absorption	(5.00)	-1.8	5607 ± 99	15.57		
Ca I						3.25
S-S Scattering	(5.07)	-1.8	4532 ± 23		15.34	
S-S Absorption	(5.05)	-1.8	5256 ± 151		15.38	
M-E Scattering	4.90	(-1.4)	4671 ± 215	14.45		
M-E Absorption	4.75	(-1.8)	4667 ± 206	14.38		
Ti I-NBS						
S-S Scattering	4.95	(-1.4)	4728 ± 240		14.30	
S-S Absorption	4.85	(-1.8)	4713 ± 218		14.14	
M-E Scattering	5.00	(-1.4)	5239 ± 320	14.86		
M-E Absorption	4.85	(-1.8)	5252 ± 375	14.79		
Ti I-King						
S-S Scattering	5.04	(-1.4)	5410 ± 310		14.64	
S-S Absorption	4.90	(-1.8)	5257 ± 305		14.51	
M-E Scattering	4.95	-1.8	6600 ± 478	17.06		
M-E Absorption	5.05	-1.3	8141 ± 614	17.05		
Ti II						
S-S Scattering	5.00	-1.8	5933 ± 309		17.00	
S-S Absorption	5.07	-1.3	7985 ± 608		16.79	
M-E Scattering	4.70	-1.8	6187 ± 292	14.82		
M-E Absorption	4.65	-1.8	6239 ± 352	14.77		
Cr I-NBS						2.35
S-S Scattering	4.95	-1.4	6071 ± 242		14.78	
S-S Absorption	4.80	-1.8	6114 ± 305		14.60	
M-E Scattering	5.05	-1.8	4449 ± 146	15.44		
M-E Absorption	5.00	-1.8	4335 ± 182	15.52		
Cr I-Hill						2.35
S-S Scattering	5.10	-1.8	4484 ± 151		15.24	
S-S Absorption	5.05	-1.8	4370 ± 182		15.24	

TABLE XVIII (Continued)

	log c/v	log a	Excitation Temperature (^{o}K)	log N/$\rho\overline{\pi}$	log NH	Δlog η
M-E Scattering	(5.06)	-1.4	4693 ± 130	15.46		
M-E Absorption	(5.00)	-1.3	4752 ± 95	15.35		
Mn I						2.05
S-S Scattering	(5.07)	-1.4	4678 ± 164		15.29	
S-S Absorption	(5.05)	-1.3	4714 ± 124		15.12	
M-E Scattering	5.06	-1.8	5219 ± 279	17.57		
M-E Absorption	5.00	-1.8	5522 ± 511	17.67		
Fe I-NBS						1.79
S-S Scattering	5.07	-1.4	5358 ± 263		17.06	
S-S Absorption	5.05	-1.8	5383 ± 501		17.48	
M-E Scattering	4.97	-1.4	3741 ± 165	17.45		
M-E Absorption	4.90	-1.3	3730 ± 153	17.41		
Fe I-King						1.79
S-S Scattering	5.05	-1.4	3732 ± 267		17.38	
S-S Absorption	4.95	-1.3	3790 ± 201		17.17	
M-E Scattering	(4.97)	(-1.4)	4420 ± 310	17.48		
M-E Absorption	(4.90)	(-1.3)	4394 ± 447	17.49		
Fe I-Carter						1.79
S-S Scattering	(5.05)	(-1.4)	4578 ± 306		17.29	
S-S Absorption	(4.95)	(-1.3)	4487 ± 456		17.21	
M-E Scattering	(5.06)	(-1.8)	5142 ± 425	15.63		
M-E Absorption	(5.00)	(-1.8)	5241 ± 458	15.55		
Co I						1.58
S-S Scattering	(5.07)	(-1.4)	5204 ± 551		15.40	
S-S Absorption	(5.05)	(-1.8)	5259 ± 517		15.29	
M-E Scattering	(5.06)	(-1.4)	5686 ± 437	16.42		
M-E Absorption	(5.00)	(-1.8)	6004 ± 619	16.33		
Ni I						1.42
S-S Scattering	(5.07)	(-1.4)	5625 ± 383		16.19	
S-S Absorption	(5.05)	(-1.8)	5840 ± 574		16.09	

line relating $\Delta\log X$ and $\overline{\chi}_e$, thus producing a large variation in the excitation temperature.

Comparison of Results Obtained Using Different Sets of f-Values

Most of the lines included in the Ti I-King, Cr I-Hill, Fe I-King, and Fe I-Carter data were also present among the NBS lines. For these common lines the NBS f-values are compared in Figure 69 with those from the other sources. The NBS f-values are on an absolute scale, while those from the other sources are on relative scales. The values of $\Delta\log gf$ used in the abundance calculations for Ti I-King, Cr I-Hill, Fe I-King, and Fe I-Carter are the quantities necessary to convert from the relative to absolute scales. This can be seen from Equation (31) of Chapter IV. However, there is no guarantee that the absolute scales determined in this manner will be the same as the NBS scale. In Figure 69 the values of $\Delta\log gf$ were used to establish the positions of the 45-degree lines. Points falling exactly on the lines represent perfect agreement between the absolute f-values of the NBS and the derived absolute f-values of the other sources. Some large deviations from agreement are apparent in the figure. At the appropriate points in the following discussion these deviations are taken into consideration.

For Ti I, Cr I, and Fe I many more lines were available with NBS f-values than with f-values from the other sources; hence small differences might be expected in the results obtained using the different sets of f-values. Falling into this category are variations in the values of log c/v and the excitation temperatures found from the Ti I-NBS and Ti I-King lines and in the values of log c/v found from the Fe I-NBS and Fe I-King lines. However, certain differences are present which cannot be

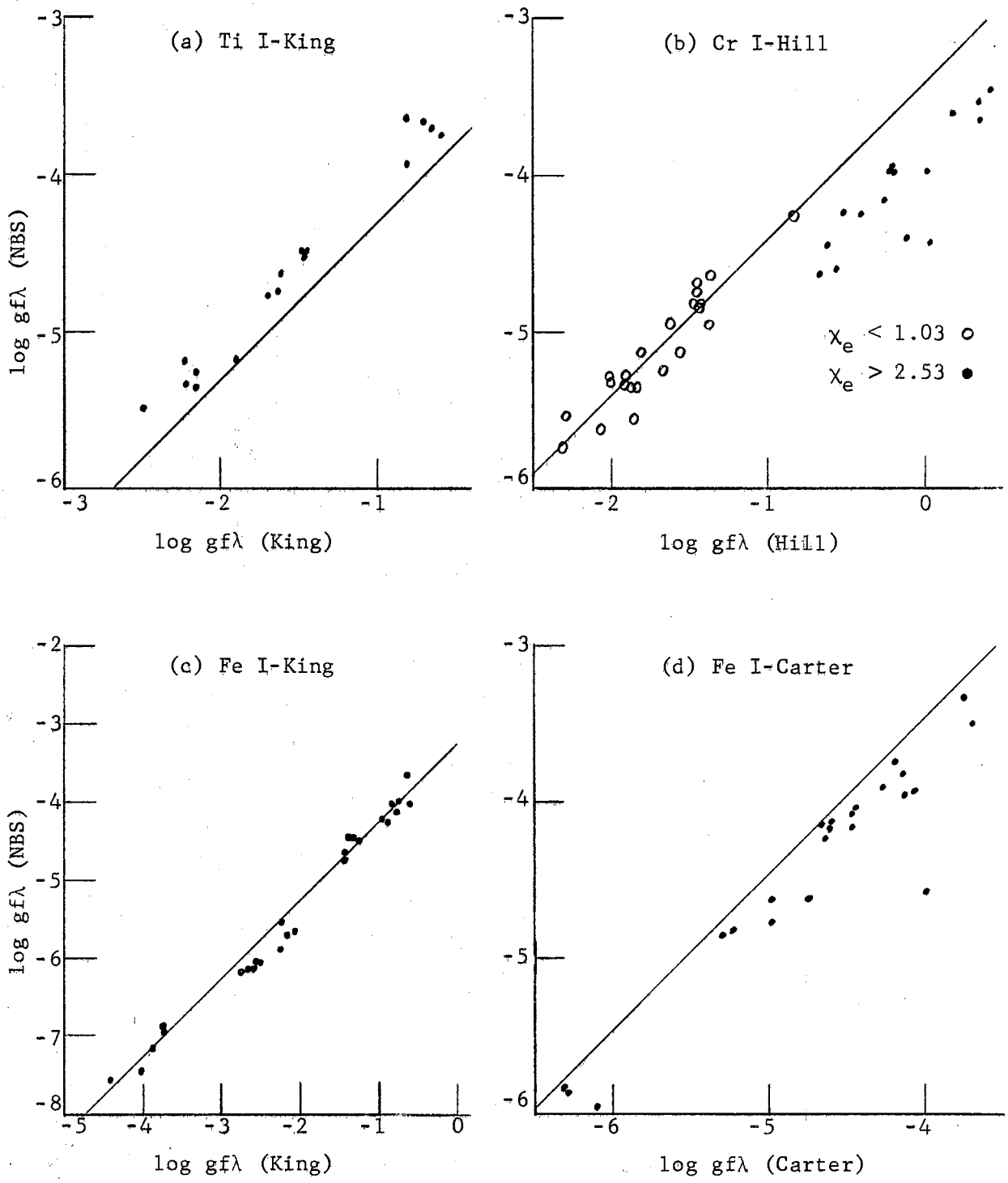

Figure 69. Comparison of the NBS f-Values With (a) the Ti I-King f-Values, (b) the Cr I-Hill f-Values, (c) the Fe I-King f-Values, and (d) the Fe I-Carter f-Values for the Lines Used in This Investigation.

attributed simply to statistical causes. These are discussed below.

Ti I

The most important differences between the Ti I-NBS and the Ti I-King results are in the abundances. As is evident in Figure 69a, the absolute scale of the NBS f-values does not agree with the absolute scale derived for the Ti I-King f-values from $\Delta\log gf = -3.30$. This disagreement may be largely responsible for the apparent differences in the abundances. The fault may lie in the value of $\Delta\log gf$, in the absolute scale used by the NBS, or in a combination of the two.

Cr I

The Cr I-NBS and Cr I-Hill results differ markedly in the values of log c/v, the excitation temperatures, and the abundances.

As remarked in Chapter IV in the presentation of the results obtained from the Cr I-NBS lines, two weak lines were very influential in the determinations of log c/v. These two lines were not included among the Cr I-Hill lines. The large differences between the Cr I-NBS and the Cr I-Hill values of log c/v are due to the effects of these two lines.

The differences between the Cr I-NBS and Cr I-Hill excitation temperatures are a result of the non-uniform relationship between the f-values used in the two cases. It is apparent from Figure 69b that the f-values for Cr I fall into two groups: those for lines with χ_e greater than 2.53 ev and those for lines with χ_e less than 1.03 ev. The excitation temperature is found from the slope of the best straight line relating $\Delta\log X$ and $\overline{\chi}_e$. The values of $\Delta\log X$ depend upon the f-values, e.g., $\Delta\log X = \log \tau_o - \log gf\lambda$ in the S-S pure scattering model. For

convenience in the discussion, consider that the Cr I-Hill f-values are placed on the absolute scale given by $\Delta\log gf = -3.42$. (Whether the scale is relative or absolute does not affect the excitation temperature determinations, but the uniformity of the scale is important.) Then, for lines with χ_e less than 1.03 ev, the values of $\Delta\log X$ obtained using the Cr I-NBS f-values should be approximately the same as those obtained using the Cr I-Hill f-values.* This can be seen from Figure 69b. For χ_e greater than 2.53 ev, the values of $\Delta\log X$ obtained using the Cr I-NBS f-values should be considerably larger than those obtained from the Cr I-Hill f-values. Hence, the slope of the best straight line relating $\Delta\log X$ and $\overline{\chi}_e$ obtained using the Cr I-NBS f-values should be substantially different from that obtained using the Cr I-Hill f-values. This is a possible explanation of the differences between the excitation temperatures found from the Cr I-NBS and the Cr I-Hill lines.

The abundances determined from the Cr I-NBS lines are smaller than those found from the Cr I-Hill lines. The abundances in each of the four models are dependent upon the quantity

$$\text{shift} + \log u - \log c/v.$$

The shift is given by $\Delta\log X + (5040/T)\overline{\chi}_e$, where T is the excitation temperature. Larger excitation temperatures give smaller shifts, and thus smaller abundances. This effect is partially offset by the increase of log u with temperature. However, the variation of log u with temperature

---

*This assumes that the same vertical shift (log c/v) is used for both cases. Although this was not true in the actual analysis of the Cr I lines, inclusion of this consideration would only complicate the argument and not alter the outcome. This can be seen by noting that a change in log c/v is accompanied by a change in $\Delta\log X$, and for Cr I, where most of the lines are weak, most of the changes in $\Delta\log X$ should be approximately the same. Hence, the slope of the best straight line relating $\Delta\log X$ and χ_e should not be altered appreciably.

is comparatively small. Hence, the much greater excitation temperatures obtained for Cr I-NBS than for Cr I-Hill produced to a large extent the differences in the calculated abundances.

Another consideration of importance in the abundance calculations is the connection between Δlog X and log c/v. By considering the shape of the curve of growth, it can be seen that as log c/v increases so does Δlog X. In the region well below the knee of the curve of growth, the slope of the curve is unity. For lines confined to this region, increases in log c/v are accompanied by like increases in Δlog X, and the effects of these changes exactly cancel one another in the abundance calculations. For stronger lines, however, an increase in log c/v produces a larger increase in Δlog X, with a resulting increase in the calculated abundance. In the case of Cr I most of the lines were weak, and it would be expected that the differences between the values of log c/v found for Cr I-NBS and Cr I-Hill would be largely compensated in the abundance calculations by the resulting differences in the values of Δlog X. This would be true were it not for the non-uniformity in the relationship between the f-values used for the two sets of lines, and the effect of this on the values of Δlog X. Because of this non-uniformity the values of Δlog X found from the Cr I-NBS lines with χ_e greater than 2.53 ev were disproportionately larger than the corresponding Cr I-Hill values. This acted in such a way as to decrease, but not nullify, the effect in the abundance calculations of the differences between the excitation temperatures.

Fe I

Important differences exist in the excitation temperatures found from the three sets of Fe I lines. These differences seem to reflect

the differences in the ranges of the excitation potentials applying in each case. For Fe I-King the values of χ_e ranged from 0.05 to 1.54 ev, for Fe I-Carter from 0.11 to 3.56 ev, and for Fe I-NBS from 0.03 to 4.53 ev. As a point of interest, excitation temperatures were calculated from the Fe I-NBS values of $\Delta \log X$, obtained from the S-S pure scattering model, covering first the same range in χ_e as represented by the Fe I-King lines, and second the same range in χ_e as represented by the Fe I-Carter lines. For χ_e in the range 0.05 to 1.54 ev the temperature found was $3616^{\circ}K$, and for χ_e in the range 0.11 to 3.56 ev the temperature determined was $5009^{\circ}K$. The first value corresponds closely to that obtained for the Fe I-King temperature ($3732^{\circ}K$ for S-S pure scattering), and the second is not greatly different from the Fe I-Carter value ($4578^{\circ}K$). It appears that the value determined for the excitation temperature depends upon the range of χ_e, with lower temperatures being characteristic of the lower levels of excitation. This lends weight to the reasonable assumption that lines arising from the higher levels in the atom are more likely to be formed principally in deeper layers of the atmosphere where the temperature is higher. In a curve of growth analysis the assumption is made that a single value of the excitation temperature can be specified which yields the correct distribution of atoms among the various energy levels. As is apparent from the above discussion, this assumption may be open to serious question when a wide range of excitation potentials is involved.

As described in the discussion of the Cr I results, differences in the excitation temperatures have a rather strong influence in producing differences in the calculated abundances. However, this is not apparent in the abundances found from the three sets of Fe I lines. In the

abundance calculations for Fe I-NBS and Fe I-King, the differences in the values of log c/v exert a greater influence than the differences in excitation temperature. Most of the lines included in these two sets are strong lines, and for strong lines an increase in log c/v produces a larger increase in Δlog X. Since the Fe I-NBS values of log c/v are larger than the Fe I-King values, this effect acts in a manner contrary to that of the excitation temperatures in the abundance calculations for Fe I-NBS and Fe I-King. Also, the fact that smaller values of log a were obtained from the Fe I-NBS lines than from the Fe I-King lines* (except for the S-S pure scattering case) tends to cause further increases in the Fe I-NBS values of Δlog X over those of Fe I-King. The result is that the Fe I-NBS abundances are larger, except for the S-S pure scattering case, than the Fe I-King abundances.

In Figure 69d it is apparent that the derived absolute scale for the Fe I-Carter f-values does not agree with the absolute scale of the Fe I-NBS f-values. This disagreement is mainly responsible for the differences between the Fe I-Carter and Fe I-NBS abundances.

Comparison of Results Obtained Using Different Idealized Models

A comparison of the results found from the four different sets of theoretical curves of growth reveals well defined trends in the values of log c/v and the abundances.

Except for Ti II, the S-S pure scattering model produced the largest values of log c/v, and the M-E pure absorption model the smallest values.

---

*The different values of log a were brought about by the different values of log c/v obtained from the two sets of lines. This can be seen by referring, in Chapter IV, to the description of the procedures used in determining log a.

The reason for this is apparent from an examination of Figure 70, where theoretical curves with log a = -1.8 for the four models are compared. Even if the S-S pure scattering curve were to be shifted horizontally so that the Doppler portions (i.e., the portions below the knees) of all four curves were coincident, the transition portion of the S-S pure scattering curve would still be higher than the transition portions of the other curves. Hence, the largest vertical shifts, and thus the largest values of log c/v, should result from the application of the S-S pure scattering curve. Conversely, the smallest value should be given by the M-E pure absorption curve.

It should be noted that for use with the M-E pure scattering model, the M-E pure absorption model, and the S-S pure absorption model the observed curves of growth were altered from those used with the S-S pure scattering model by the application of the limb darkening corrections--log $2R_c$ and $\Delta\log \eta_o$. However, the limb darkening corrections in most cases were not large enough to change the trend discussed in the preceding paragraph.

In the case of Ti II the damping parameter was important in the determination of log c/v. The plot used to determine log c/v extended from the knee well into the damping portion of the curve of growth; therefore this plot was also used to determine log a. Log a = -1.8 was found for both scattering models and log a = -1.3 for both absorption models. The curves for log a = -1.3 rise more rapidly than those for log a = -1.8. This, combined with the effects produced by the inclusion of the limb darkening corrections, caused the S-S pure absorption model to give the largest value of log c/v and the M-E pure scattering model the smallest value.

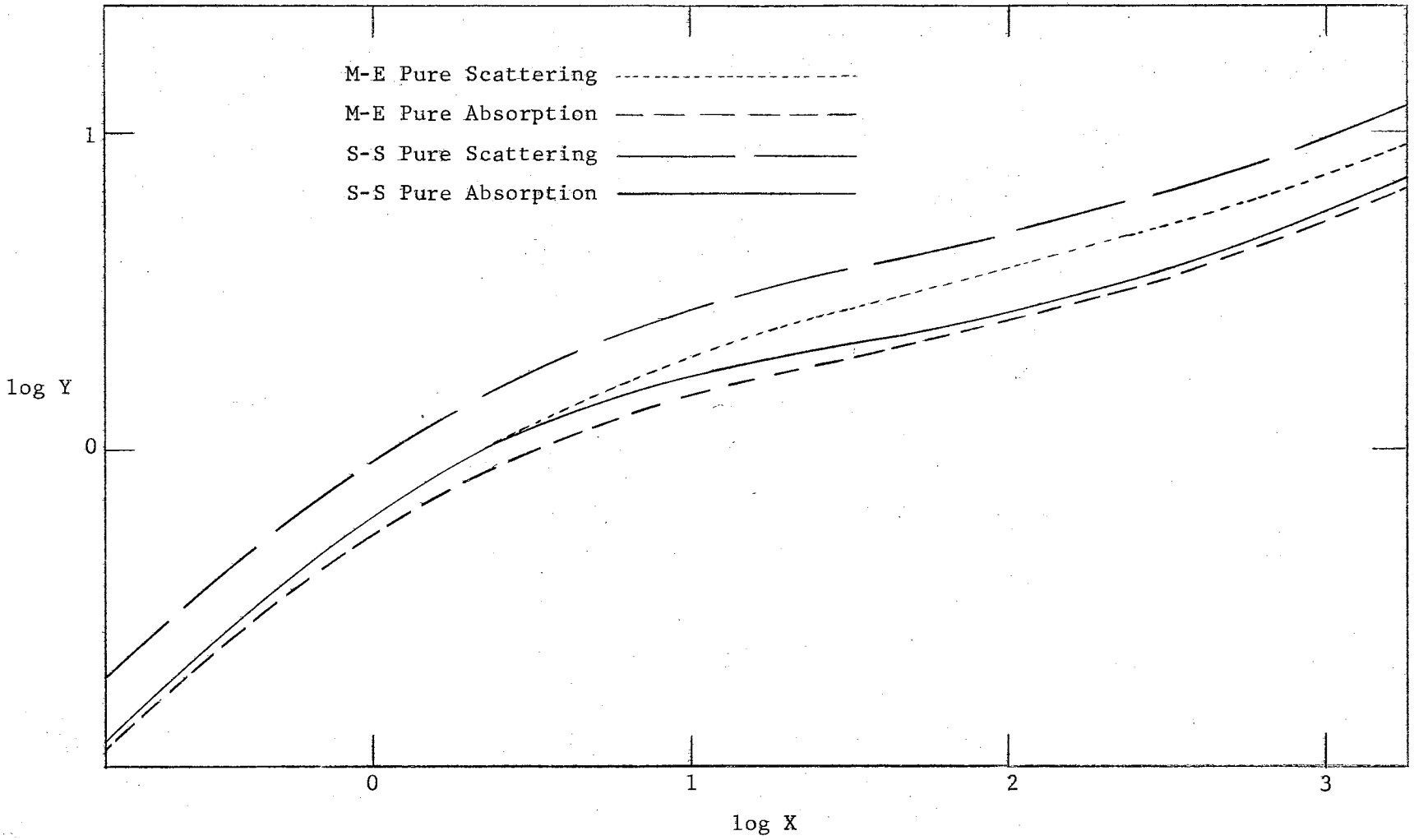

Figure 70. Comparison of the Theoretical Curves of Growth for the Four Models. The curves are for log a = -1.8.

For M-E Pure Scattering, $X = \eta_o$, $Y = W/b$. For M-E Pure Absorption, $X = \eta_o$, $Y = W/2R_c b$.

For S-S Pure Scattering, $X = \tau_o$, $Y = W/b$. For S-S Pure Absorption, $X = 3\tau_o/2$, $Y = W/2R_c b$.

The values of log $N/\rho\bar{\kappa}$ found from the M-E models are larger, in most cases, than the values of log NH determined from the S-S models. From Figure 70 it can be seen that the curves of growth for the M-E models tend to give either smaller values of log c/v or larger values of Δlog X than the curve for the S-S pure scattering model. The result in either case is that the M-E abundances tend to be larger than the S-S pure scattering abundance. The S-S pure absorption curves of Hunger are plotted with log $3\tau_o/2$ as abscissa rather than simply log τ_o. This amounts to shifting the curve horizontally so that the Doppler portion coincides with the similar portions of the M-E curves. Hence, the differences in the values of Δlog X obtained from this model and the M-E models should be insignificant. However, the term log 3/2 appears negatively in the equation giving the abundance in the S-S pure absorption model. This compensates for the shift in the abscissa, and the resulting abundance should be smaller than those found from the M-E models.

Comparison of the Results of This Study With Those of Greenstein

Greenstein (1948), in his study of a group of F stars, employed observed curves of growth based mainly upon Fe I lines and Wright's solar log X_f-values. These were analyzed using theoretical curves of growth based upon the M-E model. Greenstein's values of log v, Γ/γ_{cl}, and θ_{exc}, which are discussed below, were obtained from his observed curve of growth for Fe I.

Greenstein found for θ Ursae Majoris a value of log v = 5.44. (The velocity parameter in Greenstein's notation is represented by "V.") This leads to a value of log c/v equal to 5.04, which agrees closely with the most reliable values (the Fe I-NBS values) obtained in this investigation.

He obtained a value of Γ/γ_{cl} equal to 1.7, which corresponds to log a = -2.3. Here Γ is the effective damping constant and γ_{cl} is the classical damping constant. By referring to Figure 8 of Chapter III it can be seen that for the strongest lines, which are important in the determination of log a, the values of log W/λ measured by Greenstein are smaller than those measured in this investigation. This difference could have caused the value of log a determined by Greenstein to be smaller than the values found in this study.

For θ_{exc} Greenstein obtained the value 0.98, which corresponds to an excitation temperature equal to 5150°K. The lower level excitation potentials of the Fe I lines used by Greenstein range from 0.00 to 4.09 ev. The extent of this range is intermediate to those represented by the Fe I-Carter and Fe I-NBS lines used in this investigation. As expected from the apparent relationship, discussed earlier, between the excitation temperature and the range of χ_e, the excitation temperature obtained by Greenstein falls between the values found in this study from the Fe I-Carter and Fe I-NBS lines.

Greenstein determined abundances in the stars relative to those in the sun, and these quantities cannot readily be compared with the abundances found in this investigation. The abundances obtained by Wright (1948) for the star Procyon, which has a spectrum similar to that of θ Ursae Majoris, are of the same order of magnitude as those found for θ Ursae Majoris in this study.

Comparison of Wrubel's and Hunger's M-E Pure Absorption Curves of Growth

Hunger's M-E pure absorption curves of growth were employed in this

investigation although curves for the same model by Wrubel were available. Wrubel's curves were calculated using Chandrasekhar's exact solution of the equation of transfer and therefore are regarded as the best available for the M-E pure absorption model. However, calculations were made for only two values of log a, -1 and -3, thus limiting the usefulness of these curves.

The abscissa of both Wrubel's and Hunger's curves is log η_o. (In Hunger's notation the abscissa is log C, but for M-E pure absorption C = η_o.) The ordinate of Wrubel's curves is log W/b, while for Hunger's curves the ordinate is log $W/2R_c b$. Wrubel calculated curves for two values of B^o/B^1, 2/3 and 10/3. If B^o/B^1 is equal to 2/3, then $2R_c$ is equal to unity. In this case Hunger's ordinate is simply log W/b, the same as Wrubel's ordinate. By interpolating in Hunger's tables, curves were obtained for log a = -1 and log a = -3. These were then compared with Wrubel's curves for $B^o/B^1 = 2/3$. The calculated points of Wrubel's and Hunger's curves could not be compared individually because Wrubel and Hunger did not use the same sets of values of η_o in their calculations. To compare the curves for the same value of log a, the two curves were plotted, using the same scale, and one superposed upon the other. There were no noticeable differences in the two curves with log a = -1 nor in the two curves with log a = -3.

The ordinate of Hunger's curves can be written as

$$\log \frac{W}{2R_c b} = \log \frac{W}{b} - \log 2R_c . \tag{36}$$

If B^o/B^1 is equal to 10/3, then log $2R_c$ is equal to -0.477. Hunger's ordinate in this case is

$$\log \frac{W}{2R_c b} = \log \frac{W}{b} + 0.477. \tag{37}$$

To obtain a curve which relates log η_o and log W/b for $B^o/B^1 = 10/3$, it is only necessary to subtract the quantity 0.477 from Hunger's tabulated values of log $W/2R_c b$. For log a = -1 and log a = -3 there were no noticeable differences in the curves obtained in this manner and the curves calculated by Wrubel for $B^o/B^1 = 10/3$.

The above discussion does not eliminate the possibility that significant differences might exist between the M-E pure absorption curves of Hunger and those calculated using Wrubel's method for values of log a other than -1 and -3 and values of B^o/B^1 other than 2/3 and 10/3. However, the suggestion is strong that for any values of log a and B^o/B^1 the curves should be substantially the same.

The four sets of curves of growth used in this investigation are based upon idealized models which represent extreme approximations as to the structure of the stellar atmosphere and the mechanism of line formation. None of these models can be expected to perfectly characterize the actual structure and radiation processes of the atmosphere of θ Ursae Majoris.

In the case of the star Procyon, Schroeder (1958) has pointed out that the S-S model is to be preferred for the lines of low and intermediate excitation potential since these lines are formed well above the photosphere. For lines of higher excitation potential, which are formed primarily in the same region as the continuum, Schroeder concluded that the M-E model would be more appropriate. Due to the similarity of Procyon and θ Ursae Majoris, it seems likely that the above remarks should also apply to θ Ursae Majoris.

In the spectrum of θ Ursae Majoris the central intensities of the strongest lines are not zero. This indicates that the lines are not formed solely by the scattering process, which requires zero central intensities for the strongest lines. The lines are most likely formed by a combination of the processes of scattering and absorption.

Although the four idealized models (i.e., M-E and S-S pure scattering, and M-E and S-S pure absorption) represent extreme approximations, the results obtained in this investigation from the application of the four different models are not greatly variant.

In abundance determinations the quantity most desired is N, the number of atoms per cubic centimeter. N is inherent in the expressions NH and $N/\rho\overline{\kappa}$, which are the "abundances" determined in this study. H is the depth of the reversing layer characterizing the S-S model. In the M-E model $1/\rho\overline{\kappa}$ is a measure of the geometrical depth of the atmosphere corresponding to infinite optical depth in the continuum. It is clear that a knowledge of H or $1/\rho\overline{\kappa}$ is prerequisite to obtaining a value for N. H depends upon excitation, ionization, and varies from element to element, while $1/\rho\overline{\kappa}$ may vary strongly with optical depth. At best, average values of H and $1/\rho\overline{\kappa}$ can be obtained. Until more refined techniques are devised, curve of growth analyses will yield only NH or $N/\rho\overline{\kappa}$, the number of atoms in a one square centimeter column in the line of sight.

A curve of growth analysis yields information of a statistical nature concerning the properties of a stellar atmosphere. Such information provides a basis for more detailed studies of the individual line profiles using model atmosphere techniques. Studies of this type are called for in the further investigation of the atmosphere of θ Ursae Majoris.

REFERENCES

Allen, C. W. 1955, Astrophysical Quantities (London: Athlone Press).

Aller, L. H. 1960, Stellar Atmospheres, ed. J. L. Greenstein (Chicago: The University of Chicago Press), pp. 199, 246.

Bell, G. D., Davis, M. H., King, R. B., and Routly, P. M. 1958a, Trans. I. A. U., 10, 221.

_____. 1958b, Ap. J., 127, 775.

Carter, W. W. 1949, Phys. Rev., 76, 962.

Corliss, C. H., and Bozman, W. R. 1962, Experimental Transition Probabilities for Spectral Lines of Seventy Elements (NBS Mono. No. 53 [Washington: Government Printing Office]).

Deutsch, A. J. 1954, J. Opt. Soc. America, 44, 492.

Glennon, B. M., and Wiese, W. L. 1962, Bibliography on Atomic Transition Probabilities (NBS Mono. No. 50 [Washington: Government Printing Office]).

Greenstein, J. L. 1948, Ap. J., 107, 151.

Hill, A. J., and King, R. B. 1951, J. Opt. Soc. America, 41, 315.

Houtgast, J. 1942, The Variations in the Profiles of Strong Franhofer Lines along a Radius of the Solar Disc (Utrecht: Schotanus & Sons).

Hunger, K. 1956, Zs. f. Ap., 39, 36.

Johnson, H. L., and Morgan, W. W. 1953, Ap. J., 117, 313.

Keenan, P. C., and Morgan, W. W. 1951, Astrophysics, ed. J. A. Hynek (New York: McGraw-Hill Book Co.), p. 12.

King, R. B. 1942, Ap. J., 95, 78.

King, R. B., and King, A. S. 1938, Ap. J., 87, 24.

Menzel, D. H. 1936, Ap. J., 84, 462.

Minnaert, M., and Slob, C. 1931, Proc. Amsterdam Acad., 34, Part I, 542.

Moore, C. E. 1945, Contr. Princeton U. Obs., No. 20.

Schroeder, L. W. 1958, Ph.D. Thesis, Indiana University, unpublished.

Strömgren, B. 1937, Ap. J., 86, 1.

Struve, O., and Elvey, C. T. 1934, Ap. J., 79, 409.

Swensson, J. 1946, Ap. J., 103, 207.

Thackeray, A. 1936, Ap. J., 84, 433.

Unsöld, A. 1955, Physik der Sternatmospharen (2d ed.; Berlin: Julius Springer).

Wright, K. O. 1948, Pub. Dom. Ap. Obs. Victoria, VIII, No. 1.

_____. 1962, Astronomical Techniques, ed. W. A. Hiltner (Chicago: The University of Chicago Press), p. 83.

Wrubel, M. H. 1949, Ap. J., 109, 66.

_____. 1950, ibid., 111, 157.

_____. 1954a, ibid., 119, 51.

_____. 1954b, Proceedings of the Indiana Conference on Stellar Atmospheres, ed. M. H. Wrubel (1955), p. 126.

_____. 1956, published Aller (1960) above, p. 199.

VITA

Hugh Oscar Peebles

Candidate for the Degree of

Doctor of Philosophy

Thesis: A STUDY OF LINE INTENSITIES IN THE SPECTRUM OF θ URSAE MAJORIS

Major Field: Physics

Biographical:

Personal Data: Born in Kountze, Texas, May 4, 1933, the son of Hugh O. and Gladys L. Peebles.

Education: Attended grade school in Kountze and San Antonio, Texas; graduated from Kountze High School in 1950; received the Bachelor of Science degree from the University of Texas, with a major in Physical Education, in January, 1955; attended Lamar State College of Technology, Beaumont, Texas, for two years, beginning in 1957; attended the University of Texas during the summer, 1959; received the Master of Science degree from the Oklahoma State University, with a major in Natural Science, in August, 1960; completed requirements for the Doctor of Philosophy degree in May, 1964.

Professional experience: Taught in the Kountze High School, Kountze, Texas, from September, 1955, through May, 1959.